Master's thesis

NTNU
Norwegian University of Science and Technology
Faculty of Engineering
Department of Geoscience and Petroleum

Solveig Tegelsrud Kolstad

The controlling factors for runout lengths for "steinskred" in Hordaland, developing of a new α-β method for "steinskred" and analyses of the flow behavior "steinskred" event in Modalen, 1953

Master's thesis in Geology
Supervisor: Reginald Hermanns
Co-supervisor: François Noël and Ingrid Skrede
September 2021

NTNU
Norwegian University of
Science and Technology

Solveig Tegelsrud Kolstad

The controlling factors for runout lengths for “steinskred” in Hordaland, developing of a new α-β method for “steinskred” and analyses of the flow behavior “steinskred” event in Modalen, 1953

Master’s thesis in Geology
Supervisor: Reginald Hermanns
Co-supervisor: François Noël and Ingrid Skrede
September 2021

Norwegian University of Science and Technology
Faculty of Engineering
Department of Geoscience and Petroleum

NTNU
Norwegian University of
Science and Technology

Abstract

"Steinskred" is a Norwegian term for a small rock avalanche or large rock fall. This is a well-known phenomenon in Norway and the threat can cause fatalities if it interacts with houses or other infrastructure. Despite this, there is a lack of experience and methodology for handling these types of events in hazard zone assessment. The line between rock avalanche and "steinskred" is poorly understood.

216 deposits with volume ranging from ~800 to 8 500 000 m^3 were digitally mapped in Hordaland, located as a part of the county Vestland in Norway. This mapping is based on aerial photos, topographical maps, hill shade maps and DTMs. Large dataset from Hordaland made it possible to analyse factors controlling the runout length, testing a new $\alpha-\beta$ model for "steinskred" and discussing when rock slope failures develop flow behaviour of rock avalanches and when not.

When analysing the angle of reach (a concept for expressing the runout length) and the volume of the deposits, the data show a threshold at 250 000 m^3. Events below 250 000 m^3 show the same behaviour, with an angle of reach >31°. Higher volumes show flow like behaviour of rock avalanches and can possibly have excessive travel lengths (angle of reach <31°). When analysing the angle of reach with the effect of substrate, the events with smaller deposit volume than ~0.09 Mm^3 will have a higher angle of reach when propagating on liquefiable, soft or rocky material. In comparison, for events having larger deposit volumes than ~0.09 Mm^3, the angle of reach will be lower when propagating on liquified or soft material. In addition, the channelized runout paths seem to increase the runout length for event with larger deposit volume than ~0.08 Mm^3, while smaller events than this, the rock will lose the energy in each impact. Events with undisturbed runout path have therefore the smallest angle of reach when the volume is below ~0.08 Mm^3. With such a large dataset as collected in this work, a new $\alpha-\beta$ method has been automized using Excel. It is tested with different factors based on the earlier $\alpha-\beta$ equation for rock falls (Domaas, 1994). The best fitted $\alpha-\beta$ equation for "steinskred" is $\alpha = m \cdot \beta + n = 0.75 \cdot \beta + 5°$, where the β–point is tested to be where the slope angle $\theta_\beta = 20°$.

The zone in which failures change from "steinskred" to rock avalanche behaviour are discussed to be more flexible, and a lower volume threshold to form rock avalanches may lie around 250 000 m^3. These events between 10 000 and 250 000 m^3 can be affected the same way as rock falls and rock avalanches when it comes to substrate and topographical constraint, and

also, exceptional, have a flow like motion as rock avalanches as shown in the “steinskred” event in Modalen, 1953.

Sammendrag

Steinskred er en norsk betegnelse på et lite fjellskred eller et stort steinsprang. Denne faren er et velkjent fenomen i Norge, og kan forårsake katastrofale hendelser hvis den har rekkevidde som treffer hus eller annen infrastruktur. Til tross for dette er det mangel på erfaring og metodikk for å håndtere denne typen hendelser i vurderingen av faresoner. Grensen mellom steinskred og fjellskred er fortsatt ikke godt nok undersøkt.

216 avsetninger med volum fra ~ 800 til 8 500 000 m^3 ble digitalt kartlagt i Hordaland, som utgjør en del av Vestland fylke. Denne kartleggingen er basert på flyfoto, topografiske kart, skyggekart og DTM. Det store datasettet fra Hordaland gjorde det mulig å analysere faktorer som påvirker utløpslengden, teste en ny $\alpha-\beta$ modell for steinskred og diskutere når et skred vil utvikle granulær massestrøm og ikke.

Analyser av forholdet mellom siktevinkelen (et konsept for å uttrykke utløpslengden) og volumet til avsetningene av de kartlagte hendelsene, viser dataene en terskel på 250 000 m^3. Hendelser under 250 000 m^3 viser samme oppførsel, med en siktevinkel >31 °. Ved høyere volumer enn dette viser en strømmende bevegelse av masser og kan potensielt oppnå ekstra store utløpslengder (siktevinkel <31 °). Når man analyserer siktevinkel med effekten av substrat, vil hendelsene som har avsetningsvolum mindre enn ~0.09 Mm^3 ha en større siktevinkel når de transporteres på vannmettede sedimenter, mykere materiale eller ur. Til sammenligning vil siktevinkelen hos hendelser med høyere avsetningsvolumer enn 0.09 Mm^3 være lavere ved transport på vannmettede sedimenter eller mykt underlag. I tillegg ser det ut til at hendelsene med kanalisert utløpsbane øker utløpslengden for hendelser med større avsetningsvolum enn ~ 0,08 Mm^3, mens ved mindre hendelser enn dette, vil blokkene miste energien i hvert støt. Hendelsene som har uforstyrret utløpsbane, fører dermed til den minste siktevinkelen når volumet er mindre enn ~0,08 Mm^3. Med en så stor database har en ny $\alpha-\beta$ metode blitt automatisert ved hjelp av Excel, og testet med forskjellige faktorer basert på tidligere $\alpha-\beta$ ligninger for snøskred, steinsprang og jordskred (Bakkehoi et al., 1983, Lied and Bakkehøi, 1980, Lied and Kristensen, 2003, Norem and Sandersen, 2012). Den best tilpassede $\alpha-\beta$ ligningen for "steinskred" er $\alpha = m \cdot \beta + n = 0.75 \cdot \beta + 5°$, hvor β–punktet er testet til å være der hvor helningen på fjellsiden $\theta_\beta = 20$ °.

Grensen hvor et skred endres fra å være definert som et steinskred til å bli definert som fjellskred blir diskutert til å være mer fleksibel, og et minimum volumgrense for fjellskred kan ligge rundt

250 000 m^3. Disse hendelsene mellom 10 000 og 250 000 m^3 kan påvirkes på samme måte som steinsprang og fjellskred når det gjelder underlag og begrensninger, og har også, unntaksvis, en strømmende bevegelse som fjellskred. Dette er observert ved steinskred hendelsen i Modalen, 1953.

Acknowledgement

This thesis is the final work of the two-year master in geology at the Norwegian University of Science and Technology (NTNU). It is written in collaboration with the Geological Survey of Norway (NGU) and the Norwegian Water Resources and Energy Directorate. My supervisor has been Reginald Hermanns (NGU) and my co-supervisors have been François Noël (NGU) and Ingrid Skrede (NVE).

I would like to thank my supervisors for the good feedback, guidance, and discussions thorough out this work. I am glad to have been a part of this interesting topic of “steinskred”, it has been exciting! Thank you also to all that have helped me with small and larger questions for my thesis.

Ingeborg, I am very grateful for the help in the field. We got to experience most parts of Hordaland. Even though there were some dead ends and with a lot of walking in scree, the weather was with us and I have only good memories from the ten days. Also, thank you to my fellow students for all the motivation, and to my father which have showed large interest in my thesis and have contributed to good discussions.

Molde, 01.09.21

Table of contents

ABREVIATION

DEM	Digital Elevation Model
LiDAR	Light Detection and Ranging
NGU	Geological Survey of Norway
NGI	Norwegian Geotechnical Institute
NTNU	Norwegian University of Science and Technology
NVE	Norwegian Water Resources and Energy Directorate
RSF	Rock slope failure
SLBL	Sloping Local Base Level
TLS	Terrestrial Laser Scanner

1. Introduction

1.1 Rock slope failures in Norway

Rock slope failures in Norway, and their secondary effects, have through the years caused several fatalities and will statistically lead to more in the future. These events are of various size, can move in a velocity of tens of meters per second (Nicoletti and Sorriso-Valvo, 1991), and the large events, have flow-like motion leading to long runout lengths (Mitchell et al., 2020b). The high occurrence of rock slope failure events in Norway is, among other reasons, due to the mountainous landscape with narrow valleys and deep fjords. People will continue to settle in these small valleys and near the fjords, even in landslide prone areas (Hermanns et al., 2012). To mitigate the threat for houses and infrastructure in rock slope failure events it is important get more knowledge on the controlling factors of runout length and to develop methods for hazard assessment.

The Norwegian water resources and energy directorate (NVE) have, since 2009, had the responsibility of the administrative tasks within the prevention of landslide accidents. In 2019, NVE initiated the work of making a new guideline or industry standard for rock slope failures in Norway (NVE, 2020). The new guidelines are made in order to increase the overall quality of the hazard mapping. It will make it easier to perform and contribute to better documentation, which follows and corresponds to the plan and the building act (pbl § 28-1) and the building code (TEK 17 § 7-3).

The Norwegian term “steinskred”, which is considered as a large rock fall or a small rock avalanche, is less studied than rock fall and rock avalanches. It is found to have a lack of experience and methodology for handling these threats. There are missing guidelines for predicting the runout length for “steinskred”, and runout models are not yet developed for these types of events, such as with rock falls and rock avalanches. In hazard zone assessment the lines used for these events will be too conservative compared to the actual runout length and will take up unnecessary large areas. Detailed mapping of historic “steinskred” events will help to better understand the controlling factors for the runout length and can be used to test already existing modelling programs for rock fall and rock avalanche to suit for “steinskred” events. In 2019, NGU developed a new database with a systematic mapping of rock failure events in Norway (Velardi et al., 2020). This database exists of 174 events, spread in Troms, Sogn og Fjordane and Møre og Romsdal.

1.2 Aim of the study

In this thesis systematically mapping of rock slope failure deposits with volume in the range of ~800-8 500 000 m^3 was carried out in Hordaland. The aim is to better understand the travel length of rock slope failures in order to develop predictive tools. A special interest is to find out what rock slope failures develop flow behaviour of rock avalanches and when not. The data mapped will also contribute to a large database of events that can later serve as a valuable empirical base for calibration of simulation models. The main work includes:

- Map prehistorical rock slope failures in Hordaland (e.g. deposits and source areas) based on orthophotos, hill shade maps and terrestrial high-resolution digital elevation models (DEMs).
- Measure parameters as height (H), length (L), H/L and angle of reach (α) for the events and note the certainty level, volume, slope profile geometry, topographic constraints and substrate.
- Measure the volume of the deposit of each event based on the method "sloping local base level (SLBL)" (section 3.2.1).
- Based on the measured parameters, make statistical analysis of the controlling factors of the runout length.
- Develop an alpha-beta method with suitable coefficients for estimating the runout length of "steinskred" based on the mapped events. This follows the empirical approach of coefficients in the already existing $\alpha-\beta$ equation of rock falls.
- Fieldwork of the interesting 1955 "steinskred" event in Modalen, which had a runout with flowing masses such as in rock avalanches. This fieldwork includes LiDAR scanner, roughness analyses, measure of tree density, measuring of block sizes and collecting of sediment samples.

1.3 Available data and previous work

The analyses in this thesis are based on both data from field mapping and digital analyses. The fieldwork was carried out by the author and Ingeborg Aalstad Grønvoll and was performed during ten days in June/July 2020. For the digital analyses and inventory mapping, already existing data have been used, and are listed in table 1. Earlier work from Velardi et al. (2020) in Troms, Møre og Romsdal and Sogn og Fjordane and the development of the national database on geological landslide database have been a good base of this thesis. This thesis will partly be a further work on her dataset by mapping rock slope failures in Hordaland.

Table 1 Available data

Available data	Source
Quaternary geological maps	NGU
Bedrock maps	NGU
Aerial photo (WMS)	The Norwegian Mapping Authority (Kartverket).
Topographical data	The Norwegian Mapping Authority (Kartverket)
Quaternary map (Aga)	NGU w/Lena Rubensdotter, Gro Sandøy
DEM (1x1 m and 10x10 m)	The Norwegian Mapping Authority (Kartverket)
Data from mapped rock fall failures in Møre og Romsdal, Sogn og Fjordane and Troms county.	Velardi et al. (2020)
Hill shade map	The Norwegian Mapping Authority (Kartverket)

1.4 The study area and the geological and climatic conditions

The study area and the sites included in this study are located in the southern part of Vestland county, earlier Hordaland county (figure 1). The rest of Vestland, Sogn og Fjordane, was previous studied by Velardi et al. (2020). Hordaland is located in the western part of Norway and are characterized by high mountains, valleys and fjords. Due to the morphology with relief from 0 to 1863 masl. Hordaland is one of the counties with the most landslide events in Norway (skrednett.no). Also, one of Norway's main fjords, Hardangerfjorden, is situated in Hordaland, and is the second longest fjord in Norway (Mangerud et al., 2016). Hordaland also consists of two ice caps (platou glaciers), Hardangerjøkulen and Norway's third largest glacier, Folgefonna, both with several minor outlet glaciers.

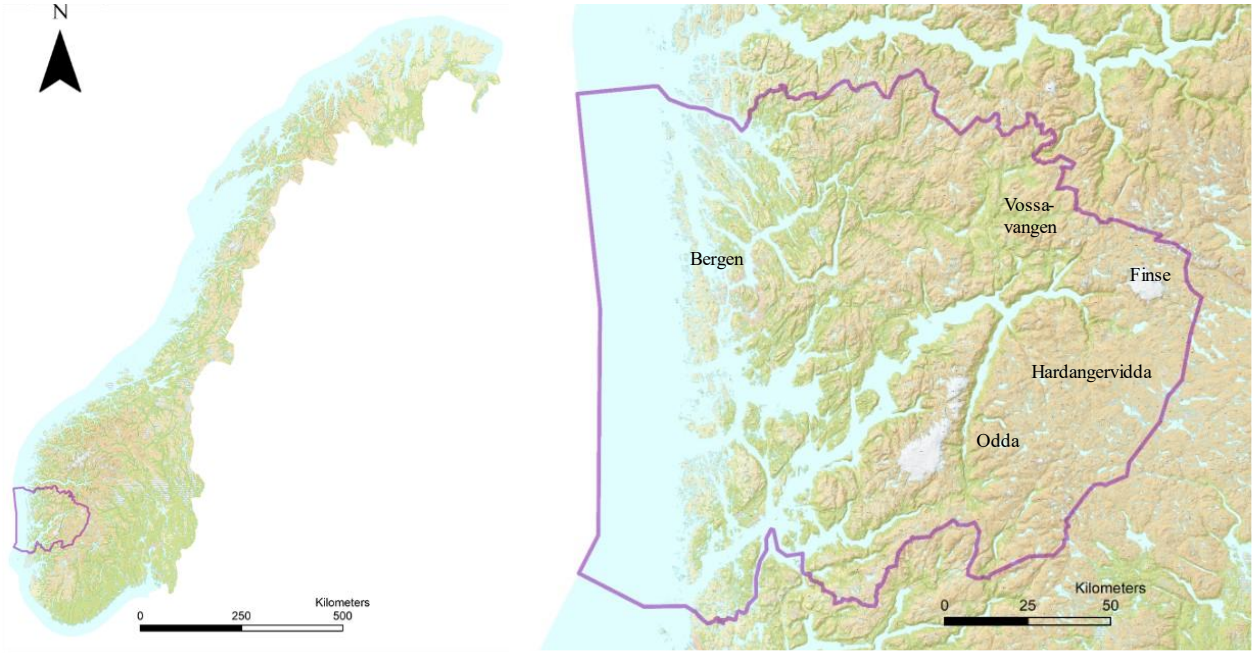

Figure 1 Overview map of Norway, and Hordaland

1.4.1 Geology in Hordaland

The bed rock in Hordaland consists of gneiss and granite from Precambrian, which is overlayed with sedimentary rocks. On top of these layers there are over thrusted nappes deriving from the Caledonian orogeny. This is followed by subsequent orogenic collapse with back-sliding of Caledonian nappes (Sigmond, 1998). These over thrusted nappes and the backsliding collapse make up important parts of the geology in Hordaland today (figure 2).

The Caledonian orogeny happened 490-390 million years ago due to collision between the two former continents Laurentia and Baltica. During this collision, plutonic rocks (dypbergarter) and metamorphic rocks (omdannede bergarter) from Proterozoic and early Paleozoic (Kambrosilur) were thrusted as nappes from a northwest direction. After the collision and when the continents started drift apart, the mountain belt started to collapse (McKerrow et al., 2000). Because of these processes Hordaland exists of several brittle faults like the Lærdal–Gjende fault system and shear zones like the Hardangerfjord shear zone, the Nordfjord–sogn shear zone and Bergensbue shear zone (marked with grey dotted lines on figure 2).

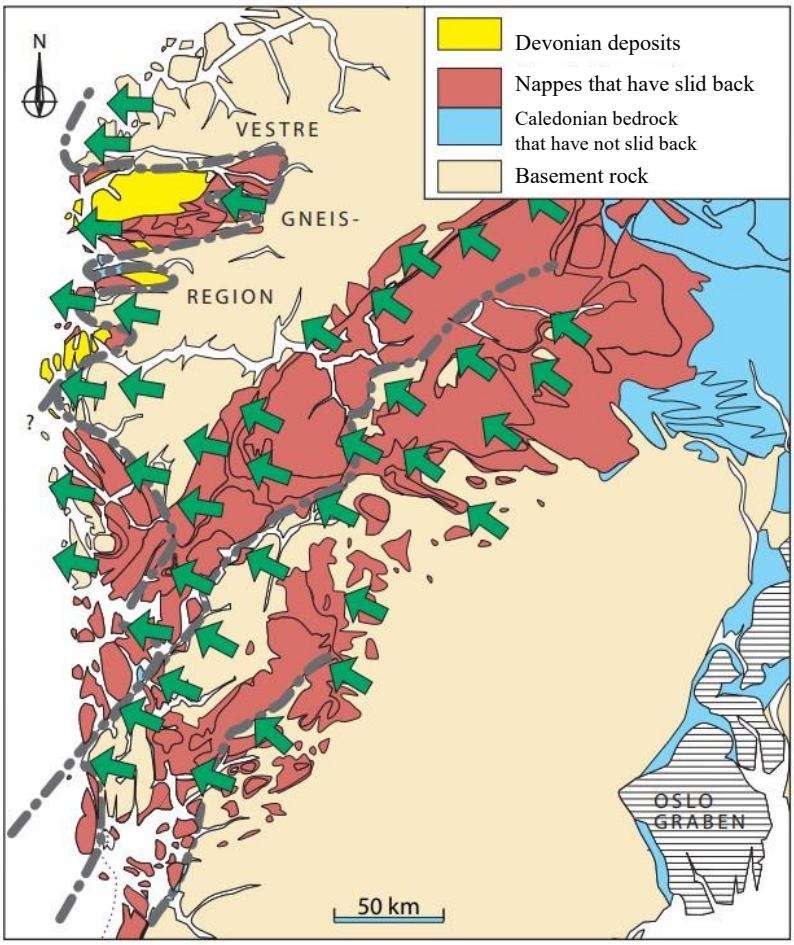

Figure 2 Overview map of the geology in Hordaland, showing the over thrusted nappes and the backsliding and the shear zones marked in grey dotted lines. Modified from Fossen et al. (2008)

1.4.2 Glacier and glacial history

Together with the large influence of the Caledonian origin and the collapse with back-sliding, the steep mountains, large fjords and u-shaped valley landscape that exists in Hordaland today are largely impacted by the quaternary glaciations. The quaternary time period have lasted the past ca. 2.6 million years, and was characterized by variated climate with temperatures oscillating between ice-age conditions and relative mildness (Fredin et al., 2013).

The last ice age, Weichel (ca. 115 000-11 700 years ago), is from many points of view, the most important glaciation for the making of the land as it exists today (Mangerud, 1976). This is because this glaciation erased most of the traces from earlier ice ages and middle ice ages. By erosion, the ice has deepened pre-existing valleys, and weakness zones and fault zones have likely been exploited by the ice. Therefore, Sørfjorden to Odda and Veafjorden east for Osterøya both goes North south direction along the already existing fault. These valleys, weakness zones and fault zones are explicit for the reason for rock slope failures in Norway. The margin and the flow direction of the last glacial maximum (LGM) are shown in figure 3.

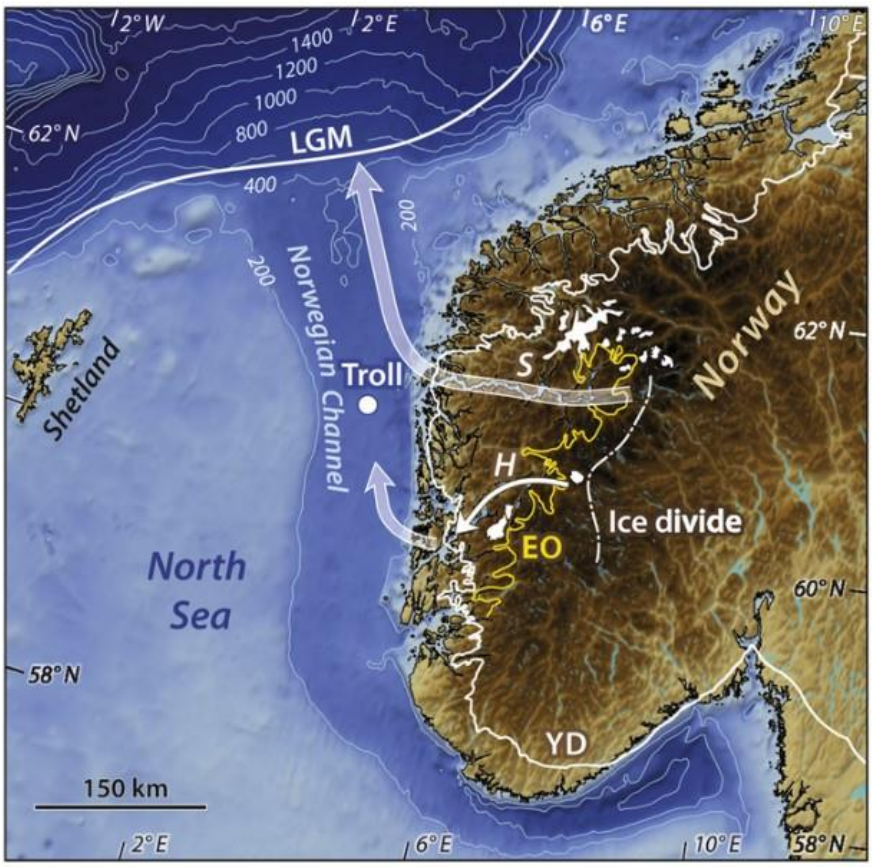

Figure 3 Shows the margin and the flow path of the ice in southern Norway at the Last Glacial Maximum (LGM). The thin white arrow shows the flow direction in Hardangerfjorden in Hordaland. The Younger dryas ice margin is marked with a thin white line while the Eidfjord-Osa (EO) moraine is marked with a yellow line (Mangerud et al., 2016)

Rock slope failures can be explained with the actions of quaternary geomorphological processes (Fredin et al., 2013). (1) The erosion of the landscape makes the relief large and the mountain sides steep. This causes increased overburden stresses in the rock mass. (2) The deglaciation of the landscape can lead to buttressing, stress recreation that can be built up in the rock mass during glaciation loading (Augustinus, 1992, Ballantyne, 2002). (3) Seismic activity in already susceptible areas, because of isostatic rebound after the melting of ice sheet, can trigger rock slope failure (Lagerbäck, 1990).

1.4.3 Modalen, an historic event in Hordaland

A known rock slope failure event in Hordaland happened on 14th of August 1953 in Modalen (figure 4). A block loosened from Storfjellet and dragged the masses in the slope with it. The masses had a granular flow motion just as rock avalanches, despite the other indication of a "steinskred" (section 2.1). In an early publication (Kolderup, 1955) it was reported that the deposited volume was multiple times larger than the failed volume, and the deposits reached further out of the slope than the frequent rock fall events. The event happened in the middle of the day, around the time 14.30. The masses travelled 200 meters over the cultivated land named Nedre Helland, had a width of ca. 200 meters and the masses height was 5-10 meters high. The rock slope failure event dammed the river that ran along with the slope. A result of both the avalanche itself and its secondary effect (damming of the creak) five of the six farms situated below the slope were affected (figure 5 and 6). It is not clear why this block set the scree in movement and propagated further out than the rest of the rock fall activity next to the failure. This event is one of the events that are mapped and analysed further in this thesis.

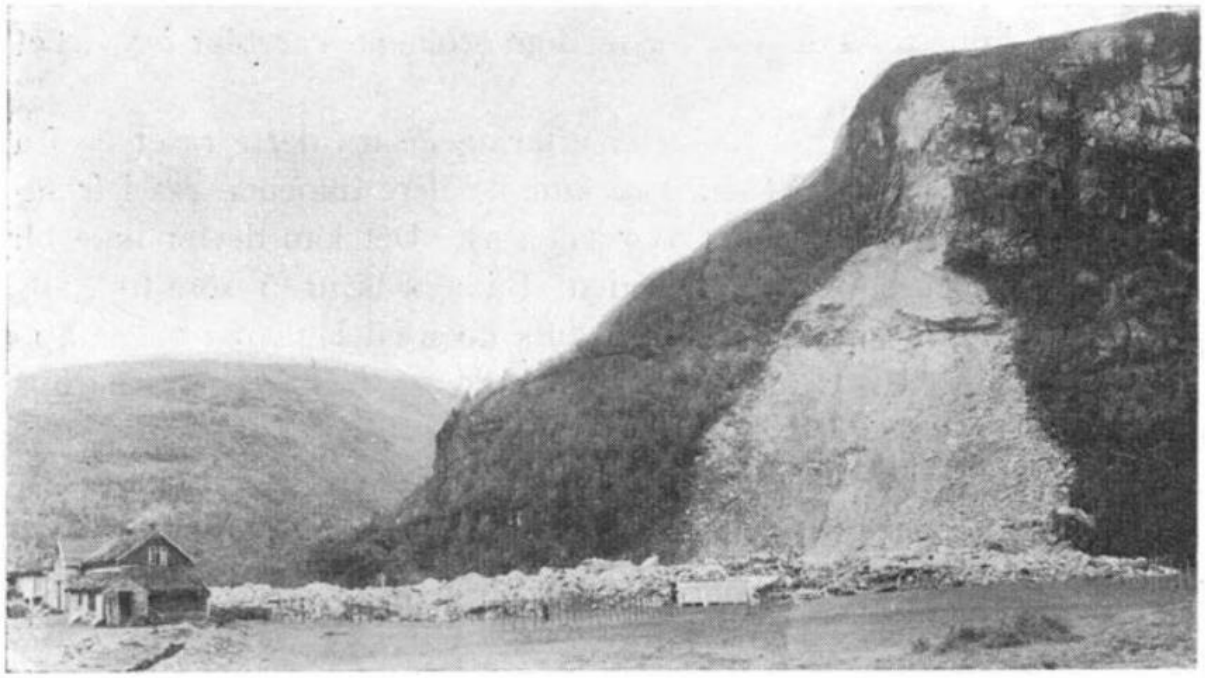

Figure 4 Overview picture of the event in Modalen (Kolderup, 1955)

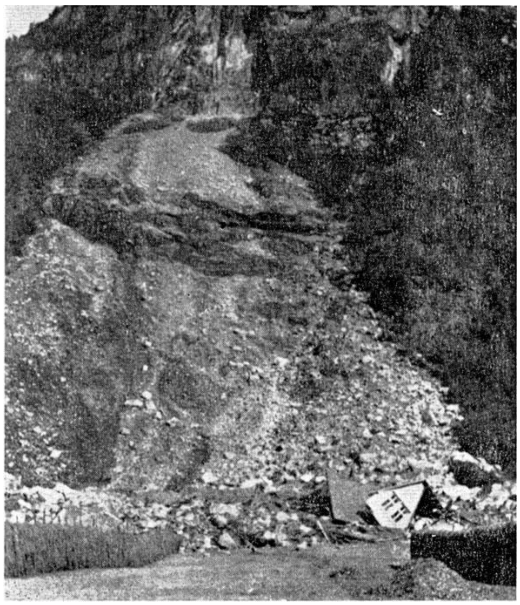

Figure 5 Picture of the distribution of the flowing masses down the slope. The picture is sent from Astor Furseth

Figure 6 The large impact of the event in Modalen and the destroyed houses. The picture is sent from Astor Furseth

2. Theory

As the flow-like motion event in Modalen and the database of landslides in Norway indicates, the needs of more knowledge of the controlling factors for runout length and how to handle and mitigate the hazard of the different RSF are important. The following sections introduces the landslide phenomena, landslide classification, the mechanics and its controlling factors, and the hazard mapping in Norway.

2.1 Landslides and landslide classification

Landslide is a complex phenomenon. Hermanns (2018) has defined landslide with the following definition:

> "A landslide is the gravitational downslope movement of solids on natural or artificial slopes. The solids are geotechnical materials that can contain water, ice, and air; however, the solids are volumetrically dominant over the transport medium (water, ice, and air)."

2.1.1 International classifications, Norwegian terminology and definitions of terms used in this thesis

To classify different types of landslides the Varnes classification system (Varnes, 1978) is, internationally, most commonly used. This classification is mainly based on movement type and landslide material. Hungr et al. (2014) has later updated the classification to correspond with geotechnical and geological terminology accepted for rocks and soils. The movement types are divided into fall, topple, sliding, spread, flow and slope deformation (figure 7) and the material is divided into rock and soil. In this thesis, only the rock material for the unstable mass prior to the failure are of interest and are summarized in table 2. Other types of materials can then be involved and incorporated from entrainments during the transport process until formation of the deposit.

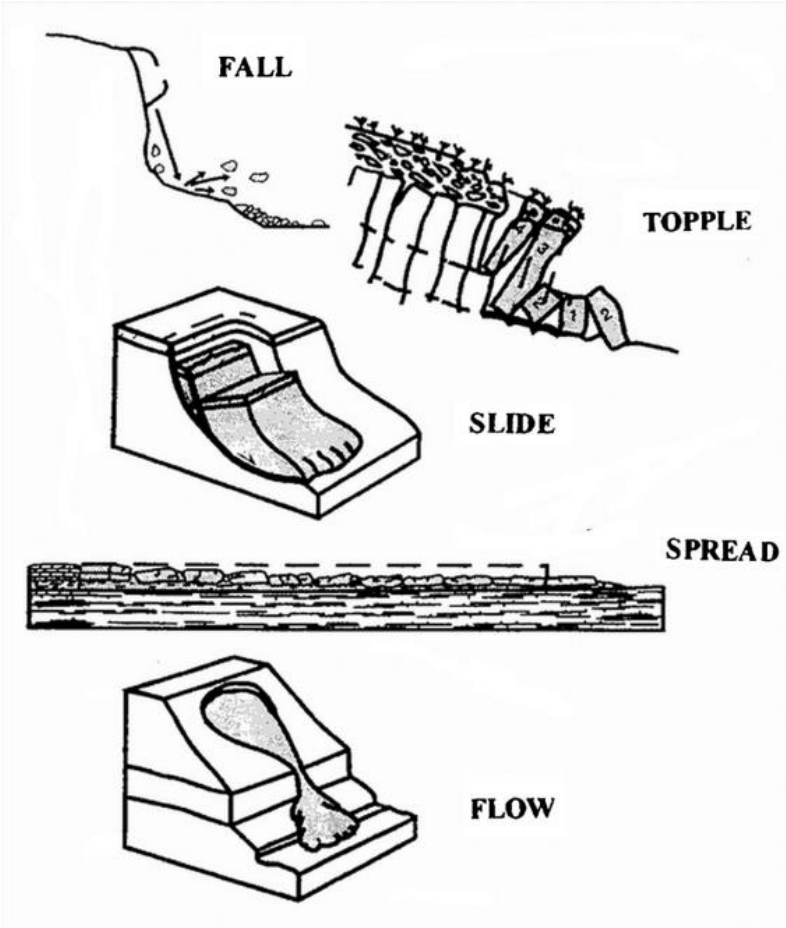

Figure 7 The different movement types of landslides. This is divided into fall, topple, slide, spread and flow (from Hungr et al. (2014), after Cruden and Varnes (1996))

Table 2 The updated classification of the movement type simplified with only the rock material. Modified after Hungr et al. (2014)

Type of movement	**Rock**
Fall	Rock fall
Topple	Rock block topple Rock flexural topple
Slide	Rock rotational slide Rock planar slide Rock wedge slide Rock compound slide Rock irregular slide
Spread	Rock slope spread
Flow	Rock avalanche
Slope deformation	Mountain slope deformation Rock slope deformation

In Norway, the terminology for rock slope failures is partly based on the volume of the falling masses (Devoli et al., 2011). It is divided into “steinsprang” (rock fall), “steinskred” (rock collapse) and “fjellskred” (rock avalanche). “Steinskred” is a Norwegian term and are not used internationally. The closest term will be rock collapse, which is discussed by (Hungr et al., 2014). Hungr et al. (2014) defined the term rock collapse as “sliding of a rock mass on an irregular rupture surface consisting of a number of randomly oriented joints, separated by segments of intact rock (“rock bridges)”. Since this classification does not have a term describing “steinskred” absolutely and this work is implemented for the Norwegian database, the term “steinskred” will be used in this thesis. For the Norwegian terms “fjellskred and “steinsprang” the international terms rock avalanche and rock fall will be used. The different terms are defined in table 3.

Table 3 Definitions of both the Norwegian landslide terms and the international terms in parenthesis together with umbrella term RSF

Term	Definition
"Steinsprang" (Rock fall)	Have a volume of typically 100 m^3. There is often an individual or few blocks that is mainly falling, bouncing and rolling down the hill with hardly any interaction of the blocks (Devoli et al., 2011), but strong mechanical interaction with the slope (Bourrier et al., 2013).
"Steinskred" (Rock collapse)	Currently, "steinskred is defined as events with volumes from 10 000 m^3 up to 100 000 m^3. In a "steinskred" the blocks interacts with each other and does often split up into smaller fragments (Devoli et al., 2011).
"Fjellskred" (Rock avalanche)	Volume range of 100 000 m^3 and up to millions of cubic meters. The masses crush down to smaller fragments, have high mobility, and can travel at high speed. (Devoli et al., 2011). Rock avalanches always have a flow type movement.
Rock slope failure event (RSF event)	In this thesis, an umbrella term for rock fall, "steinskred" and rock avalanches.

"Steinskred" is a failure type laying in between rock fall and rock avalanches. The line between "steinskred" and rock avalanches is overlapping, but in contrast to rock avalanches, "steinskred" have rather reduced interaction of blocks and do not develop a granular flow type behaviour (Devoli et al., 2011). Rock avalanches do always have a high interaction between the blocks leading to a granular flow behaviour (section 2.1.4) (Hungr, 1995) and excessive travel lengths, meaning an angle of reach < 31° (Nicoletti and Sorriso-Valvo, 1991) (section 2.1.5). The controlling factors for the runout length of "steinskred" are not well understood, hence the

need to better study them and their environment to clarify that line, in other words, to make it less blurry.

2.2 Rock slope failures (RSF)

2.2.1 The geomorphology of RSF events

The different parts of a RSF event are mainly divided into backscarp, source area, transport area and deposit area (figure 8). The source area, where the masses detach from, can in theory be steeper than 45° but occurs mainly in steeper slopes with a gradient of 60-70° (Braathen et al., 2004). The back scarp, which is visible after an event, show where the event has loosened from and makes it possible to estimate the fall height of the RSF. The masses will travel down the valley side, in the transport area, and often drag vegetation with it and leave a track left in the mountainside (NVE, 2014). When the slope is flattening, the masses will lose energy and deposit in the deposition area. This deposit area will often have a lobe form, and the largest blocks seams to go the furthest (NVE, 2014). The runout path for a RSF is defined from the highest part of the backscarp to the tip of the deposit. After many years, the transportation area often gets covered with vegetation, and the source area and the back scarp have eroded. Therefore, when detecting historical events, the deposit area is the part that are the most visible.

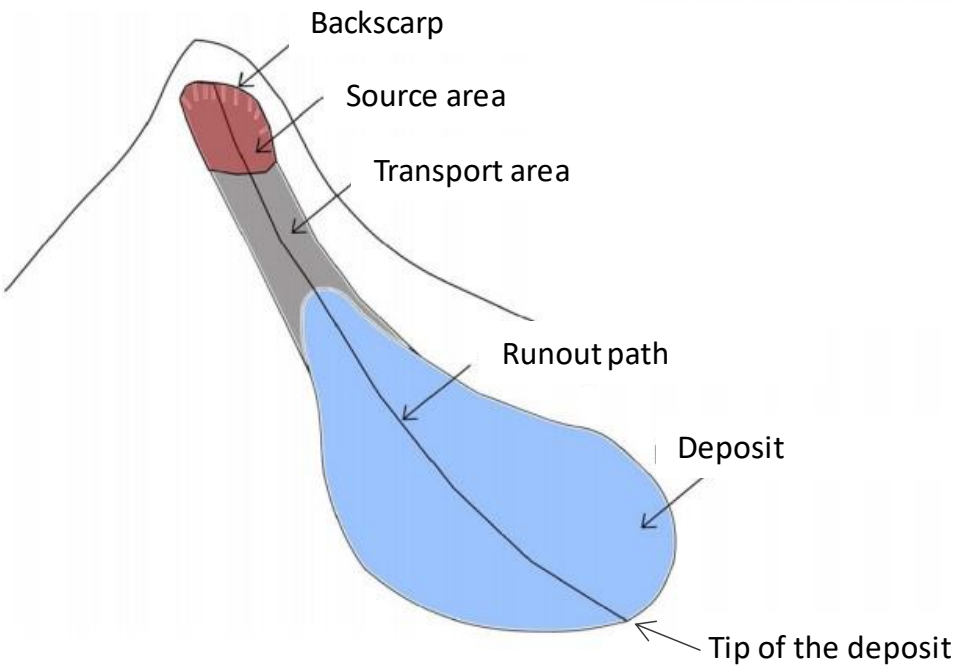

Figure 8 The geomorphology of RSF events modified by Mitchell et al. (2020a). The illustration summarizes the back scarp, source area, transport area, runout path, deposit and the tip of the deposits

2.2.2 Controlling of factors for RSF

RSF events are initiated when the driving forces overcome the shear strength of the rock mass (Braathen et al., 2004). In a slope the development of damage varies both spatially and temporally. Some parts of the slope are more disposed for pre-damage in term of water pressure, driving forces or pre-existing tectonic damage. The distribution of the damage are associated with variations in different factors, listed as by Stead and Eberhardt (2013):

- Slope topography
- Failure surface morphology
- Failure surface geometry
- Failure mechanism
- Lithological variations
- Geological structure

Factors that are affecting over time are seen to be:

- Tectonics - folds, faults, uplift, deformation phases
- Geologic processes associated with rock genesis (intrusion, metamorphism, alteration)
- Geomorphic processes – glacial erosion, glacial rebound, fluvial down cutting
- Earthquakes
- Precipitation and snowmelt events
- Long term creep

The climate and the geological history in Norway are important when it comes to factors affecting the triggering of a RSF in Norway (Braathen et al., 2004, Hermanns et al., 2017, Blikra et al., 2006). These factors include thawing of permafrost, frost activity and the processes resulting from the glaciation and the deglaciation. This is processes as oversteepening of the valley sides because of erosion from the glacier, exfoliation, and isostatic rebound (Ballantyne, 2002).

2.2.3 Mechanics of RSF events

After detaching, both rock fall and rock avalanches can change movement type along the runout path, but the two categories have different types of modes of motion.

The falling rocks in a rock fall travel down the mountain side in different modes of motion, divided into roll, bounce and fall (Dorren, 2003) (figure 9). Type of mode is depending on the slope gradient.

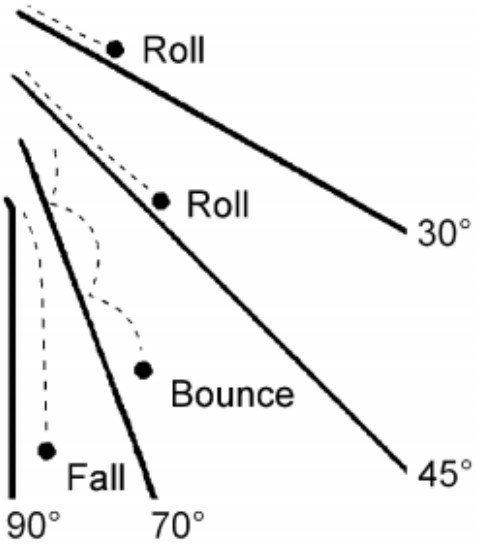

Figure 9 Illustration of the different modes of motion during a rock fall event (From Dorren (2003) after Ritchie (1963))

At slopes with an approximate gradient less than 45°, the rocks gather a rotational momentum and have a rolling motion down the slope. The rocks will often have continuous contact with the slope surface (Hungr and Evans, 1988). When the slope gets steeper, the rocks will starts bouncing down the slope. This transition between the rolling and bouncing, where the rock is in a combination of these modes, is the most economic displacement mechanism (Erismann, 1986). The rotation of the rocks occurs at a high speed, and only the edges with the largest radius are in contact with the slope. The center of gravity will move in an almost straight line. Freefall of the rocks will appear when the slope gradient is about 70°. In these cases, the center of the rock can move translational or rotational (Azzoni et al., 1995). In a rotational movement the rocks might change direction after impacting the slope and not go straight forward.

Rock avalanches are, unlike rock falls, known to have a flow like motion, a granular flow, and to usually have long runouts relative to the fall of height (Heim, 1932, Hsu, 1975). The controlling process of the motion are complex. In addition to changing during the avalanche's progress, the rheology can vary from one part of the avalanche to another (Hungr, 1995).

"Steinskred" is in between these two categories. Since "steinskred" is not yet well studied, the motion is also not clear. "Steinskred" have probably the chance to experience the modes likely for rock fall but also as rock avalanches, as seen in the event in Modalen.

2.2.4 Expressing the runout length for RSF and empirical models

There are different ways of expressing and calculating the runout length for RSF. One way of calculating the runout length is by empirical models. The empirical models are based on the topographical factors of rock fall events (Dorren, 2003). The modelling or calculation of the runout length for "steinskred" is limited, but several studies of the runout length for rock falls, and rock avalanches exist.

The fahrböschung (angle of reach)

A commonly used concept for expressing and predicting the runout length or the mobility of a RSF is the fahrböschung, also known as the energy line or angle of reach, α. The angle of reach was introduced by Heim (1932) and defines the angle of the line connecting the tip of the deposits and the back scarp of the source area of a landslide (figure 10). This is defined by the ratio of the fall height, H, and the vertical runout length, L.

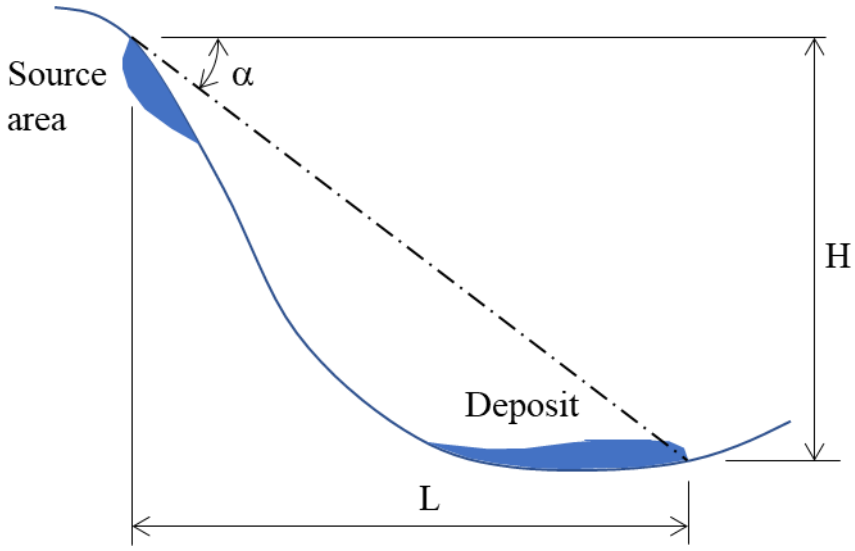

Figure 10 Simplified scheme illustrating the angle of reach in a RSF event, where H is the total fall height and the L, is the runout length. The angle of reach, α, is the angle of the line connecting the tip of the deposit and the back scarp

The shadow angle

Evans and Hungr (1993) suggested an alternative principle to predict runout length of rock fall events based on the shadow angle (figure 11), following Lied (1977). The shadow angle is represented by a straight line between the highest point of the talus slope to the tip of the deposits. Several studies (e.g. Evans and Hungr, 1993, Lied, 1977, Hungr and Evans, 1988) have tested the shadow angle principle and have found out that the angle for rock falls lie between 22° and 30°. According to Evans and Hungr (1993), who investigated 16 talus slopes, the shadow angle is preferable to the angle of reach. Note, both the angle of reach and the shadow angle is only a first approximation of the runout length of a rock fall event as many controlling factors can influence the runout length, like the terrain's geometry and roughness.

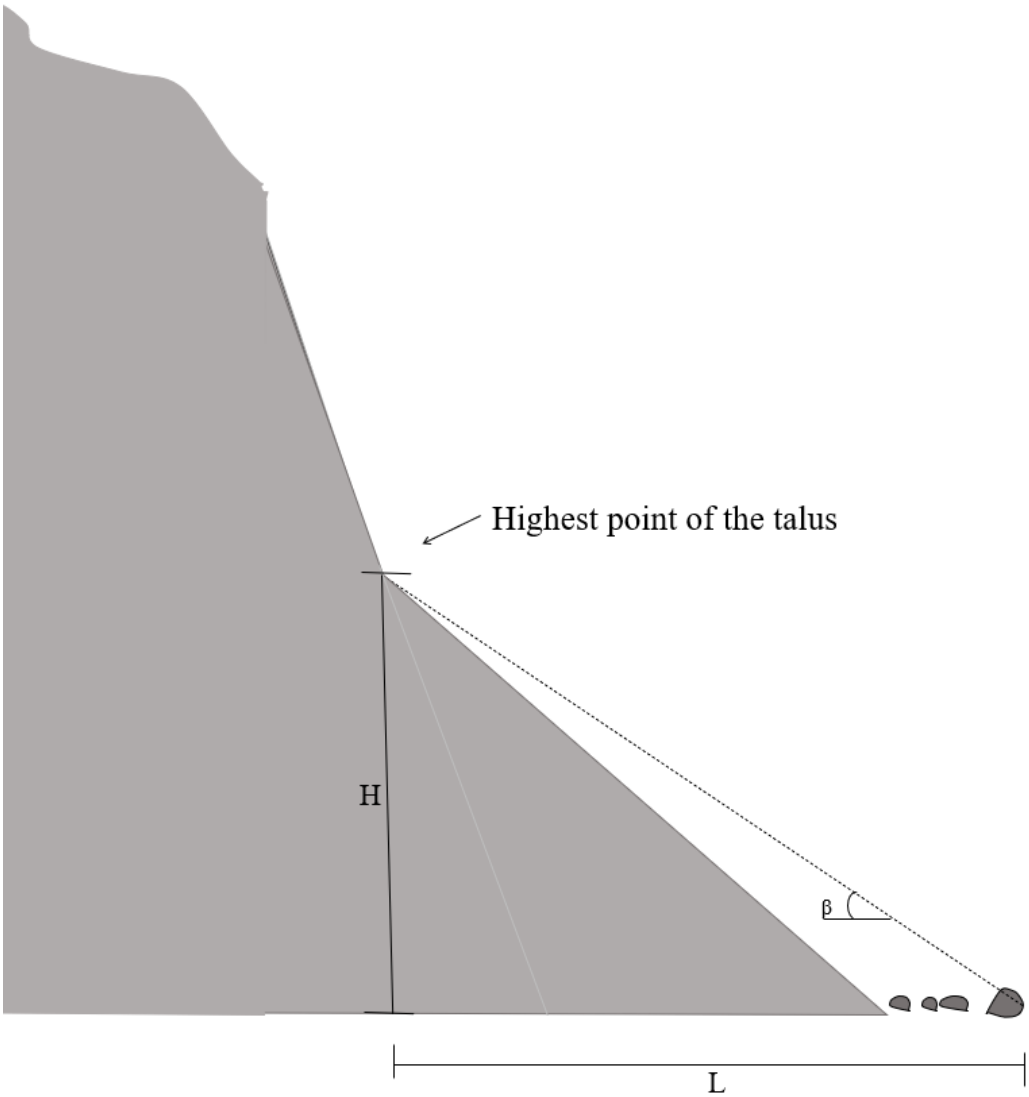

Figure 11 Illustration of the shadow angle, β. H is the height from the highest point of the talus to the height of the longest runout, and L, is defined as the length from the start of the talus to the end (longest runout). The β angle is the angle of the line connecting the tip of the talus to the highest point of the talus

The alpha-beta model

Since the geometry of the terrain can play a major role, some improved the previous mention methods by adding a correcting factor (beta) based on a simplified terrain geometry to get a better angle of reach. The alpha-beta model is an empirical model to predict the runout length of avalanches. This model was initially designed for snow avalanches, but Domaas (1994) adopted the method to rock falls. It makes a sort of bridge in between the angle of reach and the shadow angle, to include in a simplified way the effect of the geometry of the slope profile. The model is based on the relationship between the α-angle and the β-angle, and the runout for rock fall, as shown in equation 1 (Domaas, 1994):

$$\alpha = 0.77\beta + 3.9° \text{ [degrees]} \quad (1)$$

where β is the angle between the line stretching from point A (the point of release) to point B (where the slope angle θ_β =23°) and the line of the horizontal (figure 12). The α-angle is the angle of the line stretching from point A to the point C (expected runout), which is illustrating the expected runout length (Lied and Bakkehøi, 1980). This equation has a standard deviation of σ = 2.16°.

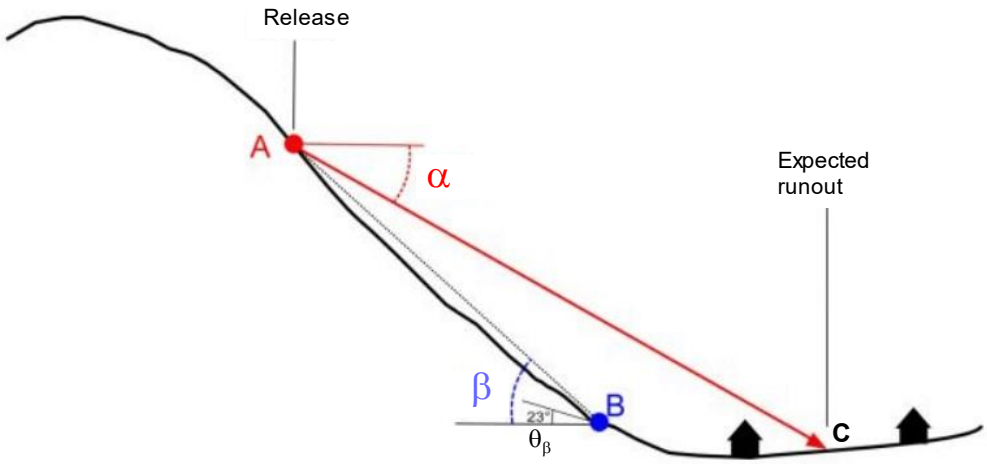

Figure 12 Illustration of geometrical principles of the α–β model for rock fall developed after Domaas (1994). Point A is the release point, the point B is where the slope angle θ_β= 23°. β–angle is the angle between the line AB and the line of the horizontal and alpha is the angle of the AC line, stretching from the release point to the maximum runout length

2.3 Controlling factors for the runout length of RSF

To perform hazard assessment, it is important to know the controlling factors for the runout length of RSF events, and how this differs for rock falls and granular flow avalanche behaviour. The controlling factors for the runout length are earlier studied by several authors.

2.3.1 Volume

Heim (1932) used the angle of reach, or Fahrböschung as Heim (1932) called it, to see if there was correlation between the angle of reach and the volume and found an inversely proportionality to the volume. Several authors (e.g. Scheidegger, 1973, Corominas, 1996, Velardi et al., 2020, Blikra et al., 2001, Hsu, 1975, Legros, 2002) have used the angle of reach in relationship with volume and have found that an increase in volume is statistically related to an increase in runout length (angle of reach). However, events with the same volume might still have largely varying travel lengths. Based on earlier world-wide rock avalanche events, Scheidegger (1973) has developed an empirical relationship between H/L and volume, V (equation 2):

$$\tan a = \frac{H}{L} = 10^{0.62419} \cdot V^{-0.15666} \qquad (2)$$

This empirical relationship forms the Scheidegger curve (figure 13), which can be used as a predictive tool. This is a best-fit curve for the 33 rock avalanche events in his study. This prediction can be utilized to forecast the reach of an imminent landslide if the volume can be estimated beforehand. Corominas (1996) has done studies with 47 rock falls and compared this to the Scheidegger curve. He concluded that a larger volume has a smaller angle of reach and when the volume is less than 250 000 m^3, the Scheidegger curve is of limited validity. In these cases, the angle of reach will, according to Corominas (1996), be about 31°. This is rather an envelope than a best-fit curves as the Scheidegger curve. Later there have been performed more studies with this Scheidegger curve by Blikra et al. (2001) and Velardi et al. (2020) who have compared with deposits of prehistoric, some historic, in Norway. They indicate that Norwegian RSF events have a higher angle of reach and have less mobility than the events Scheidegger (1973) analysed (figure 13).

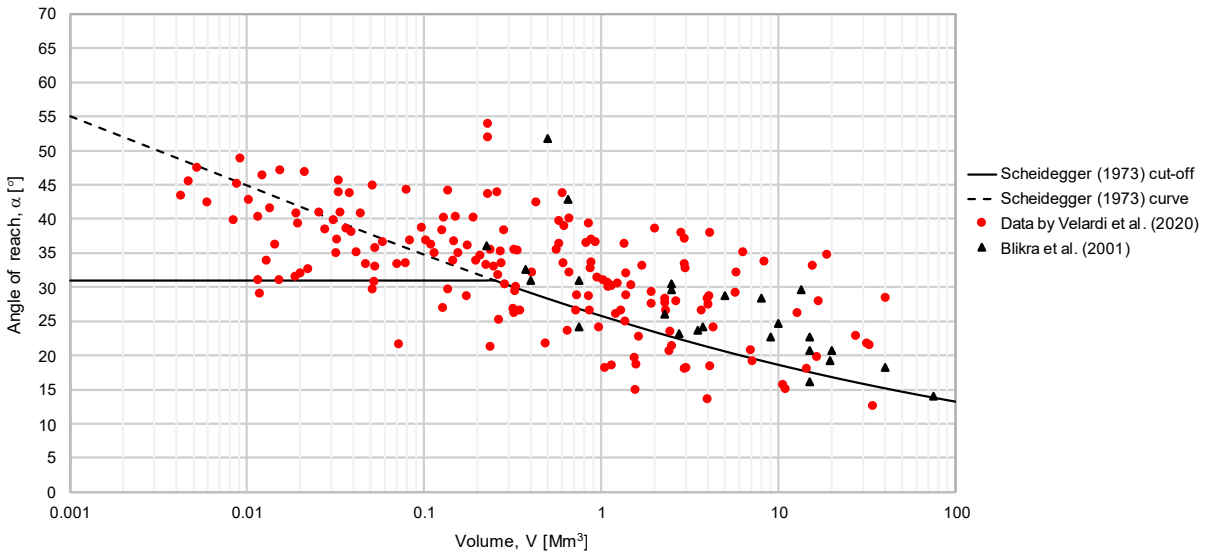

Figure 13 The data from both Blikra et al. (2001) and Velardi et al. (2020) compared with the Scheidegger cure (Scheidegger, 1973) and the cut-off of the Scheidegger curve at 31° according to Corominas (1996). These data indicate that Norwegian RSF events have a higher angle of reach and have less mobility than the world-wide events studied by Scheidegger (1973)

2.3.2 Fall height and steepness of the path

Several studies discuss if the mobility and the travel length of landslides are in relationship with, not only the volume, but also the fall height. Simple linear regression show that fall of height had a stronger correlation to travel length (Nicoletti and Sorriso-Valvo, 1991, Zhan et al., 2017) and that the runout distance are "highly sensitive" to the fall height, large fall heights leads to longer runouts (Mitchell et al., 2020a).

The fall of height is a result of the steepness of the path. The effects that the steepness of the path, or slope angle, has on the runout length have been analysed by both Crosta et al. (2017) and Velardi et al. (2020). Crosta et al. (2017) have studied granular flows and shown that a sharp slope break affects both the landslides' dynamics and runout length. The geometry of the break of slope causes a loss of momentum perpendicular to the basal layer, and smoothed slope break gives, therefore, longer runout. Velardi et al. (2020) concluded that the H/L for Norwegian failures increases linearly with events where the maximum slope angle are up to 45°, but no correlation with higher slope angles.

2.3.3 Local topography constraints

The runout length and the affected area of a rock avalanches are dependent on the morphology in the runout zone and the deposition zone. Nicoletti and Sorriso-Valvo (1991) have studied this and divided the morphology into three main groups; unobstructed, channelized and impacted against the opposite slope. These confinement conditions are also analysed by

Corominas (1996), Legros (2002), Mitchell et al. (2020a) and Velardi et al. (2020). All have concluded that the rock avalanches with channelized topography have the largest runout, while the rock avalanches that meet the opposite slope are less mobile. However, rock falls are more sensitive to obstacles and loses energy at every impact (Wyllie, 2014). In other words, a channelized path for rock fall will not necessarily make it go further on the contrary it loses the energy. But

2.3.4 Substrate and path material

In addition to the above-mentioned factors, also substrate affect the runout length for RSF events. For rock falls landing on colluvial material or bed rock the block will, because of the stiffness of the material, retain much of the energy. In contrast, blocks will lose the kinetic energy when interacting with soils which deforms when the blocks hits (Bozzolo and Pamini, 1986). Additionally, rock falls will have shorter runout lengths when interacting with wet loess soil material because of the damping of the boulder as they penetrate deeper and produces smaller rebounds (Vick et al., 2019). High roughness due to course material as scree however also reduces the runout lengths for rock falls.

Unlike rock falls, rock avalanches can develop long runout lengths when propagates over loose sediments that are saturated with water, also called liquifiable sediments (Hungr and Evans, 2004, Mitchell et al., 2020a). This might be due to rapid undrained loading of the saturated sediments with the impact of large masses (Sassa and hui Wang, 2005). Additionally, rock avalanches can potentially generate a mass flow composed of sediments from along the travel path leading to longer runout lengths and larger area of impact (Mitchell et al., 2020b). Long runout lengths are also seen with substrates of snow (Deline et al., 2011) and ice (Mitchell et al., 2020a, Velardi et al., 2020). Snow can have high saturation which leads to low strength basal layer of the substrate (Aaron and McDougall, 2019). This can also lead to higher velocities (Boultbee et al., 2006). Ice leads to small basal friction and the instantaneous melting of the ice substrate contribute to a reduction in the friction angle of the material (Sosio et al., 2012, De Blasio, 2014). For failures propagating over bedrock, the shear resistance between the bed rock and the overrunning rock masses is expected to be relatively high. This is due to the assumption that the shear resistance is in consistence with rock-on-rock sliding (Aaron and McDougall, 2019).

2.4 LiDAR as a remote sensing technique

Remote sensing techniques have made it possible to examine the earth's surface from a distance and require 3D information of the terrain with high accuracy and high spatial resolution (Jaboyedoff et al., 2012). In this project, LiDAR (Light detection ranging) and DEMs derived from LiDAR was used.

A LiDAR is an instrument sending out a laser beam towards, in this case, a slope and registers the backscattering of the pulses. This will make a point cloud of the topography and makes it possible to create a 3D model of the terrain with high resolution. The method is used to measure displacement and deformation in rock slopes. Additionally, it can be utilized to detect the source area of a RSF event, structural characterization, such as faults, fractures and joints. This detecting is possible because of the ability to "see through" vegetation. There are two different methods of LiDAR; airborne laser scan (ALS) and terrestrial laser scan (TLS), where the TLS gives the highest resolution (Jaboyedoff et al., 2012).

2.5 Norwegian hazard mapping for RSF

With the high hazard of RSF events (as seen in the NVE Atlas database and the new database by NGU (Velardi et al., 2020)), it is important to have good methodology for handling these types of natural hazards and reduce the risk for the infrastructure and the society. Therefore, in 2020, NVE developed new guidelines for avalanche assessment and safety evaluation in steep terrain (NVE, 2020). The goal for this guidance is "to give a method for hazard assessment and documentation of safety against landslides in steep terrain, which meets the requirements for safe building by the planning and building act (PPL) §28-1."(NVE, 2020). This will lead to more predictable results independent of who is doing the risk assessment.

In the mapping in Norway, there are established both susceptibility maps and hazard maps. The susceptibility maps are covering the whole country and show potential risk areas. This hazard is not stated with probability or how often this will occur but have different detail grades, depending on the methodology used. Data models makes these maps with the help of terrain data, which recognizes areas with the probability of hazard. In hazard maps, the probability of hazard is more investigated. This is done by field investigations, measurements and models. In these maps, the probability is stated by expressing yearly nominal probability (table 4) and divided the hazard into three classes. This is based on the consequence of an appearance of a RSF, including the secondary effects. This safety classification is following the planning and building act (TEK17 § 7-3).

Table 4 The safety classes for RSF events listed with the consequence and the yearly nominal probability of a failure event (TEK17 § 7-3)

Safety class for RSF events	**Consequence**	**Yearly nominal probability**
S1	Small	1/100
S2	Medium	1/1000
S3	Large	1/5000

Safety class S1 includes buildings with small consequences for personal safety and buildings where usually people do not stay. These will be buildings like a garage or a warehouse. Safety class S2 includes private houses, with less than 25 people staying. In this case the consequences are higher, and the yearly nominal probability has to be 1 per 1000 year. The last safety class, S3, applies for buildings like schools or hospitals where more than 25 people are gathered. These have the large consequence and have to be built outside the 1/5000 border.

3. Methods

The literature study showed that there is a blurry transition from rock fall behaviour to rock avalanche behaviour where methods to estimate the runout lengths based on volume or angle of reach struggles when the behaviour gets close to the definition of rock fall. To better understand this transition zone, a systematic mapping of all events in that volume range was carried on. The method used to perform this time expensive precise empirical data acquisition is first described in this section. It is followed by the description of each parameter documented from the mapped events that should help confronting existing runout prediction methods and better understand the main controlling factors of such events. Then, the method used to adapt the $\alpha-\beta$ model of "steinskred" is described, finally followed by the collecting field data from the granular flow event in Modalen.

3.1 The digital inventory mapping of Hordaland

The mapping of RSF deposits and the belonging source area of the events in Hordaland was done in the geographical information system ArcMap. ArcMap consist of several datasets and options which have been useful for determining the back scarps and the deposits:

- Download DEMs
- Hill shade map
- Aerial photo
- Topographic maps
- Draw polygons

In order to make sure that the entire area is covered in the analyses, the mapping was carried out systematically by looking at one smaller area at a time. In order to not jump over any areas, the mapped regions were marked. To obtain mapping of small events and not only the larger one the scale of the maps was shifted often. It was both looked at from a large scale to detect the larger rock avalanche events, but also at small scales like 1:10 000 to detect the smaller "steinskred" events. After detecting the event, the deposit was marked with a polygon and the backscarp were marked with a line. The detecting of the events was done by switching between the different types of maps, listed above. The hill shade map was obtained in ArcMap using one meter resolution Digital elevation models (DEMs). These were downloaded (August 2021) from Hoydedata.no, a website made by "Kartverket", and is a national collection of the height data in Norway. It was used multiple hill shade maps with different angles of azimuth, the suns

angular direction. The altitude, the suns angle above the horizon, was constant at 45°. The hill shade maps make it easier to detect the back scarp because of the shadowing in the slope. These maps also remove trees and houses from the map, making it easier to detect deposits in the landscape (figure 14). The downside with the removal is that when the blocks are large, they can be misinterpreted as houses and therefore removed from the map. This can affect the outline of the deposits and the calculation of the volume.

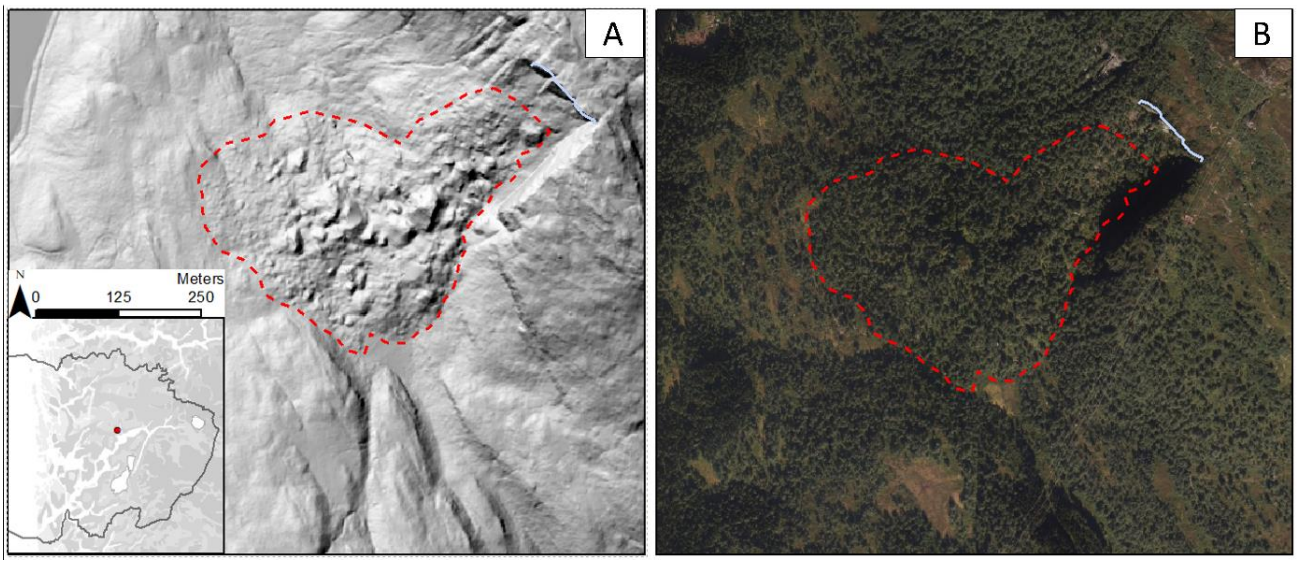

Figure 14 Illustration of the usefulness of the hill shade maps. Blocks in the terrain which are hidden by trees will be visible on the hill shade maps

"Skrednett.no" (last used 03.21) is the Norwegian database over different types of landslide events in Norway. This was used to look at the already existing registered events to ensure that the ones relevant in this database of NVE were included in the new database that includes systematic noting of the parameters for the events. The events registered in NVEs already existing database are events that caused damage or any other impact on society and consist of RSF events. The database exits of different types of landslides:

- Snow avalanche
- Debris flow/avalanche
- RSF events
- Landslides of clay
- Ice fall/avalanche

Events that have occurred in some distance to infrastructure are often not registered in this database. The registering in this database can be done by everyone. For each registered event and more details, the value of the database increases. Since everyone can add a new event, the quality and amount of detailed information of the registration vary. Therefore, not all the registered events were relevant to include in the new database, both because they were not large enough and because the deposits were not visible. In this work only the RSF events are of interest so the other types of landslides in the NVE database are sorted out of the map of the database in figure 15. Most of the mapped events in this thesis was not registered in the NVE database.

Figure 15 The rock fall events in Hordaland registered in the already exiting NVE database at "Skrednett.no"

The service "NorgeiBilder.no" was also a good tool to detect and determine the border of the deposits and decide the position of the related back scars. It has the possibility of looking at earlier orthophotos taken from the same place at different times (figure 16A and B) and look at 3D pictures of the landscape (figure 16C). This makes it possible to look at the evolution of the

sites which makes the marking of the deposits and the back scarp more certain (section 3.1.1). It is also possible to see if there are one or more events with the same source area. In some cases, pictures are taken before and after the failure, as shown in the example in figure 16. However, this data is of various coverage and resolution. For some areas pictures are available back to 1958 until 2020, while some places have only one or two pictures from the last couple of years. The 3D function was beneficial when determining both the deposits and the back scarp since the angle of view can be varied.

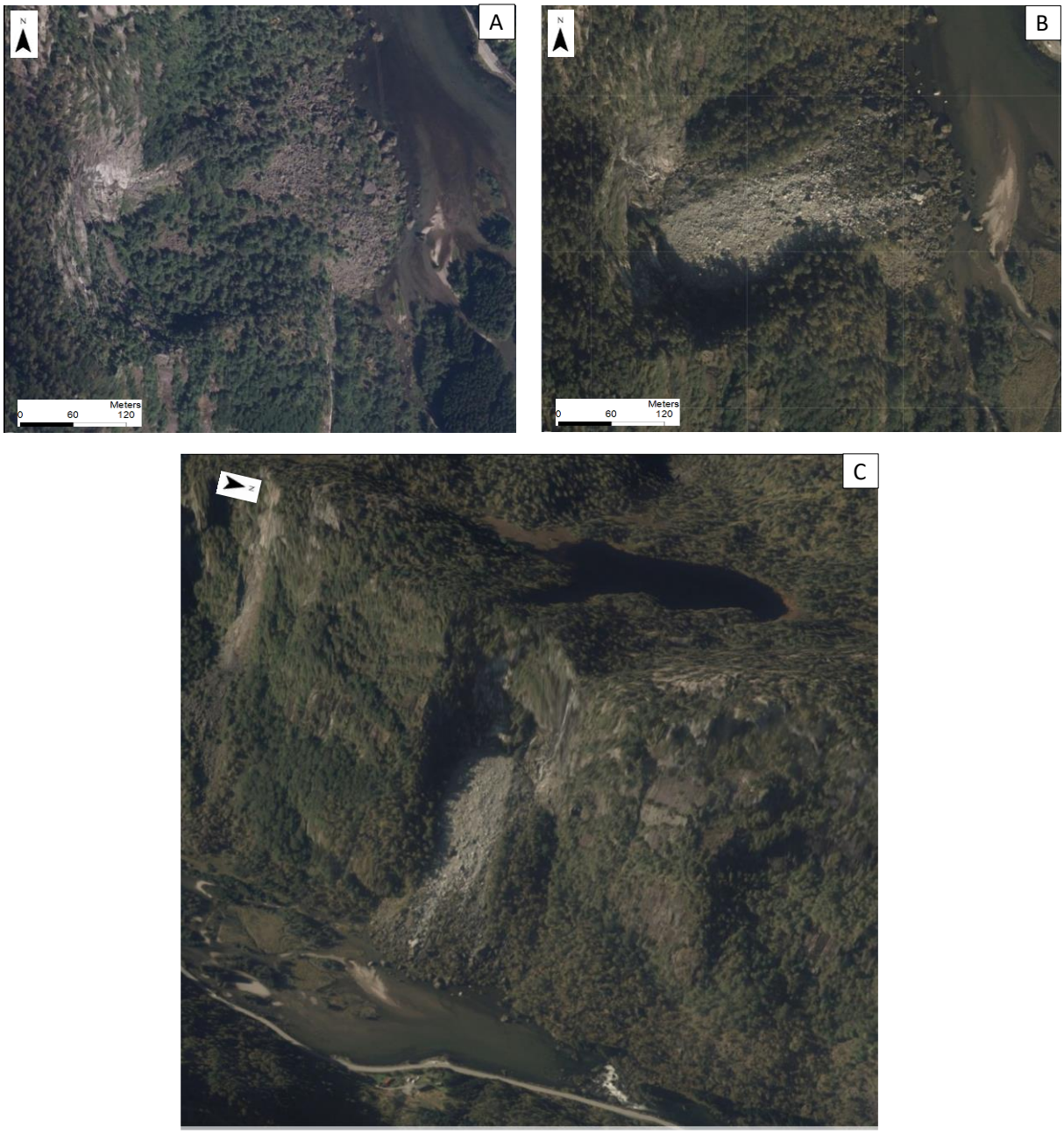

Figure 16 Pictures of a rock fall event located in Odda. A) picture before the failure, B) picture after the failure C) a 3D picture of the event taken from norgeibilder.no. This show the usefulness of picture taken from different times and how the 3D picture can be used to determine the borders for both the back scarp and the deposits

However, defining the borders for the deposits and the back scarp are often difficult because of the uncertainties of the primary morphologies of the events. Many of the RSF events are prehistoric, which leads to growth of vegetation at the deposit and erosion of the deposit and source area. When it is historic, the colors are often light and easy to detect, as seen in the example in figure 17. After erosion, the colors will be the same as the rest of the slope. A rock slope event can often be a result of several incidents at the same place and are difficult to separate if all events are old. The variation in the quality of the aerial photos affects the certainty when defining the borders, and in some photos, the deposits are covered by snow.

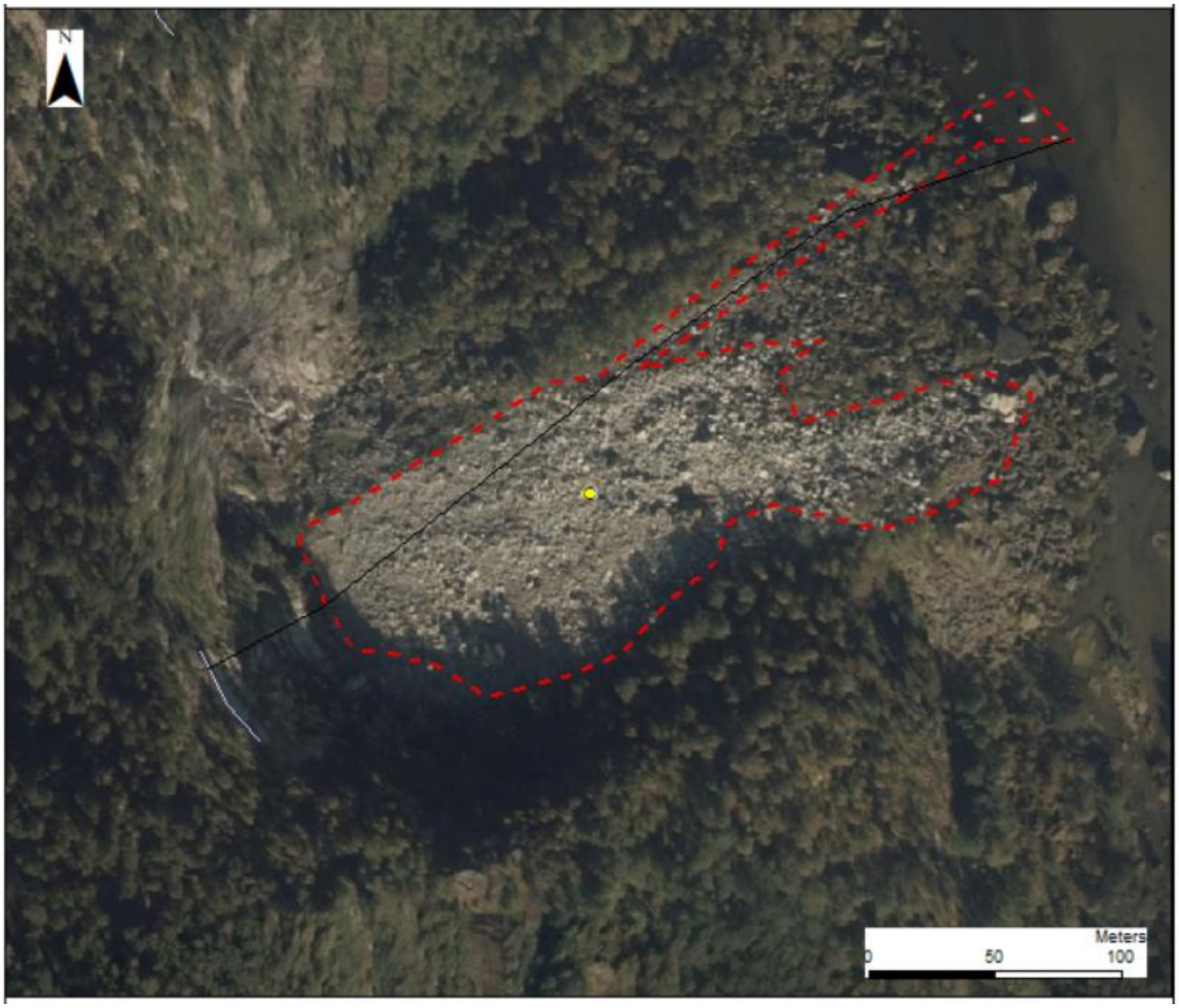

Figure 17 An example of how an event and how it is marked in the database. This is an event located in Odda. The deposits are outlined with a red dotted line, the back scarp is marked with a light blue line, the runout length is marked with a black line from the source area to the tip of the rock fall event. The yellow dot placed in the deposit contains an attribute with the parameters and information of the event

3.1.1 Certainty level of the mapped events

The events are categorized based on level of certainty when defining them. This is done to differentiate the quality of the data. The certainty level of the mapped events are, the same way as Velardi et al. (2020), categorized in four different categories:

- Certain: Events that are documented with data before and after the event or are well reported.
- Almost certain: Primary morphologies of the deposits are well-preserved, and the backscarp is visible on hill shade/DEM and orthophoto.
- Likely: The limits of the deposits and the backscarp location are quite certain, but the erosion of the deposits and back scarp have started.
- Uncertain: Mapping of the extension of the deposits and/or the location of the scarp areas are uncertain. Additionally, uncertainties related to the volume calculations or the calculation of the runout length.

Examples of the different level of certainty is shown in figures 18, 19, 20 and 21. Figure 18 show the Modalen event, which is categorized as certain. The back scarp and the deposits are clear on the hill shade map and on the pictures taken after the event. Additionally, the event is reported in an article published right after the event. Figure 19 show an example of an almost certain “steinskred” event. The deposit and the back scarp are visible on the hill shade map but are not as clear as in Modalen and has no pictures from before or right after the event. Figure 20 show the “steinskred” event in Sunndal which is categorized as likely and have landed on already existing deposit. The erosion of the back scarp has started, and the exact position is harder to tell than in the event in Kinsarvik. Figure 21 illustrates the last category, uncertain, with an event in Stølsheimen. The border of the deposit is not clear because of the river which have eroded the deposits and dragged parts of it down stream. This makes up uncertainties of the boundaries of the deposits and the volume calculations.

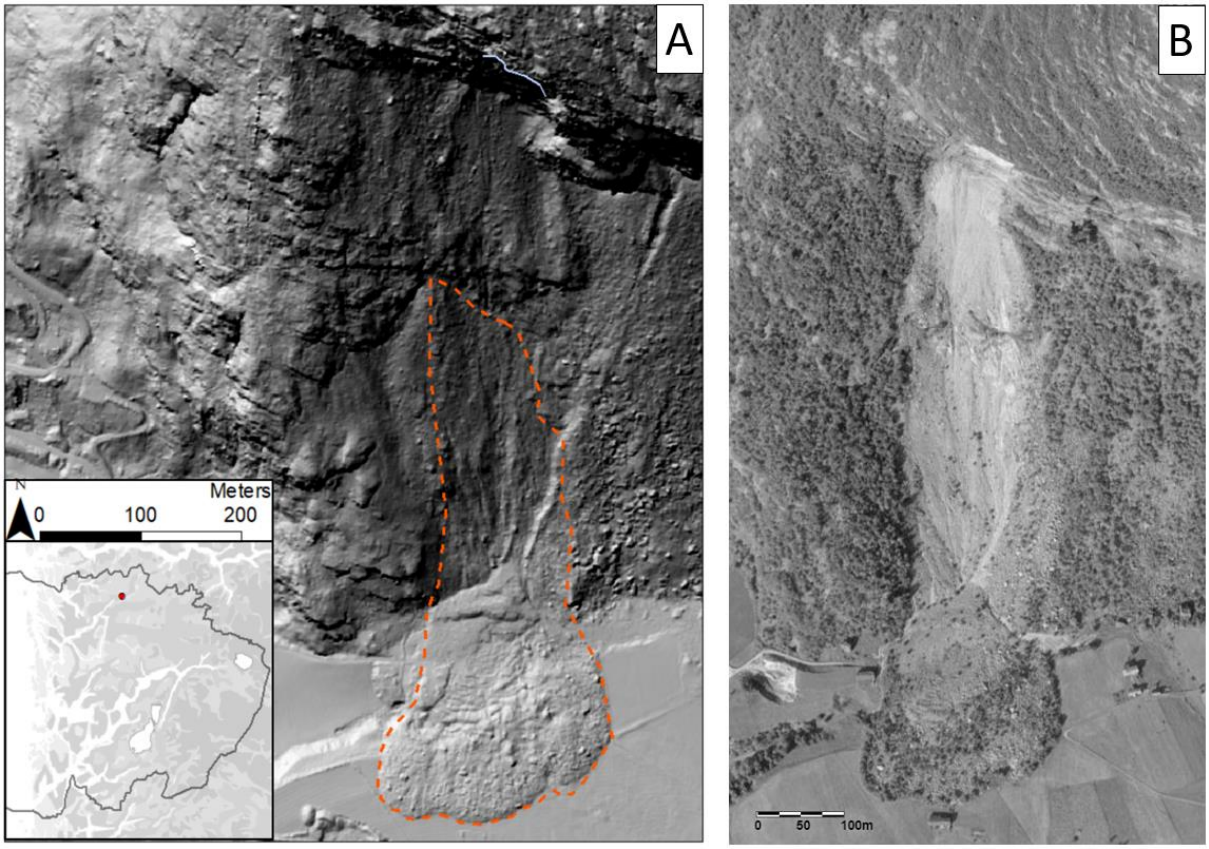

Figure 18 The rock fall event located in Modalen is classified as certain. The back scarp is marked with a light blue line and the deposits are outlined in a dotted orange line. (A)The deposits are visible on the hill shade maps (with resolution of 1 m). (B) Aerial photo (1965) taken 10 years after the event (Norgeibilder.no)

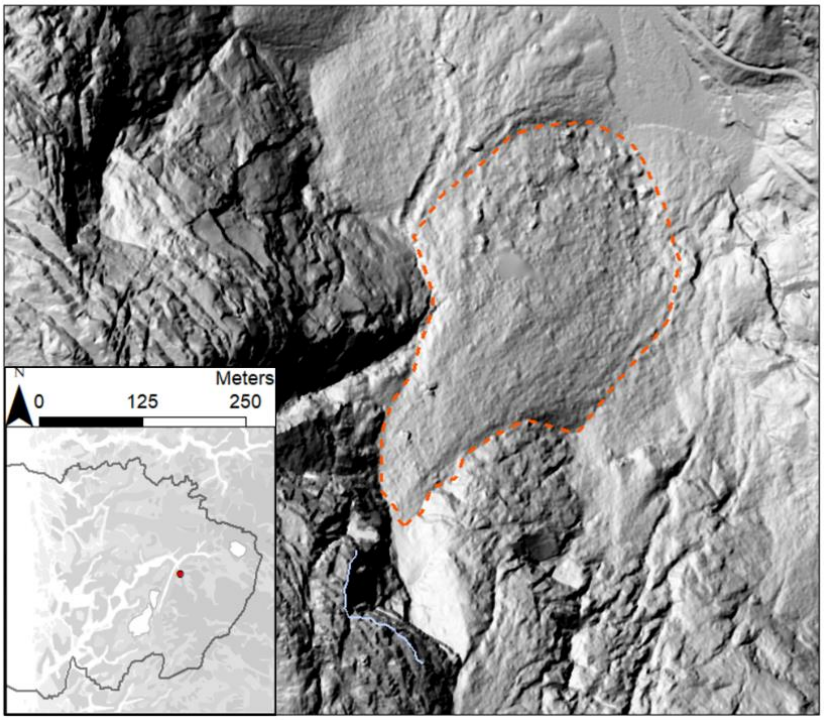

Figure 19 Rock fall event located in Kinsarvik is classified as almost certain. The back scarp is marked with a light blue line and the deposits are outlined in a dotted orange line

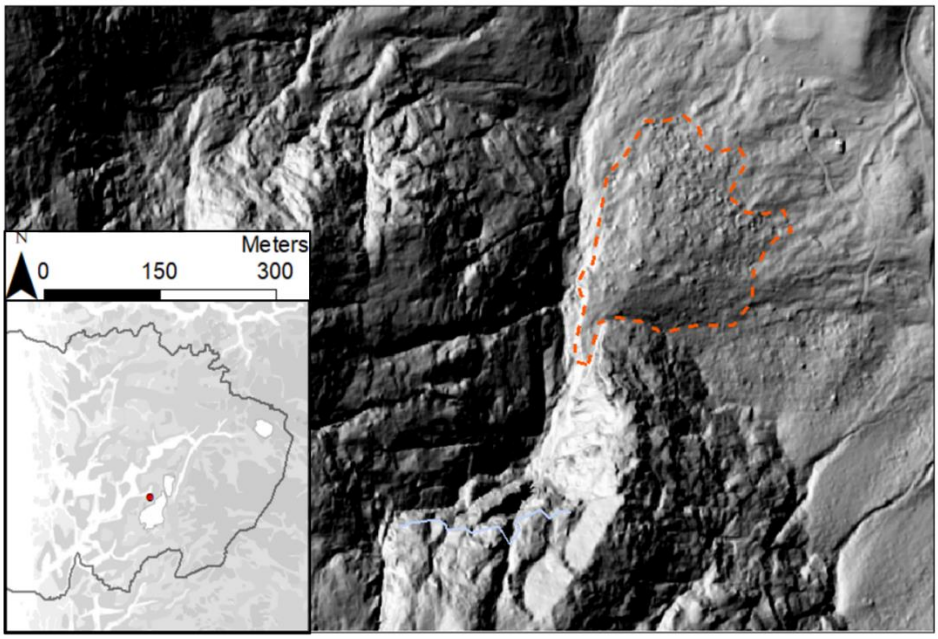

Figure 20 Rock fall event located in Sunndal is classified as likely. The deposit is outlined with an orange dotted line and the backscarp is marked with a light blue line

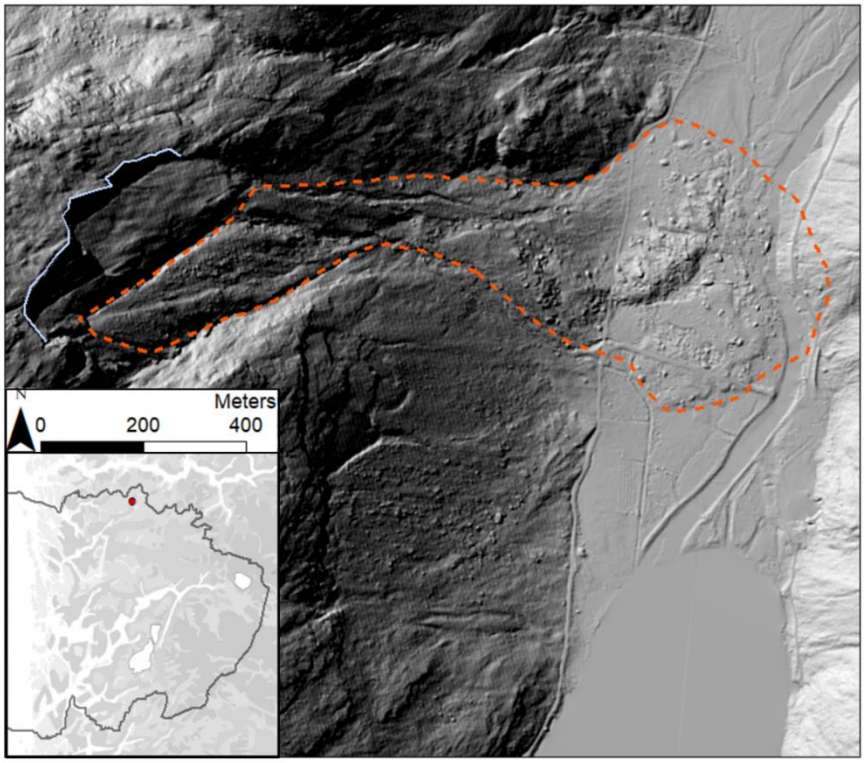

Figure 21 RSF event classified as uncertain, located in Stølsheimen. The deposit is outlined with an orange dotted line and the backscarp is marked with a light blue line

3.2 Information and the parameters in the database

For each site in the database, different parameters and information were measured and noted in the ArcMap database of NGU (Velardi et al., 2020): point ID, deposit ID, RSF event name (name of the nearest village or mountain), municipality, county, drop height (H), runout length (L), H/L, the angle of reach, confinement, propagation substrate and info about the deposits (max. thickness, average thickness, volume) (appendix A).

3.2.1 Estimation of the deposit volumes with the use of the SLBL tool

For each event, the deposit volume was calculated using the method Slope Local Base Level (SLBL). This method was developed by Jaboyedoff et al. (2004) and is based on the "base-level"-concept by Strahler and Strahler (2013). "Base level" is the lowest level a stream can erode. A further development done by NGU is used in this thesis. This tool uses a DEM to create a secondary curve for the surface prior to the deposition of the deposits (Jaboyedoff and Derron, 2005).

The input data are the DEM and the polygon for the deposits. The DEM are in a resolution of 10 m. A higher resolution is more time consuming for computation, and according to Velardi et al. (2020) the implementation with 1 m and 10 m resolution gave the same quality of results. The tolerance for the events was either chosen to be 0 or 0.1. For wide valleys and gentle dipping slopes, the tolerance was set to 0. The modelling will then make a flat underlying contact to the substrate. To make a more curved underlying to the substrate, as needed in narrow steep-sided valleys, the tolerance was set to 0.1. The method uses four neighbors and takes the average of these values, leading to a smooth surface. Max. thickness of the deposits was set to 100 000 m to make sure that the correct depth would be measured. When this depth is reached in a cell, the computation stops. If this is set to be too low, the computation will stop at too low depth. The tool also has the "not deepening" option which makes the minimum altitude in the SLBL area to be limited by the lower value of the bordering cell.

The calculated volume results when using the SLBL are produced by calculating the height difference between the topography and the created surface prior to the failure, multiplied by the area. The method is relatively new and has not been much tested. The volume calculations are based on the definition of the deposits and do not account for the possibility that the estimated deposit might come from several events.

3.2.2 Definition and estimation of the drop height, runout length and angle of reach

The drop height (H) is defined as the height difference from the top of the source area to the lowest part of the deposits. Some of the events have deposits that travels up the opposite slope. In these cases, the height will be measured from the valley bottom and not the tip of the deposits. The runout length (L) is defined as the maximal horizontal distance between the top of the source area (back scarp) and the tip of the deposits (figure 22). This parameter is measured approximately 90 degrees on the isolines, determining the travel path. The angle of reach, α, is estimated by the arctangent of the ratio of the fall height and the runout length (see equation 3).

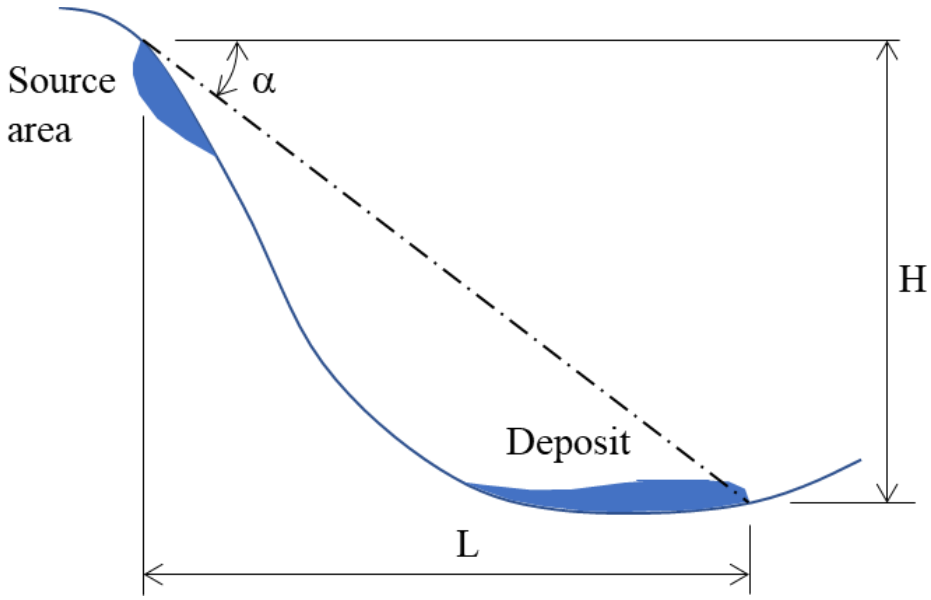

Figure 22 Scheme of a RSF event with runout length (L), fall height (H) and the angle of reach (α)

$$\alpha = tan^{-1}\left(\frac{H}{L}\right) \cdot \frac{\pi}{180} \quad \text{[degrees]} \tag{3}$$

3.2.3 Estimation of the maximum slope angle

The maximum slope angle is estimated for all the events to compare this to the runout length. This is done by calculating the angle of the steepest part of the slope (see equation 4)

$$\theta = tan^{-1}\left(\frac{h}{l}\right) \cdot \frac{\pi}{180} \quad \text{[degrees]} \tag{4}$$

The height (h) and the length (l) of the steepest part of the slope were calculated differently, depending on the slope profile geometry (figure 23). In RSF events where the runout path was straight, the maximum angle is equal to the mean slope angle, and they were measured between the back scarp and the tip of the deposits. In cases where the runout path is straight, but the deposits have travelled beyond the slopes nick point, the angle is not estimated from the back scarp to the tip of the deposits but rather from the back scarp to the nick point of the slope. Some of the RSF events have parts of the slope with a fall or bouncing area. In these cases, the max. slope angle was estimated at the steepest segment. This method does not tell how large the area of maximum slope angle represents. In some places, it covers the entire slope, and in other events, it will only represent a smaller part of the slope.

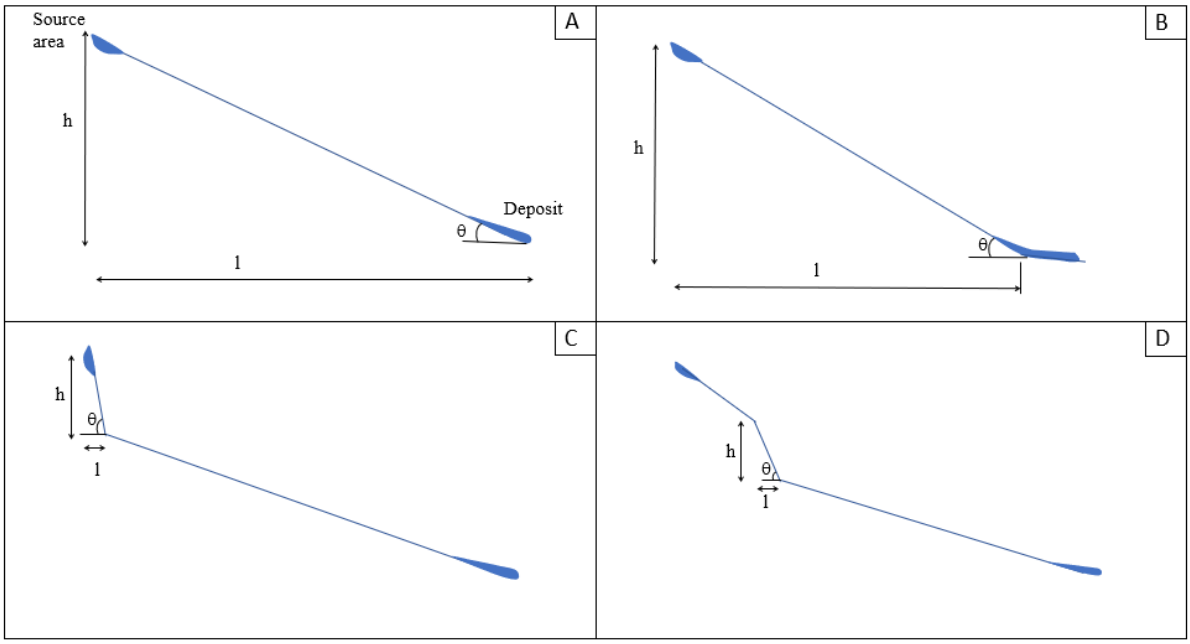

Figure 23 Illustration of a RSF event and belonging maximum slope angle (θ), height (h) and length (l) of the steepest part of the slope. Four cases are shown to illustrate how the calculation of the maximum slope angle is done: A) event with a straight runout path, B) event where the deposits have travelled further out than the slopes nick point, C) the steepest part of the slope is in the beginning of the runout path and D) the slope consist of different parts with different angles

3.2.4 Defining the slope profile geometry

The runout length for RSF events is empirically estimated using the alpha-beta method (Domaas, 1994), the shadow angle (Evans and Hungr, 1993) and the angle of reach (Heim, 1932) (section 2.1.5). Because the trend in published data shows a large variation in the data when comparing the relationship between the angle of reach and volume, several valuations have been tested for “steinskred” to look deeper into developing of a new empirical runout assessment.

None of the existing methods represents the entire slope profile geometry well and is the reason for investigateing this further in this thesis. The slope profile geometry has become easy to evaluate because of the high resolution DEMs and tools such as ArcGIS. This evaluation is done based on graphs put into Excel using the X (length) and Z (height) values for each site showing the slope profile. The categories of the slope profile geometry are divided into straight, large fall/bouncing area and small fall/bouncing area (figure 24). The specific difference between small and large fall/bouncing areas is that "small fall/bouncing area"-event is defined as the event with a fall/bouncing area covering 1/3 of the total fall height, while the "large fall/bouncing area"-events is defined as the event with a fall/bouncing area that is larger than 1/3 of the total fall height. Examples of the different categories are shown in figure 25, 26 and 27.

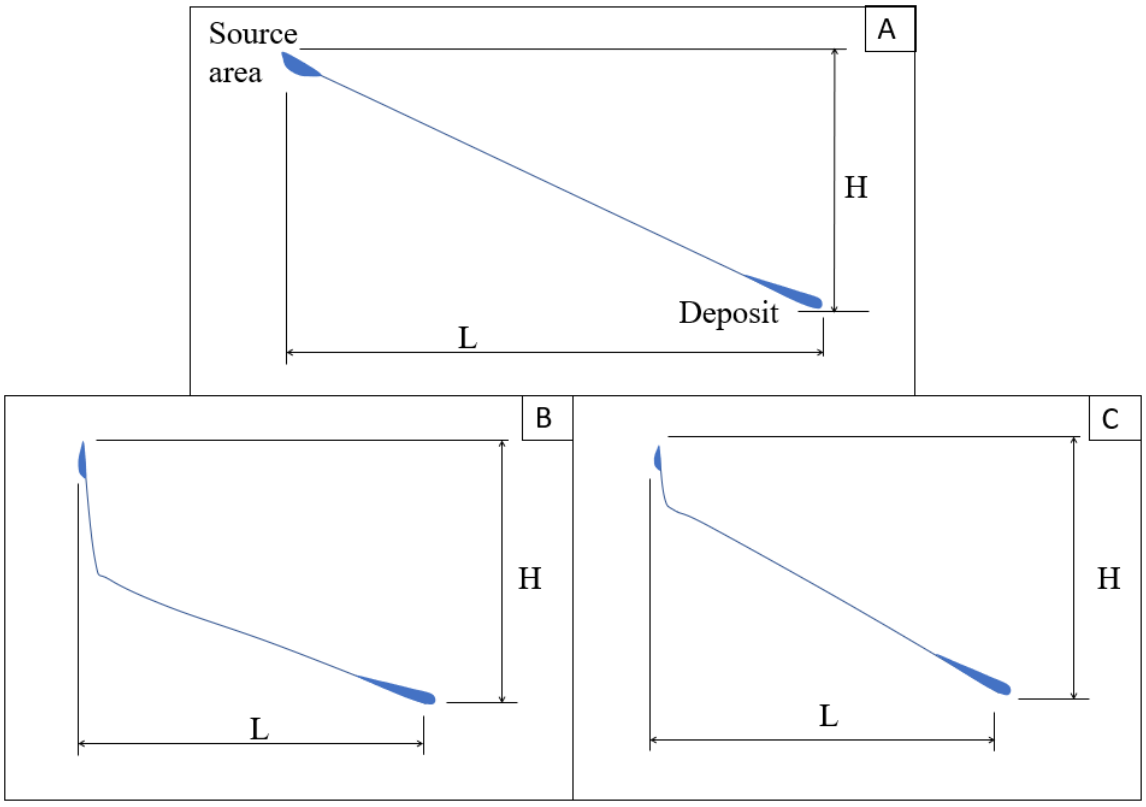

Figure 24 Simplified schemes of rock fall failures, the fall height (H), travel length (L) for the three different classifications of the slope profile geometry. A) the deposit has a straight travel path, B) the deposits have a large fall/bouncing area (>1/3 of the fall height) and C) the deposit has a small fall/bouncing area (< 1/3 of the fall height)

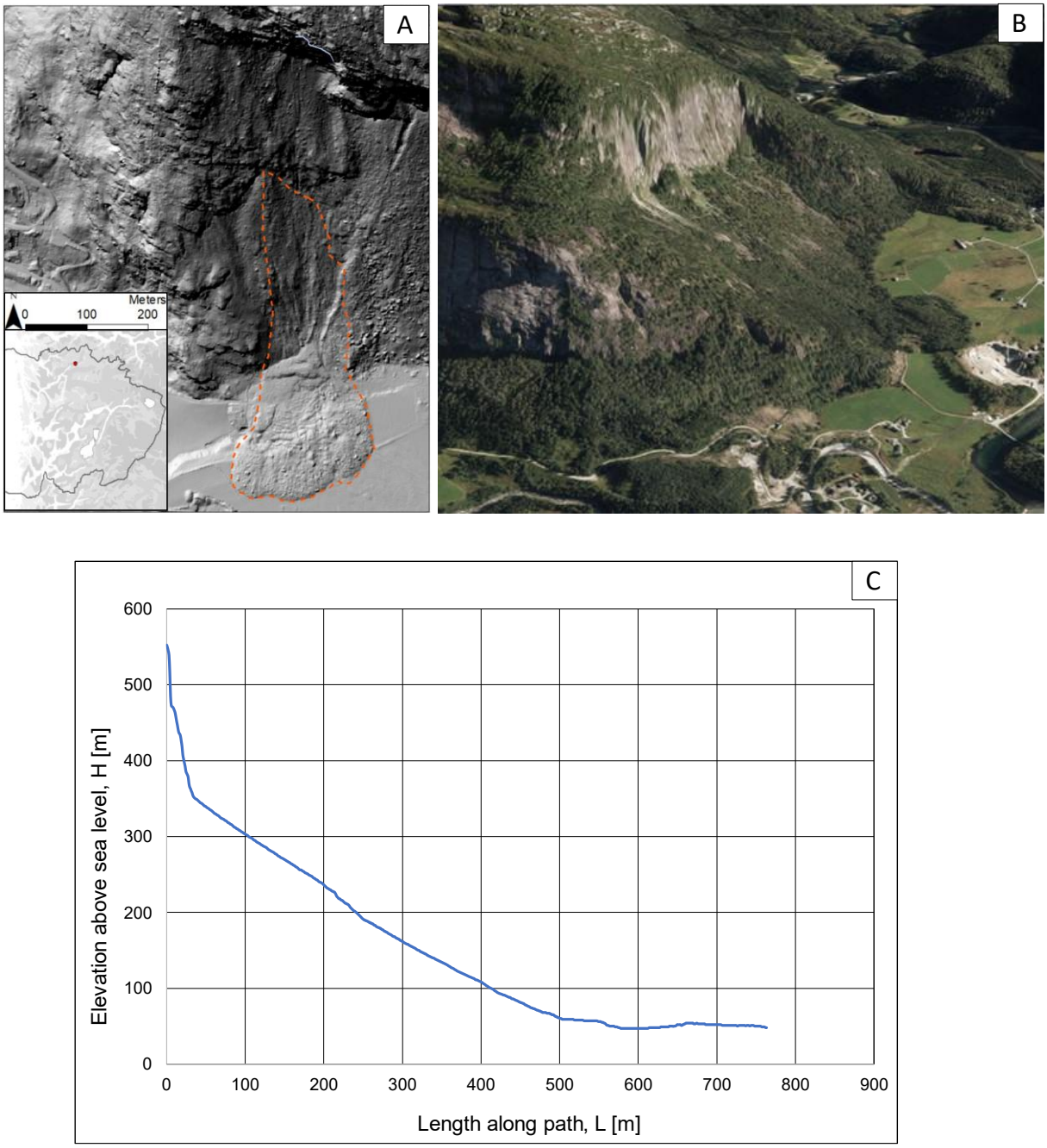

Figure 25 Example where the slope profile geometry has a large fall/bouncing area is taken from Modalen. A) Overview of the event with a red dotted line illustrating the border of the deposits and a light blue line marking the back scar, B) a 3D view of the site and C) the height profile of the slope

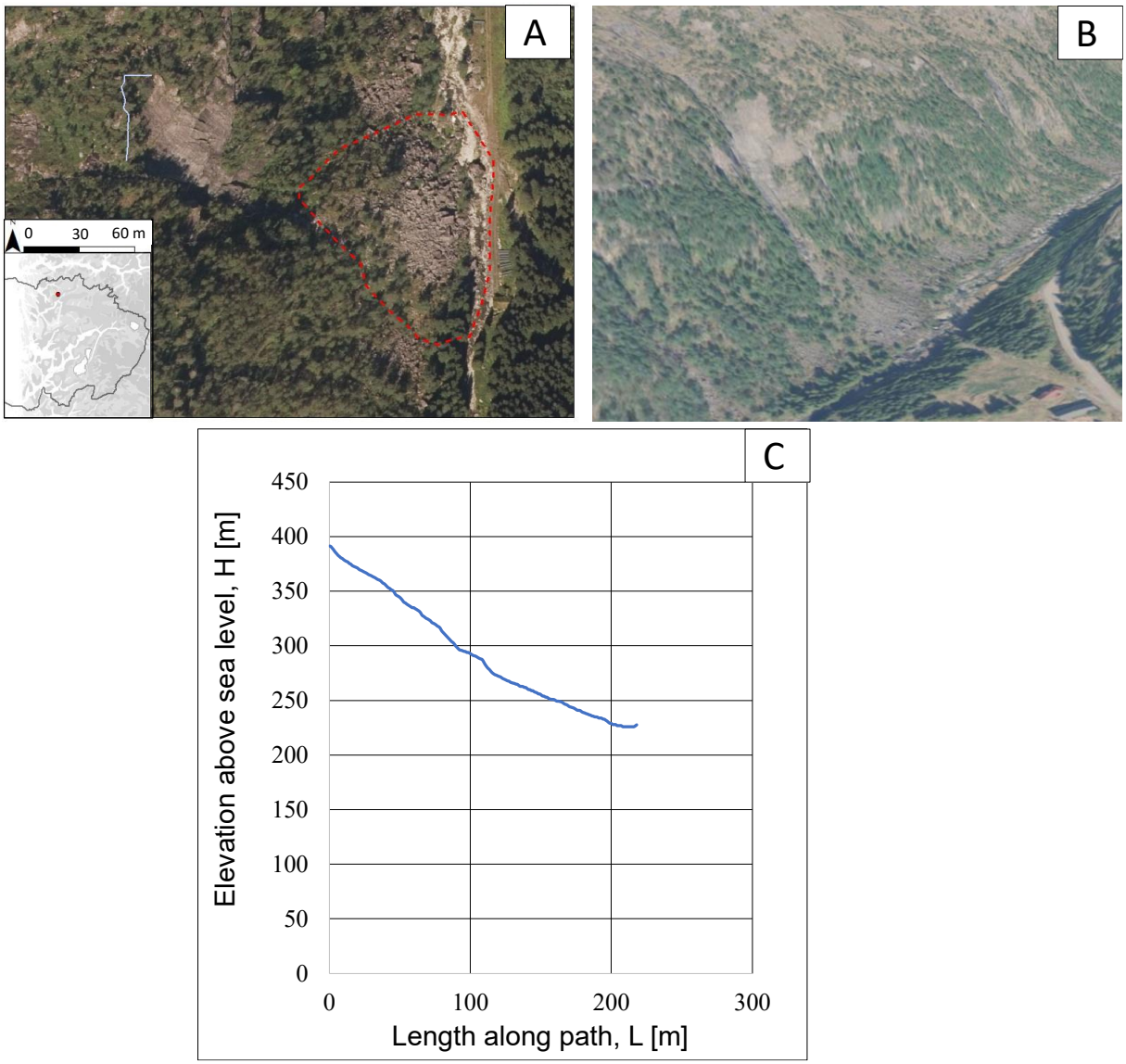

Figure 26 Example with a straight slope profile geometry. A) Overview of the event with a red dotted line illustrating the border of the deposits and a light blue line marking the back scar, B) a 3D view of the site, and C) the height profile of the slope

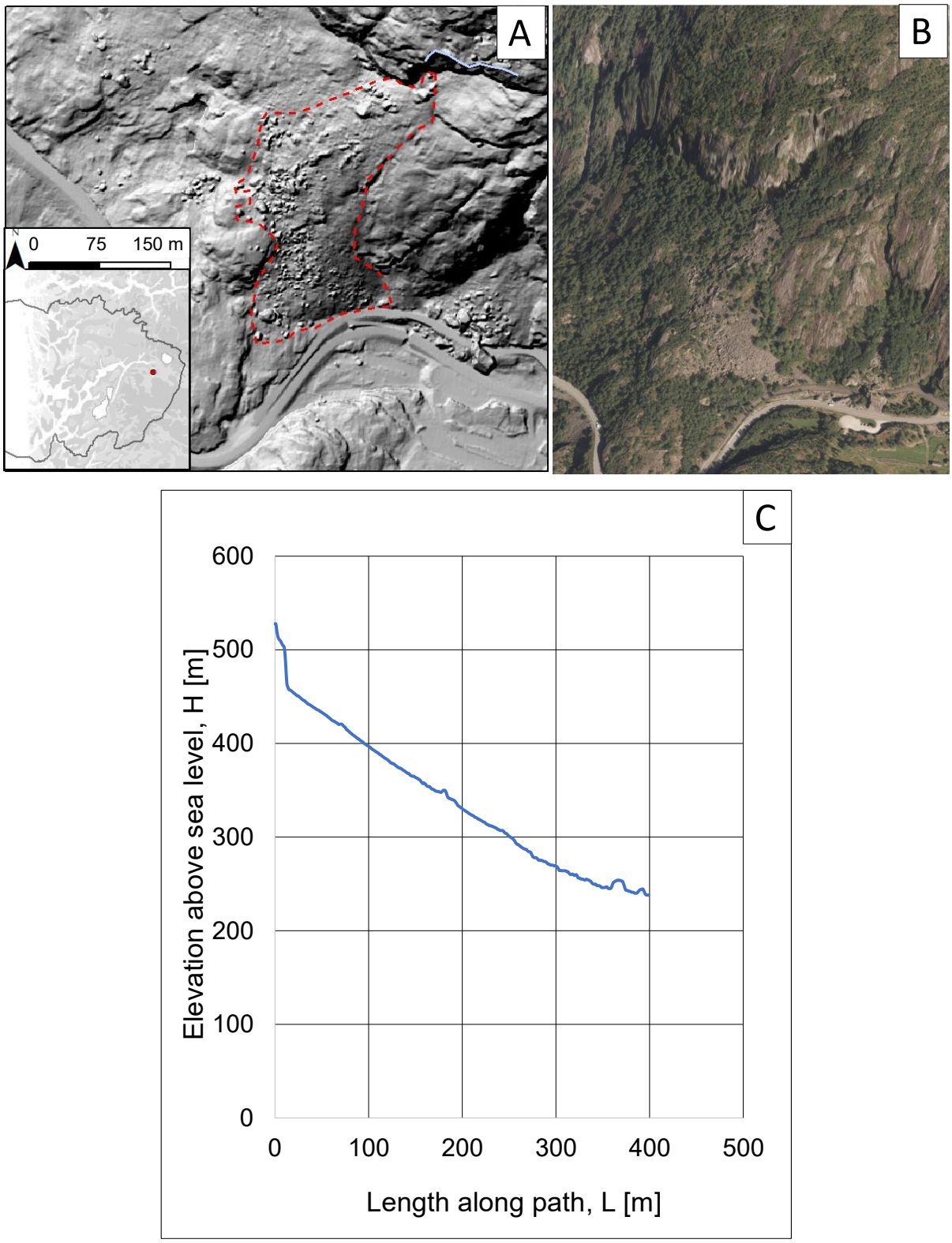

Figure 27 Example where the slope profile geometry has a small fall/bouncing area. A) Overview of the event with a red dotted line illustrating the border of the deposits and a light blue line marking the back scar. B) a 3D view of the site, and C) the height profile of the slope

Area under the graph

To further invetigate the geometry and how the slope morhology effects the runout length, the "normalized area" is estimated and compared with the angle of the energy line (corresponding to angle og reach) (section 2.1.5). The normalized area is defined as the area between the energy line and the profile of the graph. The normalized area is illustarted in figure 28.

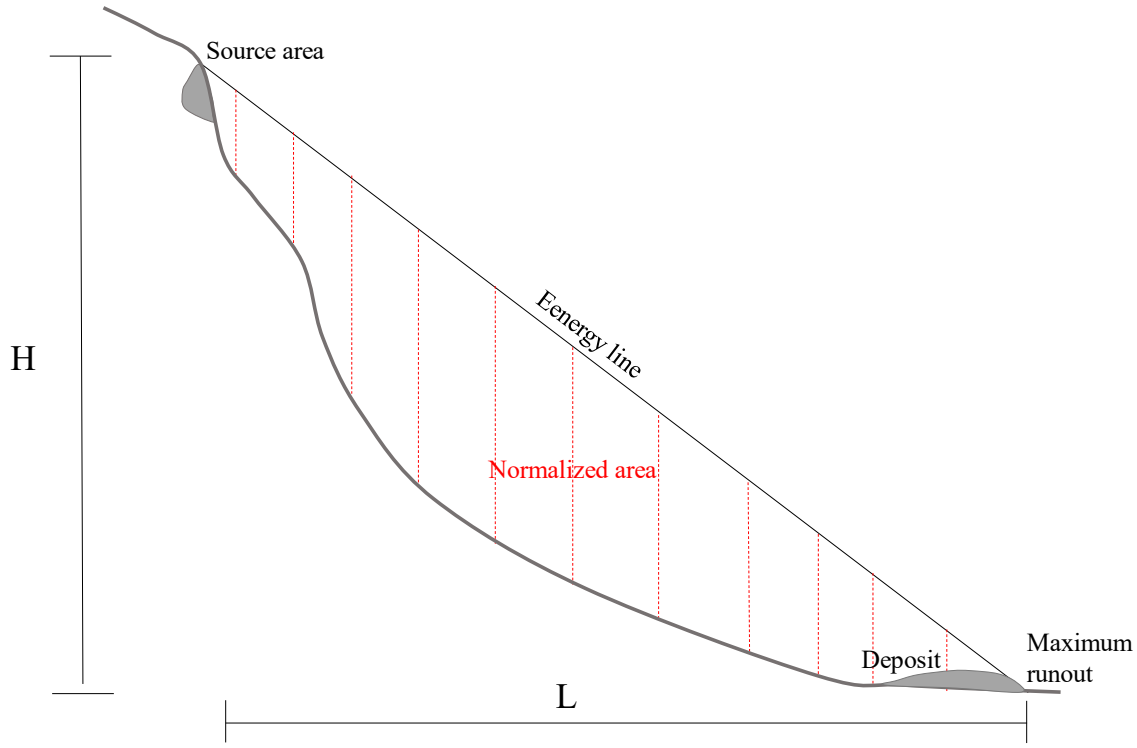

Figure 28 Simplified scheme of a rock slope event with belonging energy line and normalized area. The H is the total fall height, and the L is the vertical runout length

3.2.5 Determining the topographical constraints

The runout zone morphology was defined using a topographic map, orthophotos and hill shade maps. The morphology is divided into three categories: channelized, open slope and opposing the opposite valley wall (figure 29). This categorization is a continuation of Velardi et al. (2020), which is based on Corominas (1996) and Nicoletti and Sorriso-Valvo (1991). Examples of the different categories are illustrated in figure 30, 31 and 32.

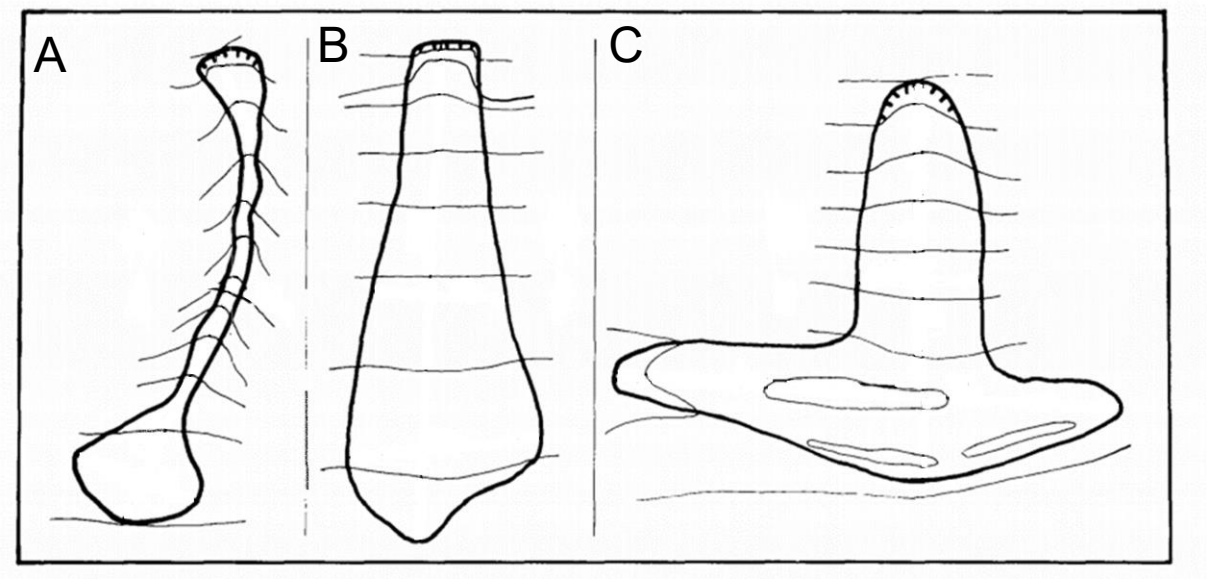

Figure 29 Illustrates of the different topographical constraints. A) illustrates a channelized confinement, B) illustrate an unobstructed event and C) illustration of an event with the obstruction of travelling up the opposing valley wall. Modified by Nicoletti and Sorriso-Valvo (1991)

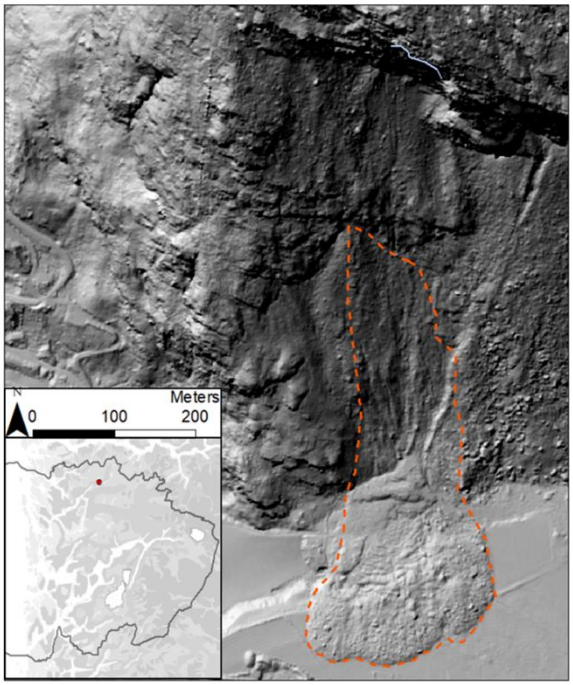

Figure 30 The event located in Modalen is classified as unobstructed. The deposit is outlined with an orange dotted line and the backscarp is marked with a light blue line

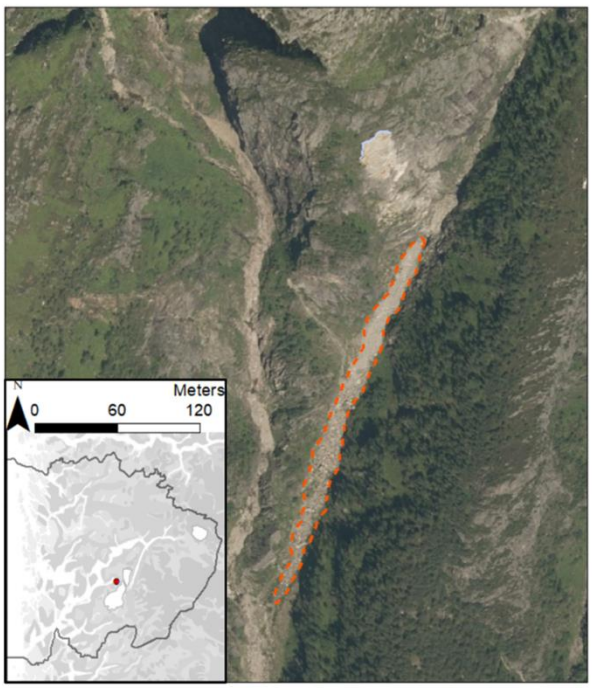

Figure 31 Channelized event, located in Mauranger. The deposit is outlined with an orange dotted line and the backscarp is marked with a light blue line

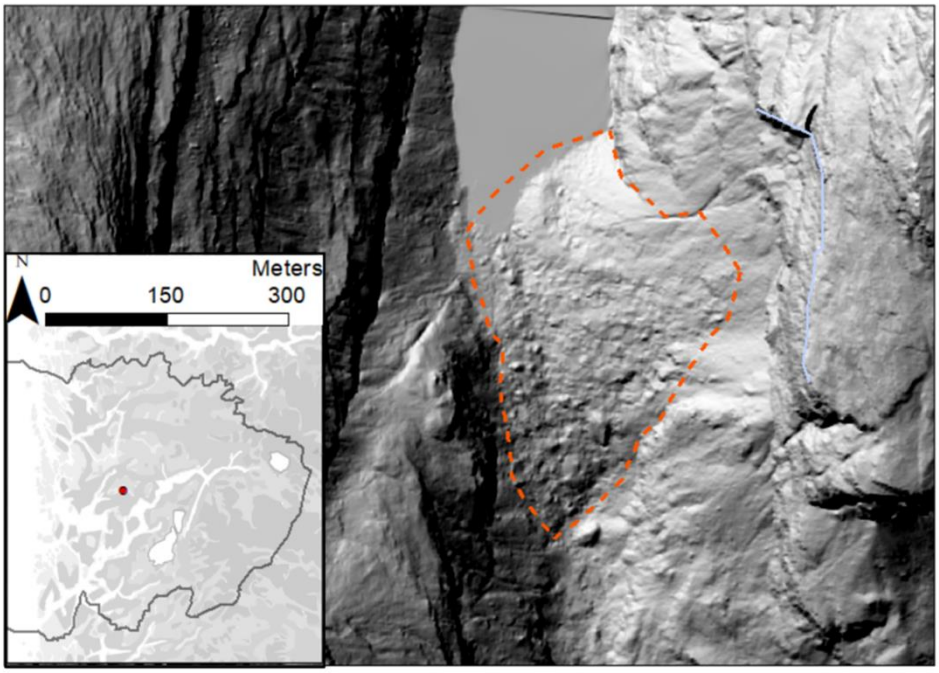

Figure 32 Rock fall event that are traveling up on the opposite valley wall are classified as obstructed or opposing wall. This event is located in Kvitingen. The deposit is outlined with an orange dotted line and the backscarp is marked with a light blue line

3.2.6 Defining of the substrate

When this work started, only the following substrates were defined in earlier work (Velardi et al., 2020) and in the NGU database: permanent snowfields, marine deposits, glaciofluvial sediments, into water bodies and across water. The field work in this thesis made it clear that the categories of the substrate had to be extended. Therefore, the following categories of substrates were added in this work: glaciofluvial sediments, debris flow, on scree, moraine, bed rock and alluvial sediments. For the events mapped, the substrate is determined by orthophoto and the quaternary map of NGU.

In most of the events, the avalanche path consists of more than one type of substrate. Therefore, two types of analyses of the substrate have been performed. In the first analyses, the dominating substrate is considered. In the second analysis, the substrate that underlies the toe area of the deposit is evaluated. Figure 33, 34, 35 and 36 show examples of events with different types of substrates.

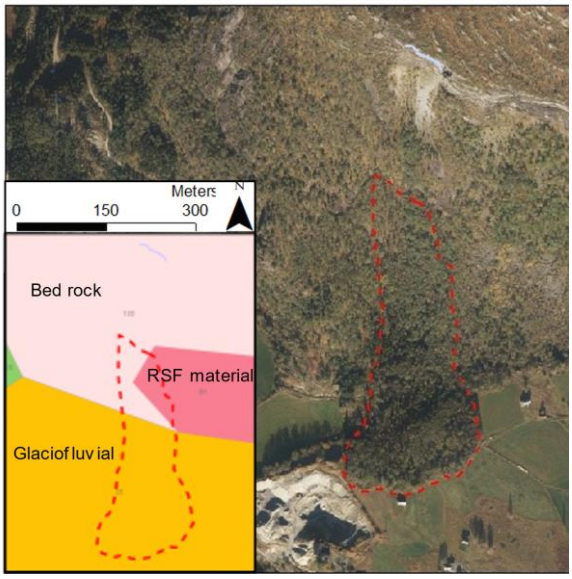

Figure 33 RSF event mainly travelled on scree (based on field aerial photos and map observations). The toe area is deposited on glaciofluvial sediments

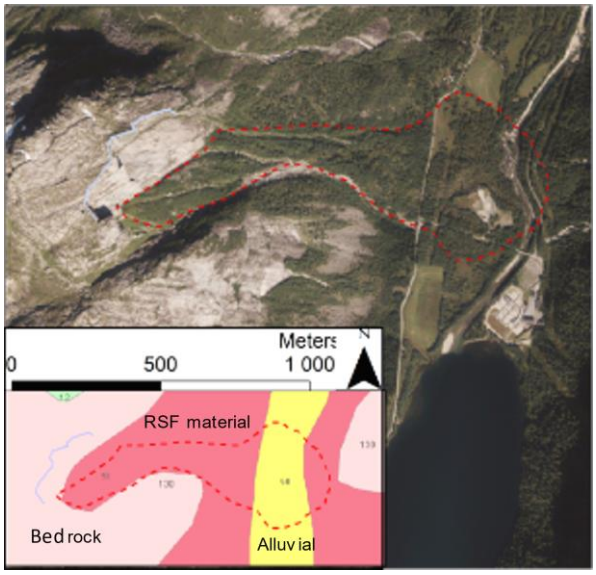

Figure 34 RSF event dominantly traveled on scree, and the toe area are mainly deposited on alluvial sediments

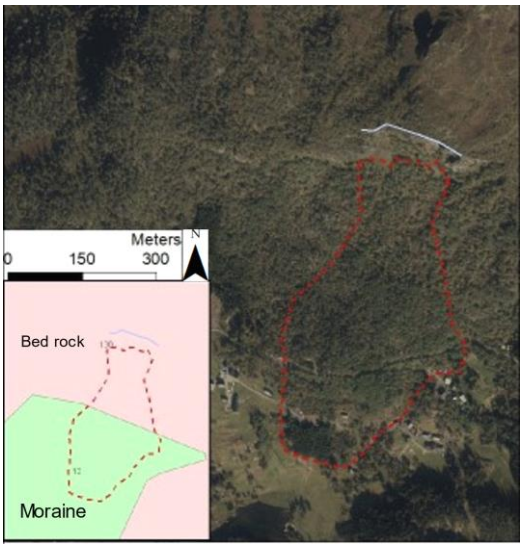

Figure 35 RSF event where the toe area consists of moraine

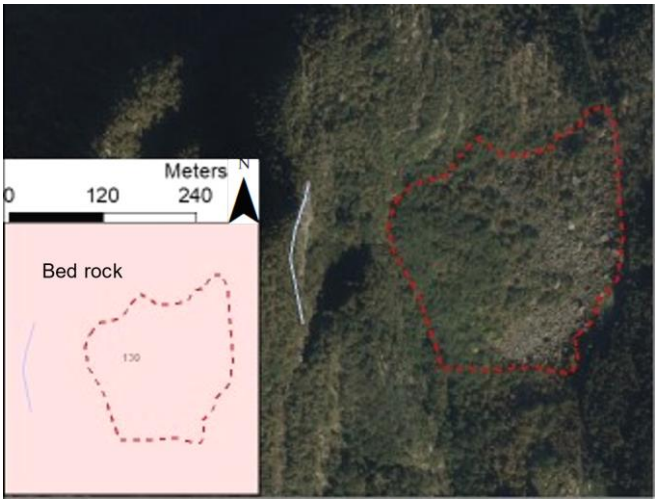

Figure 36 RSF event where the masses only propagated over bed rock

3.3 Developing of a α–β model for steinskred

Until now, the equations in the alpha-beta method are only developed for rock fall, snow avalanches, and debris flows (Lied and Bakkehøi, 1980, Lied and Kristensen, 2003, Bakkehoi et al., 1983, Norem and Sandersen, 2012). In this thesis an α–β method with suitable coefficients for estimating the runout length of "steinskred" is developed. This development follows the empirical approach of the coefficients in the already existing α–β equations for rock fall shown with equation 5 with existing standard deviation (σ):

Rock fall: $\alpha = 0.77\beta + 3.9°$ $(\sigma = 2.16°)$ (5)

The β-point is where the terrain starts flattening, and the masses start losing energy. Flattening means here where the terrain slope is $\leq \theta_\beta$ (section 2.1.5). For rock falls this is where the slope angle $\theta_\beta = 23°$.

The different factors tested is shown in equation 6:

$$\alpha = m \cdot \beta + n \quad (6)$$

Where m and n are constants.

Because of the high number of 216 mapped RSF events, largely beyond what are previously covered in literature (Schleier et al. (2017) with 33 RSF events, Corominas (1996) with 56 RSF events, Velardi et al. (2020) with 177 RSF events), the analysis was automated in Excel to

manage to cover efficiently all the events and to test a high number of parameters combination in a time effective and precise manner. The method is based on the profiles of the slope geometry used in section 3.2.4.

Each event has one sheet each in the Excel file (appendix B). For each sheet, there is the profile of the slope geometry of the event with the X (length) and Z (height) values. Additionally, the length and the height to where the β-point is placed on the graph is calculated. It is easy to test various θ_β -angles in the excel-file. If this value is changed, it will change for all the events in the entire excel-file, and a new length and height to the β-point will be estimated, for this value, for all the events. Also, the profile resolution is easily changed and is also tested with different values.

One of the sheets in the excel file is presenting the results. This sheet summarizes all the β-angles from all the different events by collecting the height and length values to the beta point from all the events. Together with the θ_β –angle the values for the two factors, m and n, could be tested. The m was tested between 0.66 and 0.84, n was tested between 3 and 5, and θ_β was tested with angles between 20° and 25°. Each interval was tested with 5 to 7 values. The θ_β, m- and n-values optimization were carried out by testing various θ_β –angles until the combination with the constants m and n giving the lowest deviation between the mapped and predicted runout length was reached.

3.4 Local mapping in Modalen

In addition to the detailed systematic mapping, fieldwork was undertaken to gather data about "steinskred" events and the runout length. The "steinskred" event in Modalen (section 1.4.3) was chosen to collect data to better understand why its behaviour deviated from most of the other cases. Indeed, the Modalen event shows granular flow geomorphologic features often seen on rock avalanches deposits but not on most mapped "steinskred" events. Because of the surprisingly large amount of RSF events located in Hordaland, the inventory mapping and analyses of the α–β method was more time consuming than expected. The planned modelling of the site was abandoned. Anyway, the mapping is still included for possible later investigation and modelling of the site.

In the field roughness analyses, measuring the block size, tree density, collecting sediment samples, doing observations of the substrate in a sand quarry on the side of the deposits and scanning with the LiDAR scanner (the TLS method) were done. The locations of the

measurements are marked on figure 37. Three roughness measurements were performed with LiDAR scanner. One is taken at 200 masl., second at 120 masl. and the third was taken 65 masl. There were three different locations where blocks were measured. This was at the tip of the deposits, at the east side of the deposits, and one in the central part. The tree density was measured both at the nick point of the slope (border of where the trees are growing and the start of the terrace) and higher up in the slope. The four sediment samples were taken around the deposit where one was taken at the east side of the deposit (nr.1), second at the tip (nr. 2), the third at the west side (nr. 3) and the fourth on the border between the scree and the terrace (nr.4).

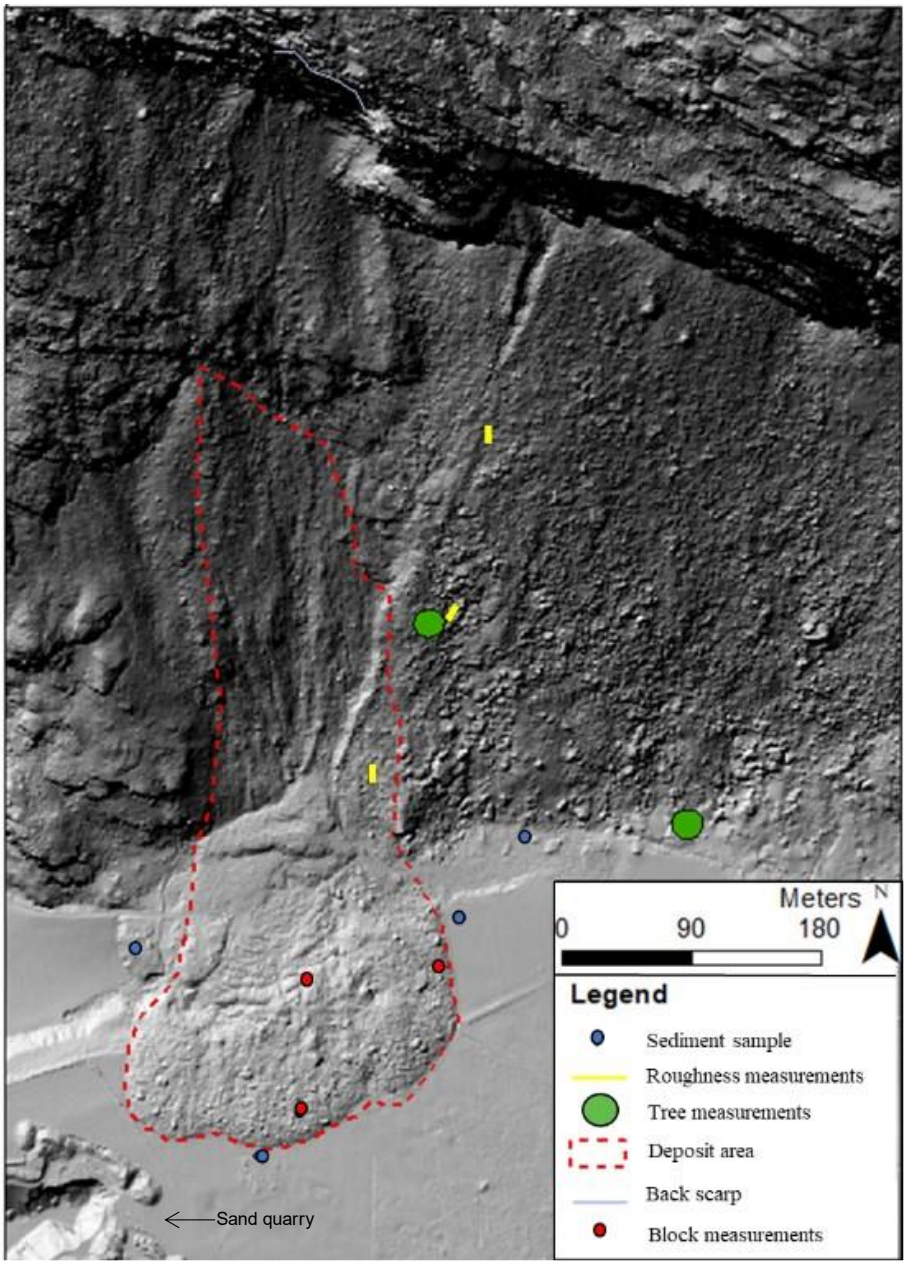

Figure 37 Overview map of the event in Modalen and the location of the different analyses performed in field and a sand quarry close to the deposit area. This was roughness analyses of the slope, measuring of the tree density, block measurements and sediment samples were taken

Roughness measurements

The roughness of the slope surface is formed by the uneven distribution of blocks on the scree slope. This was measured in the field by stretching a measuring tape (10 m) parallel to the surface over the obstacles and measure the distance from the rock/obstacles and the measuring tape (figure 38). The measurement was done for each block lying in the 10-meter distance, measured normal to the slope surface.

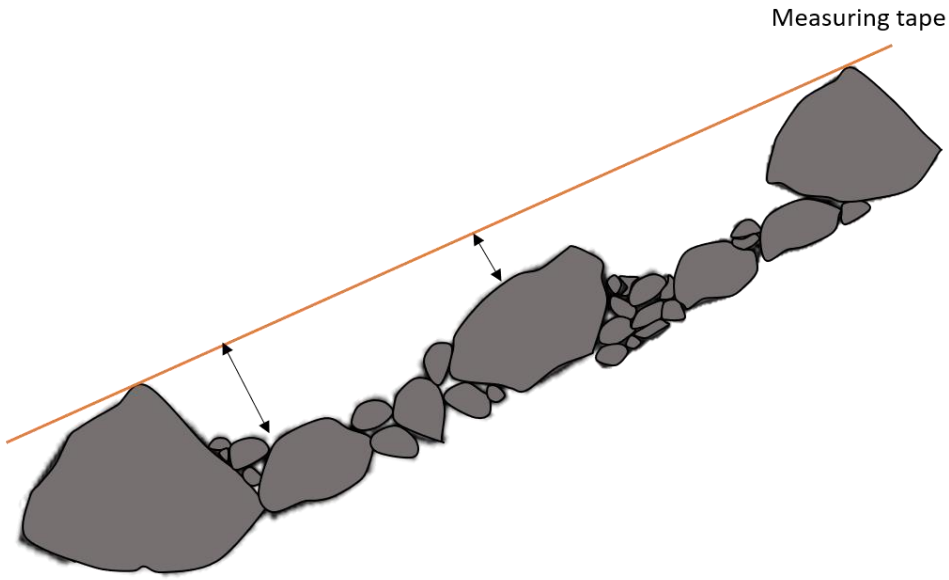

Figure 38 Illustration of scree which represents the roughness of the slope. The roughness was estimated by stretching a measuring tape (illustrated as orange line) parallel to the surface and measure the distance between the rocks and the measuring tape

In addition to measuring manually, pictures of the roughness were taken, showing the slope from above at several angles. This makes it possible to create 3D models of the roughness for use in modelling programs.

Block size measurements

The sizes of the blocks were measured to find out what size of blocks travels the furthest and to be able to enter the block size in a modelling program. The size was measured by measuring the height, length, and width of 100 blocks touching each other. This is a good way to get a reasonably accurate measure of the block sizes free of subjective surface assessments. There are some challenges with the method. Some blocks often have vegetation on top, some are eroded down into the substrate, and some are difficult to measure the height of. The difficulty with the height measurements is due to the covering by other neighboring blocks.

Sediment samples

Since the substrate is studied to influence the runout length (section 2.3.4), four substrate samples were taken in Modalen. The sampling was done to determine any effect on the runout length due to the substrate property. High water content in the substrate can lead to liquification and potentially longer runout length. Additionally, a more detailed quaternary map of the area is made.

The analyses have been done by filtering out the samples by using both wet and dry filter analyses. This is done to evaluate the distribution of the grainsizes and what effect that might have on the runout length. The wet and dry filter analyses were done after method described in Statens vegvesen' handbook 014 "Laboratorieundersøkelser" (Statens vegvesen, 2005). In the wet filter analyses the sediment samples were dissolved in water and filtered out the fragments below 63 µm. The sediment samples were dried in a heating cabinet and weighed. The fragments above 63 µm were sorted with the use of dry filtering. In the dry filtering different sizes were used; 0.063, 125, 250, 500, 1, 2, 4, 8 and 16 (mm). The material was shaken in 10 minutes and after that weighed.

Measuring of trees

The measuring of the density of trees can be entered into modelling programs, such as RockyFor3D (Dorren, 2015) and Rocfall (RockScience, 2021) , to test if the trees can affect the runout of the deposits.

One of the measurements in Modalen was taken at the neighbor slope, a few meters outside of the deposits. The neighbor slope is assessed to better represent the vegetation cover prior to the event rather than the slope affected by the event itself. The second is taken up in the middle of the slope (110 masl.). This was done by using a 5 and 10 m measuring tape. The five meters long measuring tape was used in the measurement taken at the neighbor slope and the ten meters long measuring tape was used at the measurement at 110 masl.. The measuring tape was fixed at a tree in the middle and all the trees inside a radius of 5 m or 10 m was registered. Both the type of tree and the diameter of the stem of the tree were recorded. The diameter of the stem was measured in the height of the chest.

Terrestrial laser scanning (TLS)

TLS was also used in the field (figure 39). The scanner was positioned at two different locations for the same site (figure 40). This is done to get different view directions and to optimize to cover most of the surface orientation and so that the datasets can be merged into one single model to minimize occlusion (Lato et al., 2010). The TLS has a long range, up to 3500 m, so the entire slope is covered. It has a spatial resolution of 5 to 15 cm (NGU, 2015). The scanning was taken when the entire slope was in the shadow to ensure that the result would be as good as possible. Cloudy and sun at the same time will cause poorer results. The data set can be processed and used as a terrain model in modelling programs or more easily identify the source area and measure the size of the source area.

Figure 39 Pictures of the Lidar scanning. This illustrates the position and angle of the scanner compared with the slope

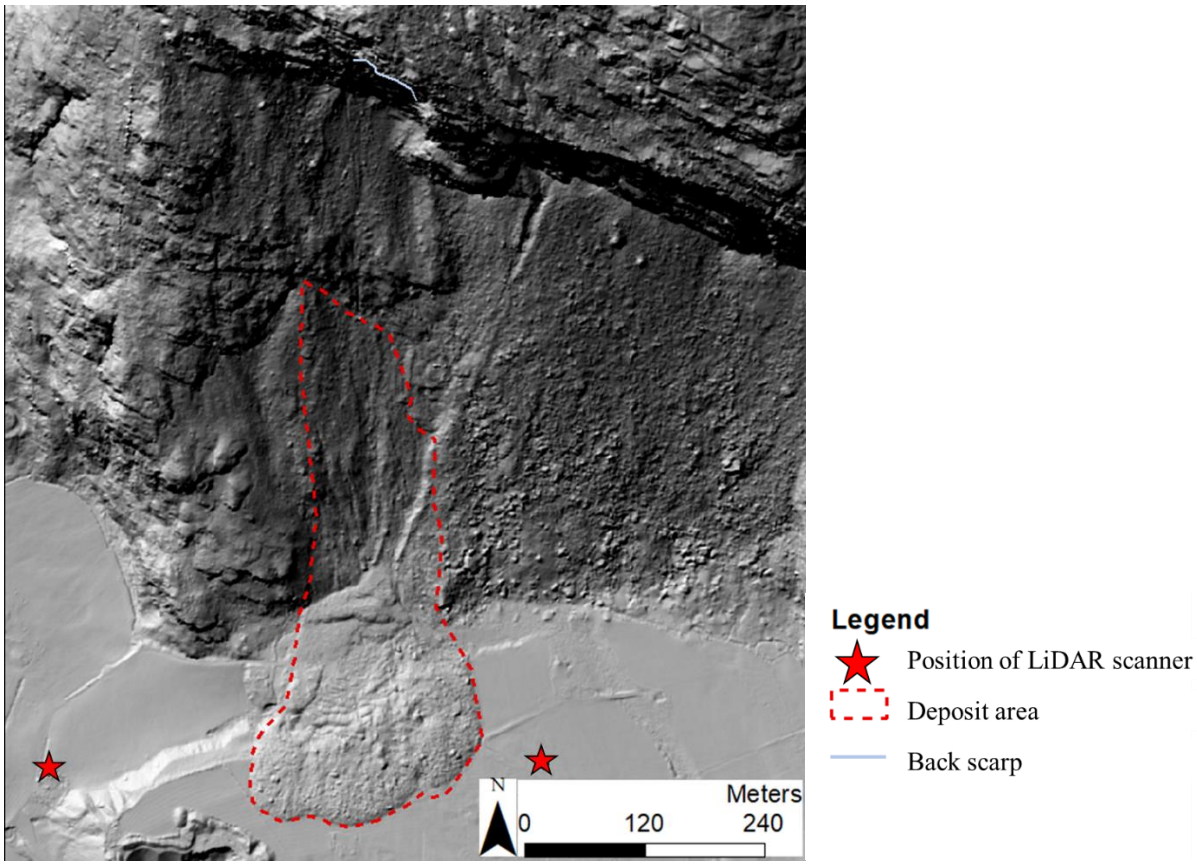

Figure 40 Overview map with the two locations of where the LiDAR scanner was placed marked with red stars

Volume estimation by the use of CloudCompare

The volume of the detached masses at the source area, the eroded masses in the slope, and the deposited masses at the deposit area were estimated in CloudCompare (cloudcompare.org). CloudCompare is a 3D point cloud and mesh processing software. The source area was estimated by using point cloud deviated from TLS scans in the field. Volume estimations of the eroded masses in the slope and the deposited masses at the deposit area, were based on already existing point cloud data in Hoydedata.no. To calculate the volume of the deposits the previous topography had to be interpolated. Then, the volume was calculated by the height difference between the interpolated plane and the point cloud made by the LiDAR scans.

4. Results

Based on the different methods described above, the inventory map of RSF events of the entire Hordaland, developing an α–β model for steinskred and field investigations/volume calculations of Modalen were performed. In the following sections, the results are presented.

4.1 Results for the regional analyses of events in Hordaland

216 RSF events were mapped in Modalen. The calculated volumes range from ca. 800 m^3 to 8 500 000 m^3 (figure 41).

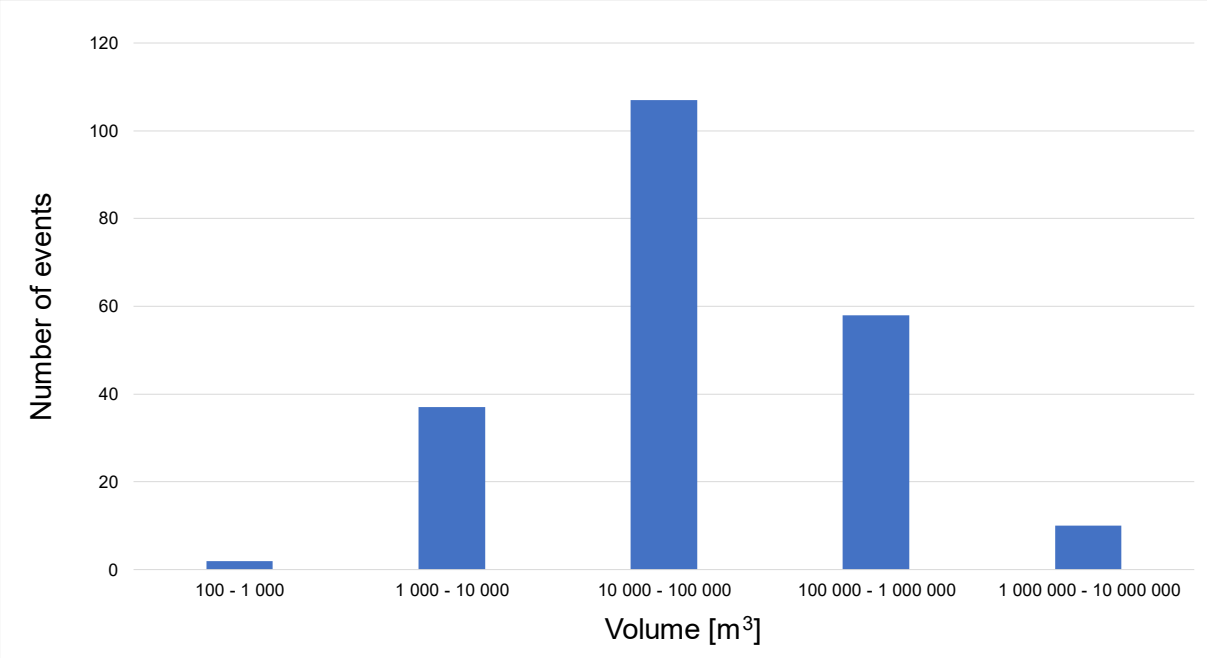

Figure 41 The distribution of the volume ranges of the mapped RSF events in Hordaland, showed in a histogram

The high concentrations of RSF events and belonging deposits collected in the study area are mainly clustered around the fjords (figure 42). At the coast and the east part (Hardangervidda) of Hordaland, the landscape has a lesser difference in the relief, reflected in the number of events.

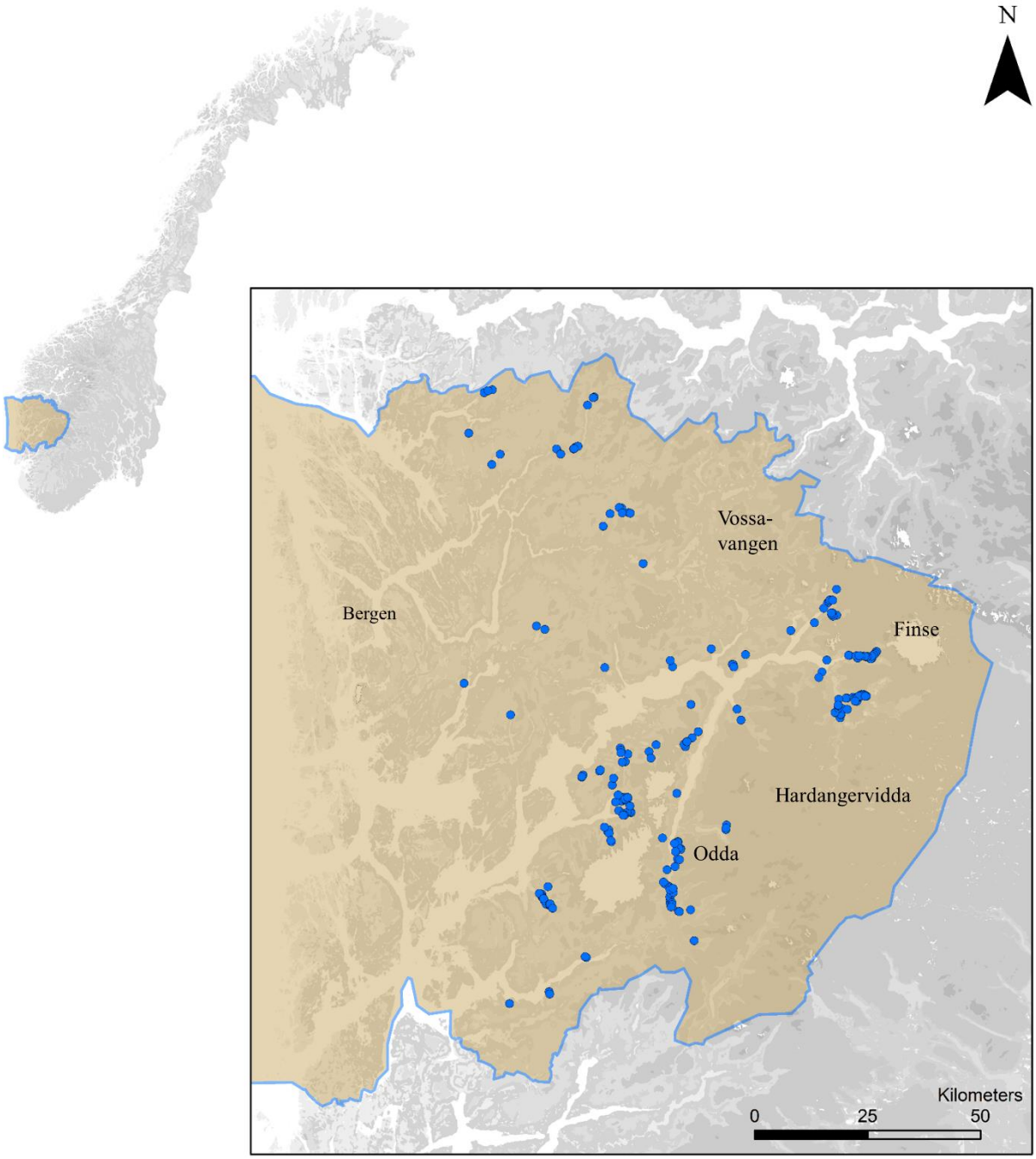

Figure 42 Overview map of Hordaland and the mapped events

As an example of how the events are mapped, figure 43 shows a detailed view of one of the valleys in Hordaland, Måbødalen, with the mapped RSF. This valley has one of the highest numbers of RSF events.

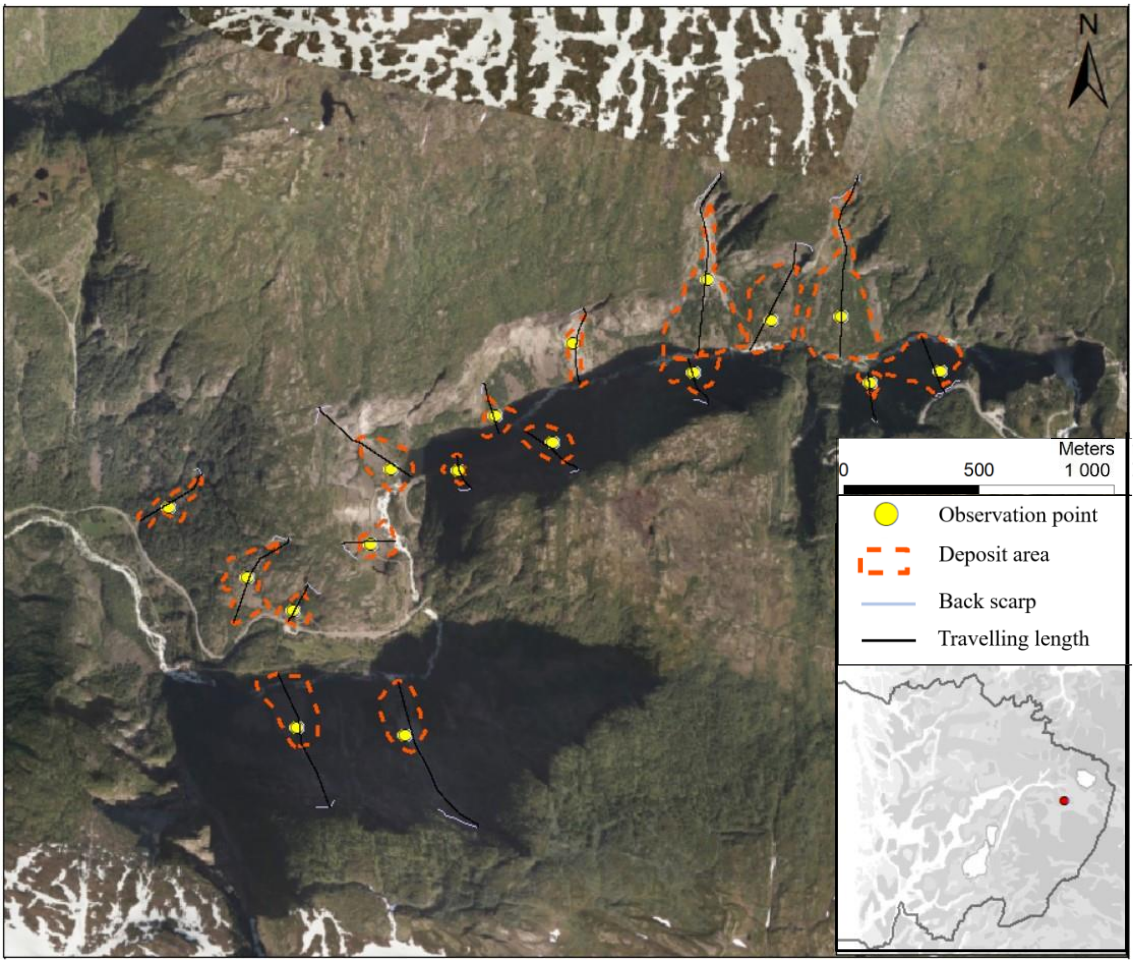

Figure 43 Måbødalen is one of the valleys that are exposed of many RSF events. The deposits of the events are marked with red, the backscarp with light blue line and the black line are indicating the estimated travel length. The yellow point is marking the event and consists of attributes with different information of the event.

The events were divided into the four certainty levels a: uncertain (n=90), likely (n=84), almost certain (n=29) and certain (n=13) (table 5). The different events with belonging certainty levels are marked on the map in figure 44, where each category of certainty level is distinguished by different colors; red (uncertain), yellow (likely), light blue (almost certain) and dark blue (certain).

Table 5 List of the different levels of certainty and the number of events in each category

Level of certainty	Number of events
Certain	13
Almost certain	29
Likely	84
Uncertain	90

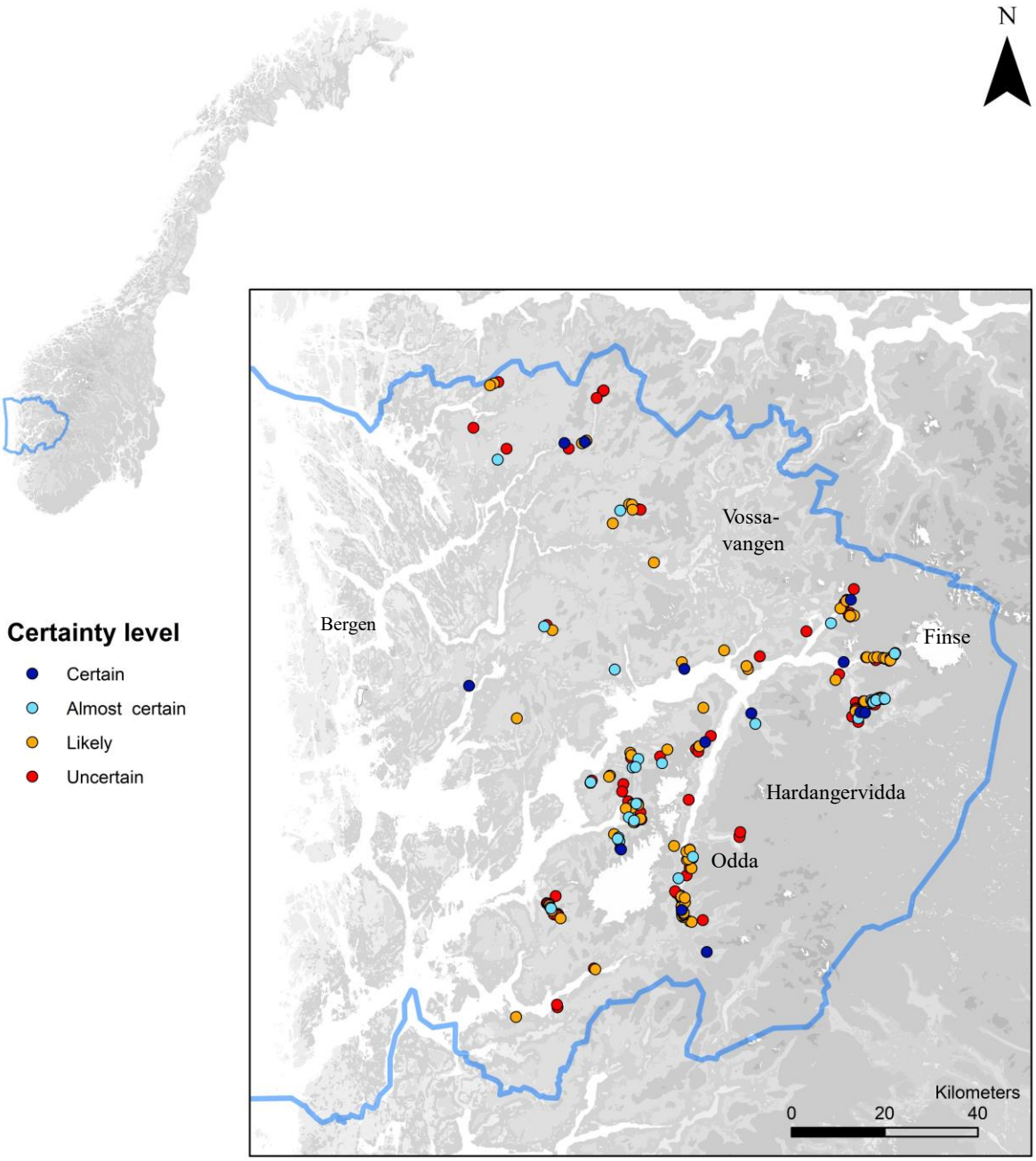

Figure 44 Overview map of the mapped RSF deposits in Hordaland, where the different certainty levels are represented by different colors. Red is indicating uncertain, yellow is likely, light blue is almost certain, while the dark blue represents the events that are certain

The certainty level is plotted in an angle of reach/volume ratio compared with the worldwide data from Scheidegger (1973) and Corominas (1996) (figure 45). Only two of the mapped events in Hordaland plot under this Scheidegger curve, while the rest are lying above. Of the two events located under the curve, one is classified as uncertain, and the other is almost certain.

The plot shows that the volume and the travel length are independent of the certainty level. The uncertainty on defining the outline of the deposit does not influence the overall outcome of the results. This is also shown in the plot with only events classified as certain and almost certain (see figure 46).

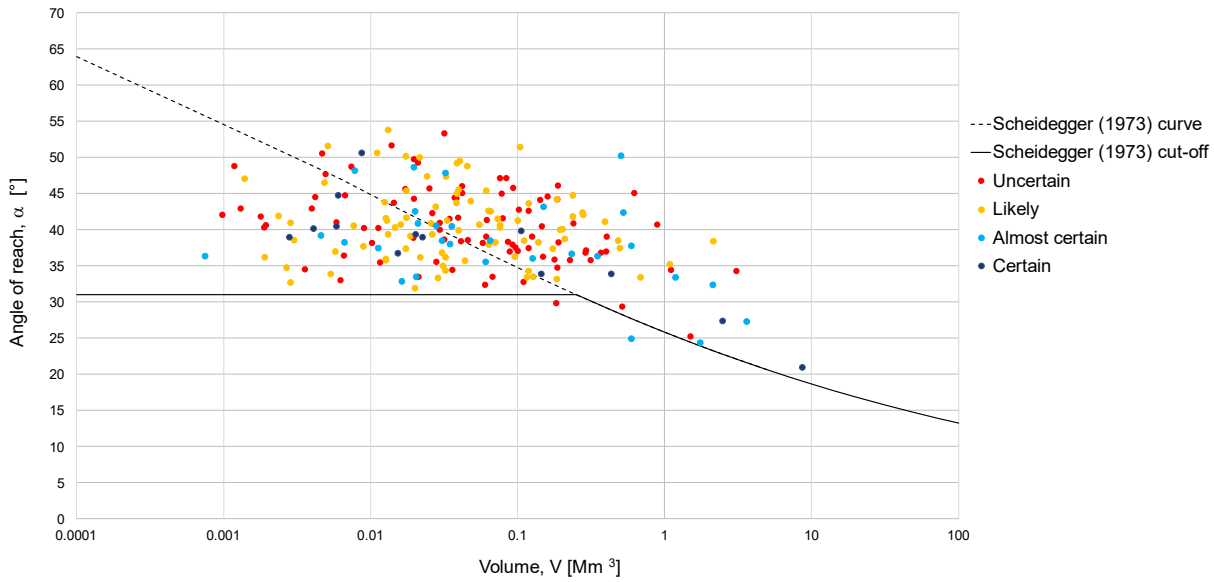

Figure 45 Graph showing the ratio between angle of reach and volume, where the events are divided into four certainty levels. The events are plotted against the Scheidegger curve (Scheidegger, 1973), and the Scheidegger cut-off at 31° according to Corominas (1996). The volume is presented in a logarithmic scale

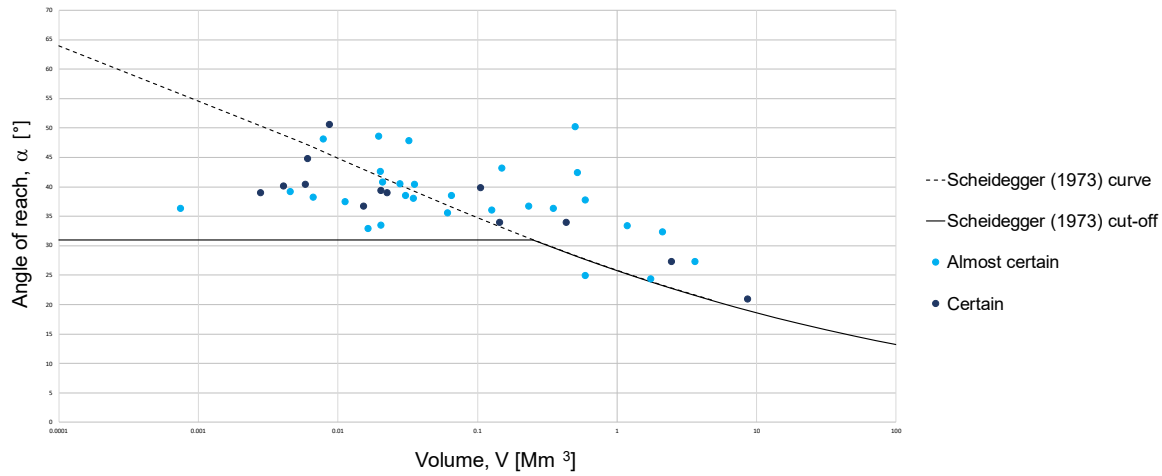

Figure 46 Graph showing the ratio between angle of reach and volume, showing only the events classified as certain and almost certain. The events are plotted against the Scheidegger curve (Scheidegger, 1973), and the Scheidegger cut-off at 31° according to Corominas (1996). The volume is presented in a logarithmic scale

4.1.1 Volume of the deposits

The mapped events are plotted in a angle of reach/ volume ratio (figure 47). This plot shows a threshold in the events at 250 000 m^3 where the events with volumes lower than this have angle of reach above 31°, while larger deposit volumes might have an excessive travel length (angle of reach <31°) as seen with rock avalanches. Seven events out of 32 with deposit volume above 250 000 m^3 have excessive travel lengths. Additionally, one with volume below 250 000 m^3 have excessive runout length. However, figure 47 show that several of the events larger than 250 000 m^3 have high angles of reach. Two of these events have larger angle of reach than 45°, which is higher than expected out from the volume.

If dividing the data at 250 000 m^3, the best-fit curves indicates that events with higher deposit volumes than 250 000 m^3 have a best fit curve following the Scheidegger curve, only more conservative. It indicates that there is a slight correlation between the volume and the angle of reach. The trend line for deposit volumes below 250 000 m^3 the angles of reach are more constant at an angle of reach about 41°.

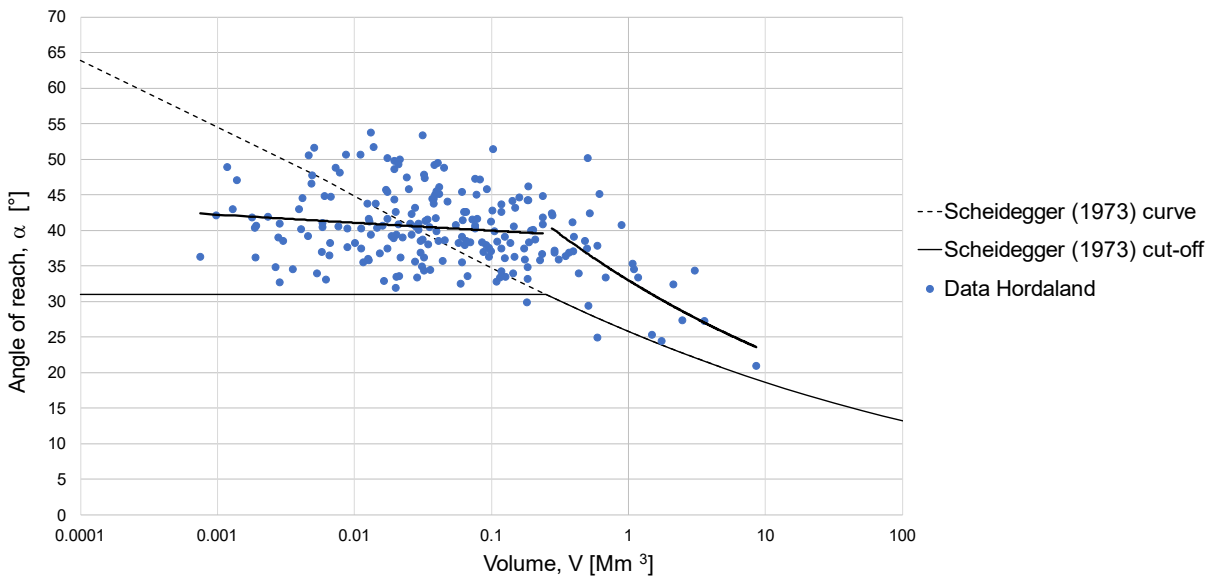

Figure 47 Deposit angle of reach/volume ratio with one best-fit curve for events larger than 250 000 m^3 and a second best-fit curve for events with deposit volume below 250 000 m^3. The volume is presented in a logarithmic scale

4.1.2 Maximum slope angle

The events estimated maximum slope angles are plotted against H/L. In general, the trend shows a larger max. slope angle with an increase in H/L ratio. However, it seems to be a change when the max. slope angle reaches ca. 45° (figure 48). For events with max. slope angle larger than 45° the plotted events do not seem to have a correlation with the H/L ratio.

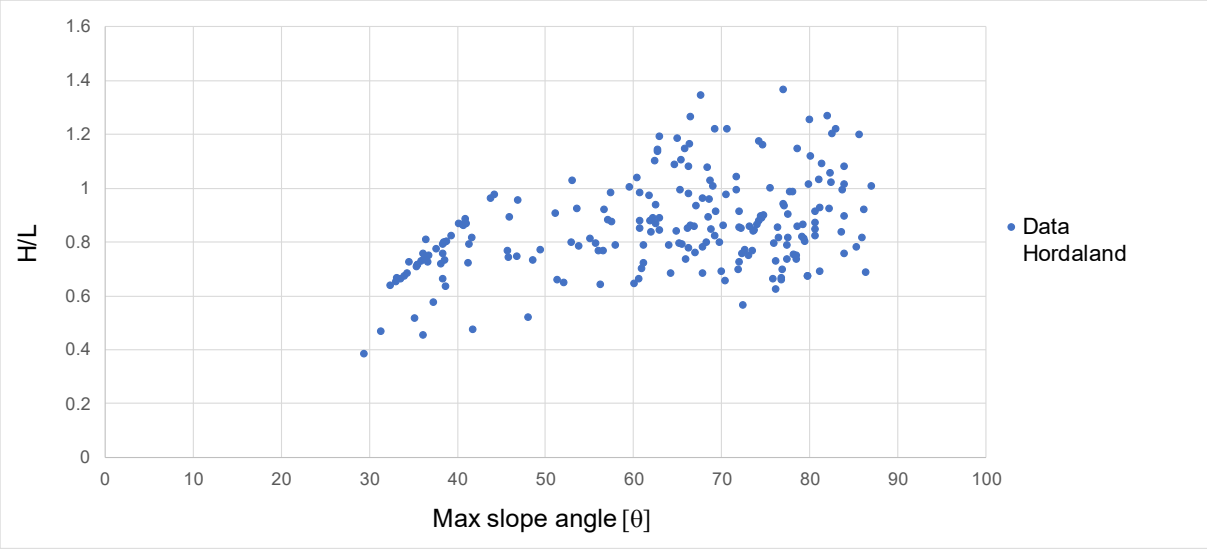

Figure 48 Graph showing the ratio between the H/L and max. slope angle.

4.1.3 Slope profile geometry

A more profound look into the impact of the slope profile geometry indicates that in Hordaland 64 events are small fall/bouncing area events, 91 large fall/bouncing area events and 57 straight path events.

When comparing the slope profile geometry classes to the angle of reach, it becomes evident that the slope profile geometry impacts the angle of reach (figure 49). The best fit curves imply that events with a straight path have the lowest angle of reach, followed by the ones with small fall/bouncing areas and the ones with large fall/bouncing areas having the highest angle of reach. The distribution of the different slope profile geometry, the formulas and R^2-values for the best fit curves are listed in table 6. The R^2-value is a measure of how close the data are to the best fit curve. A R^2-value close to one is favorable since this indicates that the data have a small scatter and a good statistical fit. As seen in table 6 the R^2-value for the slope profile geometry are not close to one which indicate scattering in the data. For the straight slope profile geometry category there are specially two outliers with an angle of reach above 45° and for the small fall/bouncing area there are two outlier events located below 30°. The large fall/bouncing area have the largest spread, illustrated with the lowest R^2-vales.

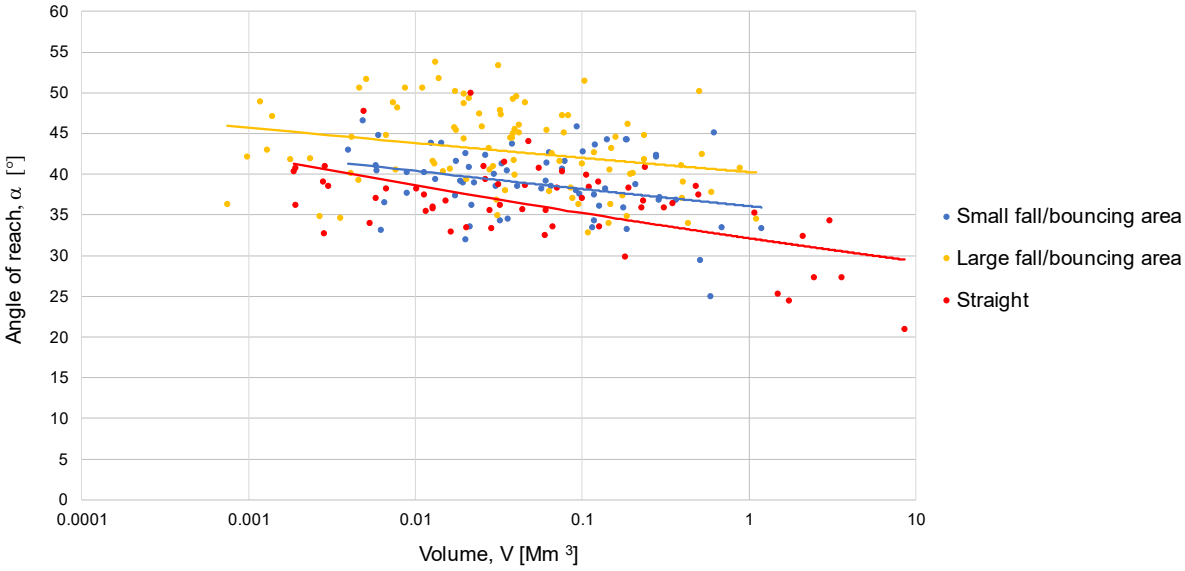

Figure 49 The different slope profile geometries are plotted in an angle of reach/volume ratio, compared to the different slope profile geometries. The best fit curves are included in the graph. The volume is presented in a logarithmic scale

Table 6 The four different categories of the slope profile geometry with the corresponding number of events in each category with formula and R^2-values for the best fit curves

Type of profile geometry	**Number of events**	**Formula**	**R^2-value**
Small fall/bouncing area	64	$y = 36.088x^{-0.024}$	0.08
Large fall/bouncing area	91	$y = 40.261x^{-0.018}$	0.0605
Straight	57	$y = 32.134x^{-0.04}$	0.2795

The slope profile geometries are also analysed with only the events classified as likely and uncertain. This show the same correlation as in the analyses with all the events (figure 50).

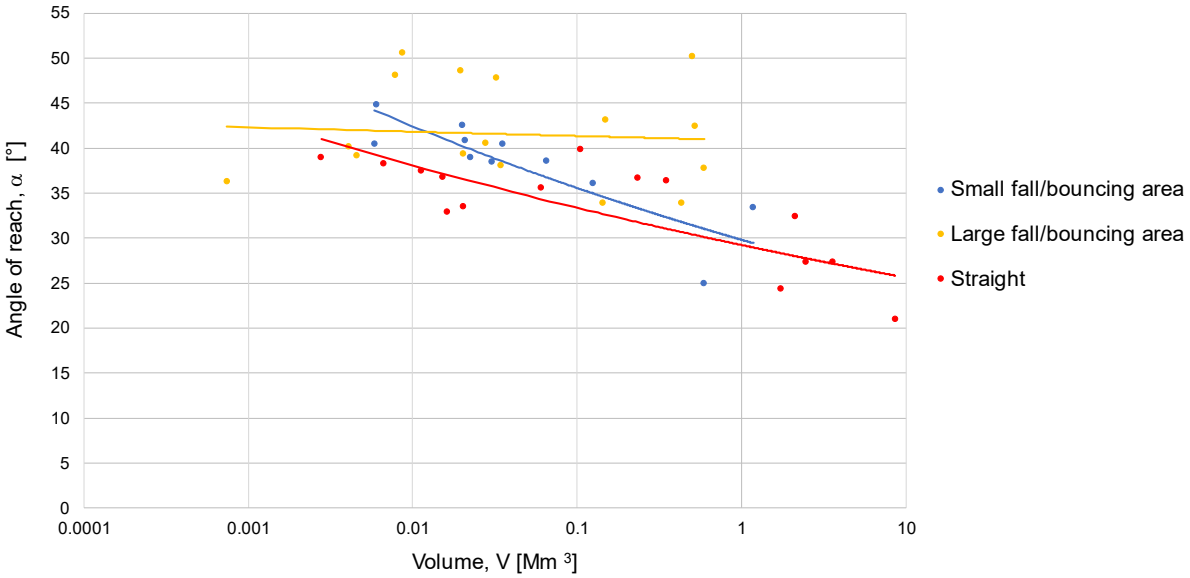

Figure 50 The events classified as certain and almost certain with the different slope profile geometries plotted in an angle of reach/volume ratio. The best fit curves are included. The volume is presented in a logarithmic scale

Area under the graph

To see if it was possible to get a more objective view on what effect the slope profile geometry has on the runout length the ratio between the angle of reach compared to the normalized area was tested. The result from this analyse is illustrated in figure 51. This ratio has no obvious correlation.

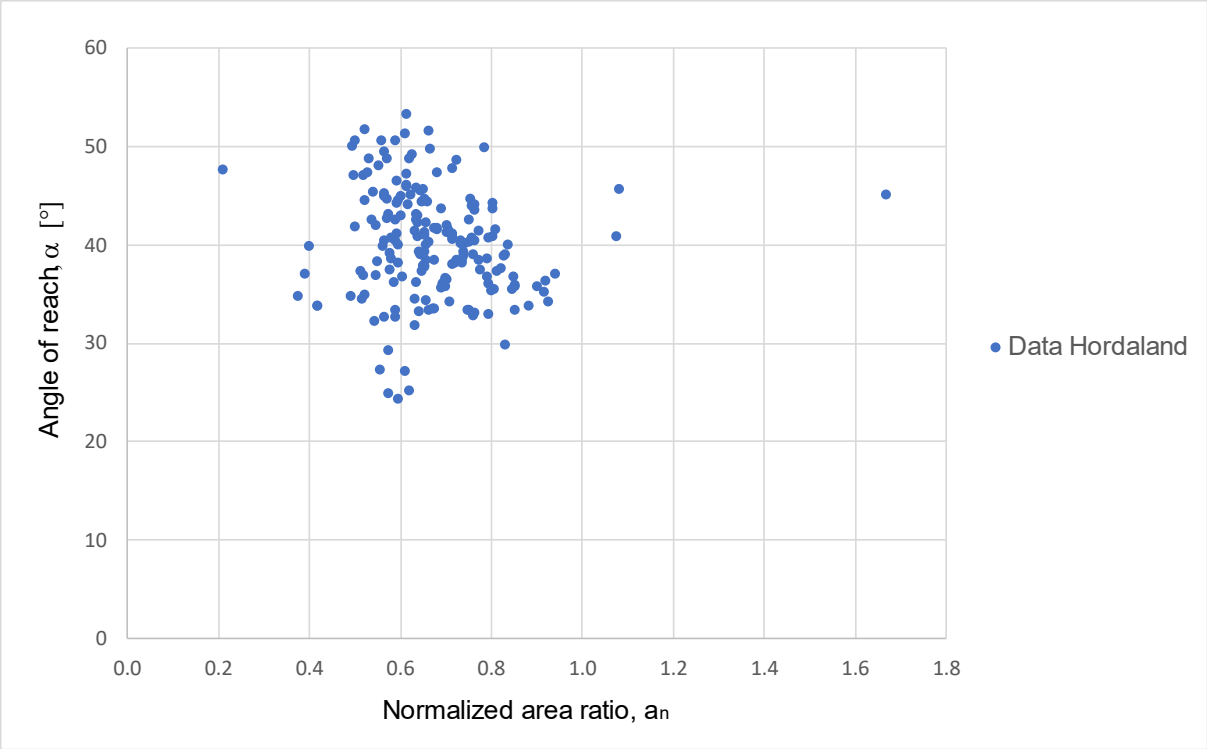

Figure 51 The event from Hordaland plotted in an angle of reach/normalized area ratio.

4.1.4 The effect of the topographical constrains

The analyses of flow path topography versus angle of reach resulted in 14 channelized, 52 opposing wall and 148 unobstructed RSF events in the study area.

Figure 52 show that for RSF events above ~0.08 Mm^3, the best fit curves for the different categories indicate that events running onto the opposite valley wall have the highest angles of reach. This is followed by the unobstructed ones, while the channelized events have the lowest angle of reach. However, for the volumes below ~0.8 Mm^3 the number of channelized events are small, and the ones that are channelized have larger angle of reach than the RSF events classified as unobstructed. The best fitting curves for channelized events and events opposing the opposite valley wall are close to following the Scheidegger curve, only more conservative (figure 53). The unobstructed best fit curve follows more the cut-off of the Scheidegger curve at 31°, by Corominas (1996). These best fit curves are summarized in the table 7 together with the curve's R^2-values. R^2-values are not close to one which indicates scattering in the data. The best R^2-values occur for the event propagating onto the opposite valley wall with a value of 0.36. The unobstructed events have shown the poorest statistical fit with an R^2-value of 0.07. The events with largest and the smallest angle of reach in the entire dataset are categorized as unobstructed.

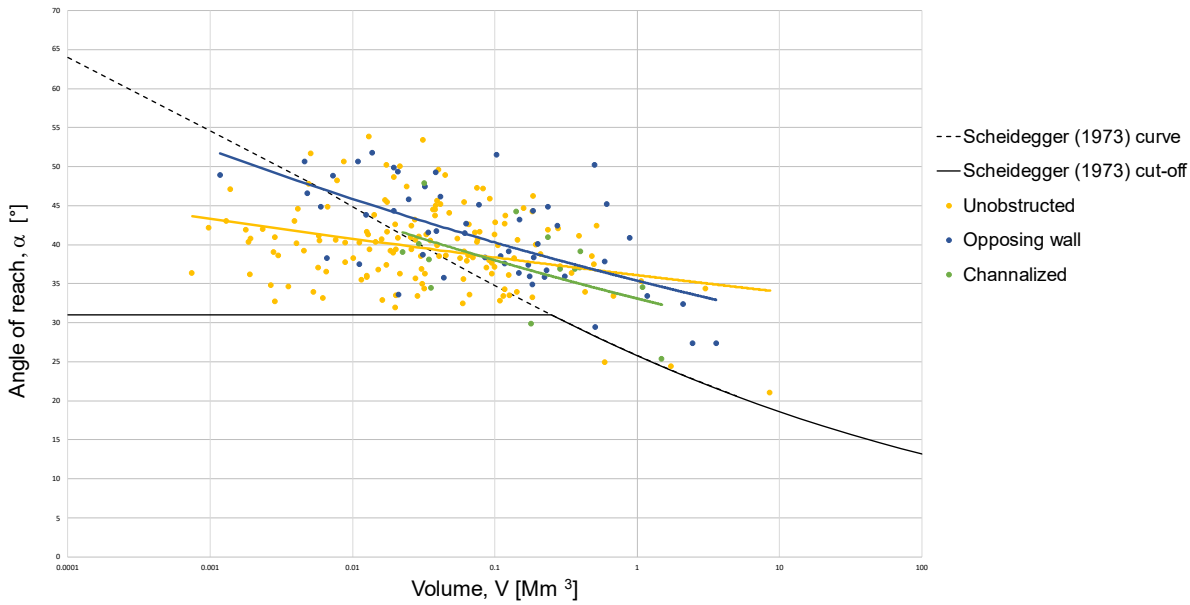

Figure 52 The angle of reach/volume ratio, compared to the different categories of topographical constraints: channelized, opposing wall and unobstructed. The events are plotted against the Scheidegger curve (Scheidegger, 1973) and the cut-off of the Scheidegger curve at 31°, according to Corominas (1996). The best fit curves for the different categories are included. The volume is in a logarithmic scale

Table 7 Number of events, formulas and R^2-values for the different types of topographical constraints of the runout paths

Type of topographic constraints	Number of events	Formula	R^2 value
Unobstructed	148	$y=36.097x^{-0.026}$	0.0755
Opposing wall	52	$y=35.391x^{-0.056}$	0.3647
Channelized	14	$y=33.101x^{-0.06}$	0.2668

Even though events propagating onto the opposing wall in general give a shorter runout length, three out of seven events with excessive travel length are propagate onto an opposing valley wall. However, they are related to larger volumes, which also are expected to go far. Additionally, two of the mapped events are located under the Scheidegger curve. The event with a deposit volume smaller than 250 000 m^3 are classified as uncertain and has a channelized topography, and the other event is classified as certain and is unobstructed. The certain unobstructed event is shown in figure 53.

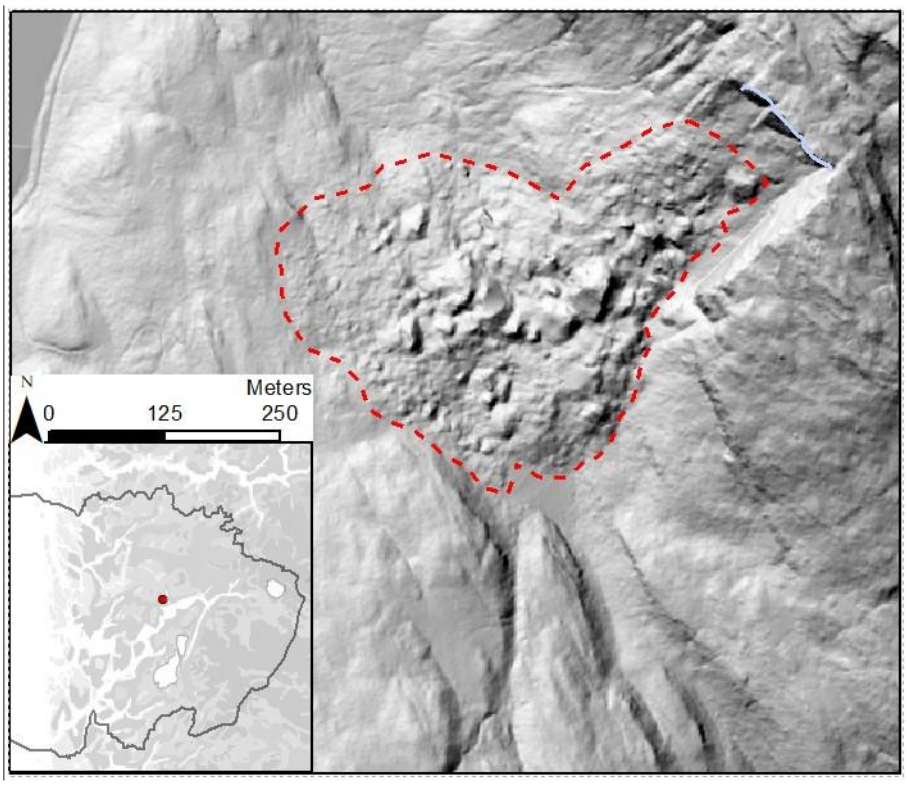

Figure 53 The unobstructed event located below the Scheidegger curve

The effect the topographic constraints have on the runout length is also tested with only the events classified as likely and uncertain (figure 54). This result indicates the same correlation with the unobstructed events and the events opposing the opposite valley wall. Only three of the events classified as certain and almost certain have a channelized runout path. All three are connected to volumes at the lower range and located above the best fit curve of the unobstructed events. These three events have a large scatter which are shown with the best fit curve. The curve is not following either the Scheidegger curve (Scheidegger, 1973) or the cut- off of the Scheidegger curve at 31°, indicated by Corominas (1996).

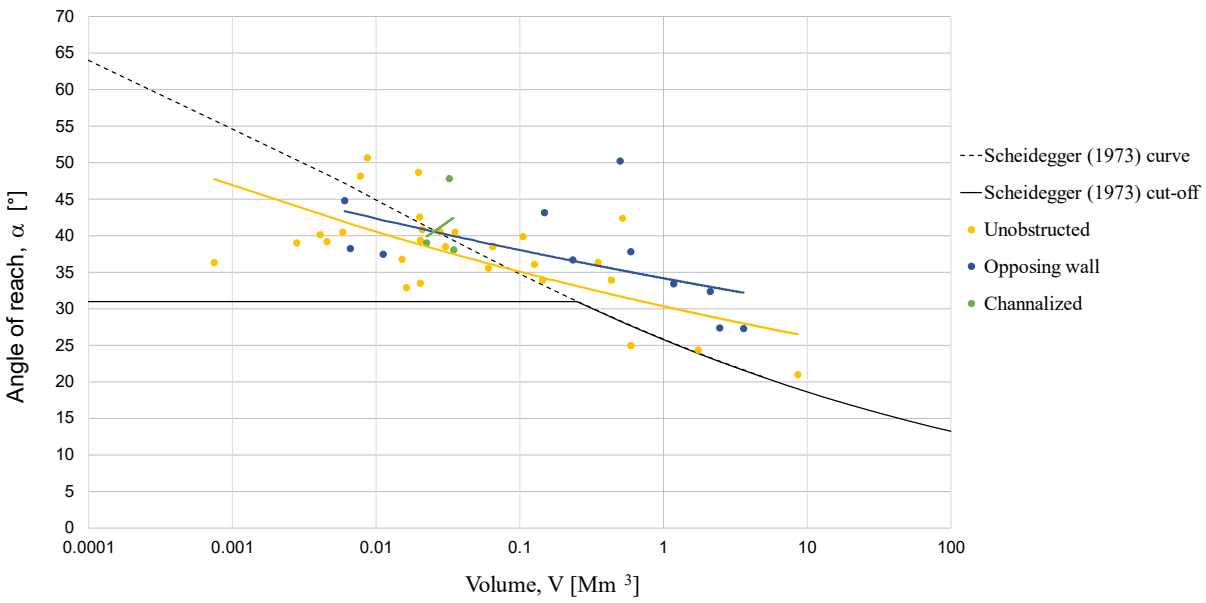

Figure 54 The angle of reach/volume ratio, compared to the different categories of topographical constraints: channelized, opposing wall and unobstructed. In this plot only the events classified as certain and almost certain are included. The events are plotted against the Scheidegger curve (Scheidegger, 1973) and the cut-off of the Scheidegger curve at 31°, according to Corominas (1996). The best fit curves for the different categories are also included. The volume is in a logarithmic scale

4.1.5 Substrate material

The substrate will, in many cases, change along the travel path. Analyses have therefore been done to see if the runout is mostly affected by what substrates there is in the toe area of the deposits, or if it is mostly affected by what substrate the runout path are dominated by. Some of the located events have their runouts into water bodies. These events are excluded from the results since the runout lengths and the volumes could not be estimated. This is because detailed bathymetric data in Norway are restricted for the public.

Analysis of the substrate in the toe area

Figure 55 shows the substrate categories in the toe area in an angle of reach/volume ratio, compared with the world-wide data from Scheidegger (1973) and Corominas (1996). For events with volumes higher than ~0.09 Mm^3 the best fit curves indicate that events crossing water bodies have the shortest angle of reach. This is followed by the events with toe area consisting of glaciofluvial sediments, moraine, alluvial sediments, bed rock and scree (figure 55). When the volume gets smaller than ~0.09 Mm^3, the events landing on bed rock has the lowest angle of reach. None of the events are crossing water or have glaciofluvial sediments which have the lowest angles of reach in the events larger than ~0.09 Mm^3. Additionally, the events with substrate as moraine and alluvial sediments are not having the smallest angle of reach as in the

events with larger volumes. The graph shows that events with smaller deposit volume (below approximately 10 000 m^3) are only landing on bed rock or scree in the Hordaland dataset.

The best fit curve for the alluvial and moraine sediments seems to follow the Scheidegger curve (Scheidegger, 1973), while the trend line for bed rock and scree are flatter and follows the cut-off of the Scheidegger curve, by Corominas (1996). Only three events are noted to land on glaciofluvial sediments, two are registered to be crossing waterbodies, and only one event is registered to land on ice or permanent snow fields. These categories are considered to be too small data for establishing a valuable best fit curve or a trend. The formulas and the R^2-values to the best fit curves and distribution of the substrate categories are listed in table 8. The best fit curve for moraine has the best R^2-values value of 0.39, but in general, the R^2-values show large scatter in the data.

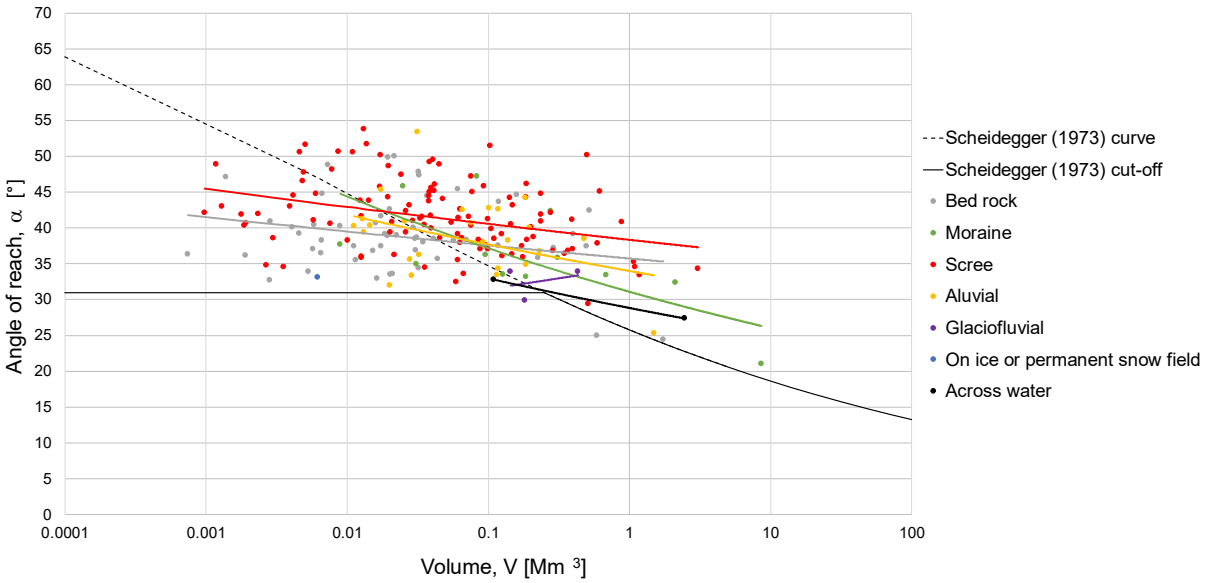

Figure 55 The angle of reach/volume ratio compared to the events with different substrates in the toe area of the RSF lands on. This is plotted together with the Scheidegger curve (Scheidegger, 1973) and the cut-off of the Scheidegger curve at 31° (Corominas, 1996). The best fit curves of the different data classes are also included. The volume is in a logarithmic scale

Table 8 Distribution of the different substrates in the toe area of the RSF event, best fit formulas and R^2-values for the mapped events in Hordaland
*Not statistical representative (only exist one or two events or lands in water)
-- Excluded from the analyses

Type of substrate, toe area	Number of events	Formula	R^2-value
Across water	2	$y=28.831x^{-0.058}$	1*
Alluvial	25	$y=33.997x^{-0.045}$	0.1231
Bed rock	54	$y=33.782x^{-0.039}$	0.1439
Debris flow	0		
Glaciofluvial	3	$y=34.547x^{-0.0404}$	0.1038
Into water body	7	--	--
Moraine	12	$y=28.441x^{-0.06}$	1
On ice or permanent snow field	1	*	*
Scree	112	$y=37.358x^{-0.028}$	0.1228

Analysis of the dominating substrate

The analysis of the dominating substrates indicates that the RSF events propagating across water have the shortest angle of reach, followed by ice and snow fields, moraine, bed rock and scree (figure 56). Only one event is registered to propagate over ice or snowfield, the same for debris flow. Two events are registered in each of the category's moraine and events crossing a waterbody. These four categories consist how too few events to be statistically representative.

The distributions of the different dominating substrate categories are listed in table 9, together with the formula and R^2-values for the best fit curves. The substrate with the highest R^2-values is 0.14. Since the R^2-values are not close to one, they indicate scattering and a bad statistically fit of the data. This means other factors are influencing the runout length of RSF events.

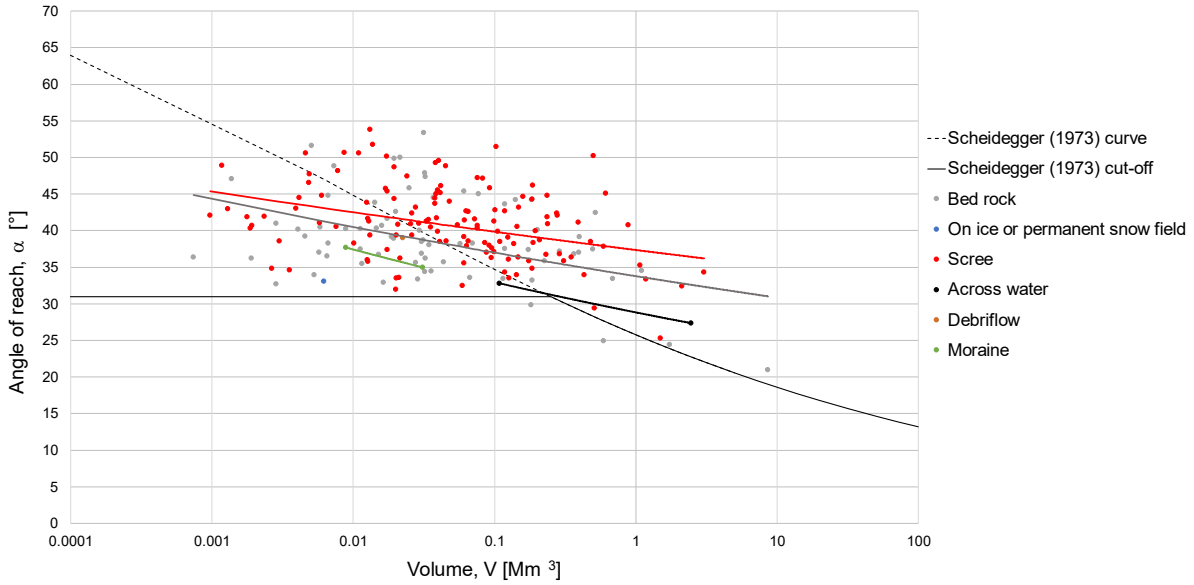

Figure 56 The angle of reach/volume ratio compared to the events with different dominating substrates. The events are plotted together with the Scheidegger curve (Scheidegger, 1973) and the cut-off of the Scheidegger curve at 31°, by Corominas (1996). The best fit curves of the different data classes are also included. The volume is in a logarithmic scale

Table 9 Distribution of the different substrates that are dominating the travelling path for the mapped events, with formula and R^2-values of the best fit curves.
*Not statistical representative (only occurring for one or two events or lands in water)
-- Excluded from the analyses

Type of substrate, dominating	Number of events	Formula	R^2-value
Across water	2	$28.831x^{-0.058}$	1*
Alluvial	0		
Bed rock	72	$34.141x^{-0.033}$	0.1378
Debris flow	1	*	*
Into water body	7	--	--
Moraine	2	$28.441x^{-0.06*}$	1*
On ice or permanent snow field	1	*	*
Scree	131	$37.358x^{-0.028}$	0.1228

4.1.6 Substrate and constraints

Since the topographical constraint seems to be a strong controlling factor, the next step is to analyse the substrate with unobstructed events. The events with obstructions in the travelling path were therefore excluded from the analyses. The results are represented in angle of reach/volume ratio, compared to the different substrates, including best fit curves, the Scheidegger curve (Scheidegger, 1973) and the cut-off of the Scheidegger curve by Corominas (1996).

The substrate in the toe of the unobstructed RSF events

In general, the analyses of the substrate in the toe area of the unobstructed events shows that the events travelling on moraine have the lowest angle of reach, followed by the ones landing on ice and snow fields, glaciofluvial, bed rock, alluvial and scree (figure 57). The events landing on moraine has higher angles of reach with smaller volume. Table 10 show the distribution of the different substrate categories, the number of events in each category and the formula and R^2-values for the best fit curves. R^2-values are highest for the best fit curve for events with moraine as the substrate in the toe area. This value is 0.45. However, the values are not close to one, so the results are scattered.

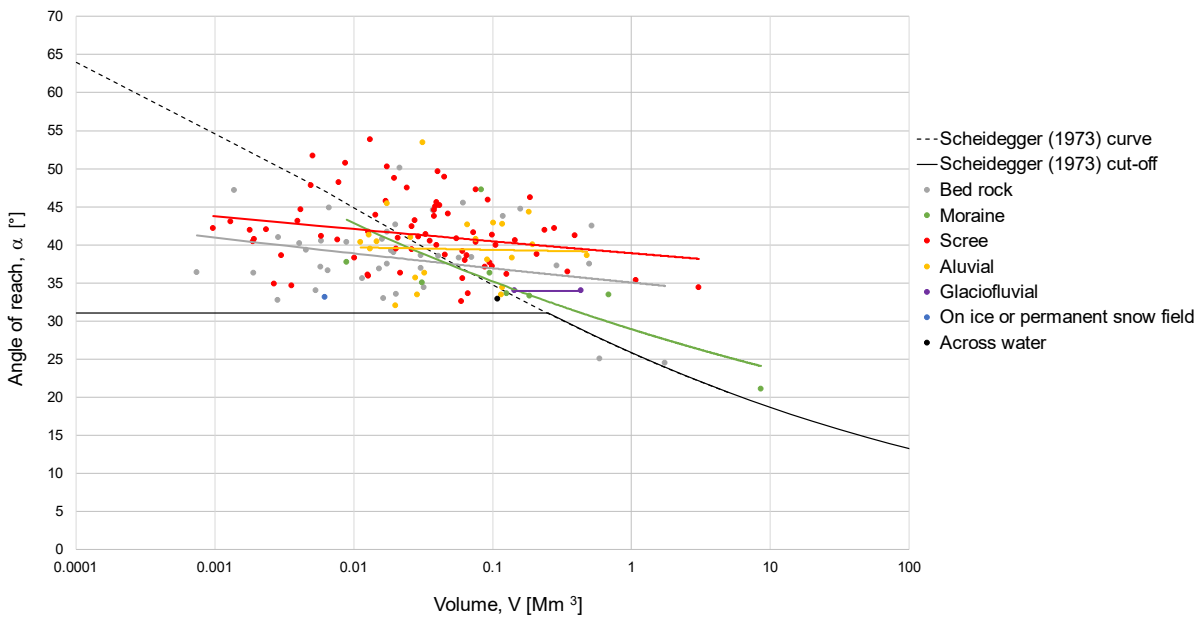

Figure 57 The angle of reach/volume ratio compared to the unobstructed events with different substrates in the toe of the RSF event. The events are plotted together with the Scheidegger curve (Scheidegger, 1973) and the cut-off of the Scheidegger curve at 31°, by Corominas (1996). The best fit curves of the different data classes are also included. The volume is in a logarithmic scale

Table 10 Distribution of the different substrates in the toe of the RSF event, with formula and R^2-values of the best fit curves.
*Not statistical representative (only occurring for one or two events or lands in water)
-- Excluded from the analyses

Type of substrate, in the toe (unobstructed)	Number of events	Formula	R^2-value
Across water	1	*	*
Alluvial	22	$y=39.017x^{-0.004}$	0.002
Bed rock	39	$y=35.603x^{-0.019}$	0.0426
Glaciofluvial	2	$y=33.932x^{-3E-15*}$	*
Into water body	5	--	--
Moraine	8	$y=28.743x^{-0.085}$	0.452
On ice or permanent snow field	1	*	*
Scree	72	$y=38.897x^{-0.017}$	0.0553

Dominating substrate for the unobstructed events

When analysing the dominating substrates for unobstructed events, the unobstructed events travelling across water and on ice or permanent snow fields have the longest runout. However, these are only represented with one event in each category. Following, the events propagating on moraine, bed rock and scree have the highest angles of reach (figure 58). Table 11 are listing the distribution of the different categories and belonging formula and R^2-values. These R^2-values indicate that the data are highly scattered with values close to zero, indicating more factors influencing the runout length for the RSF event.

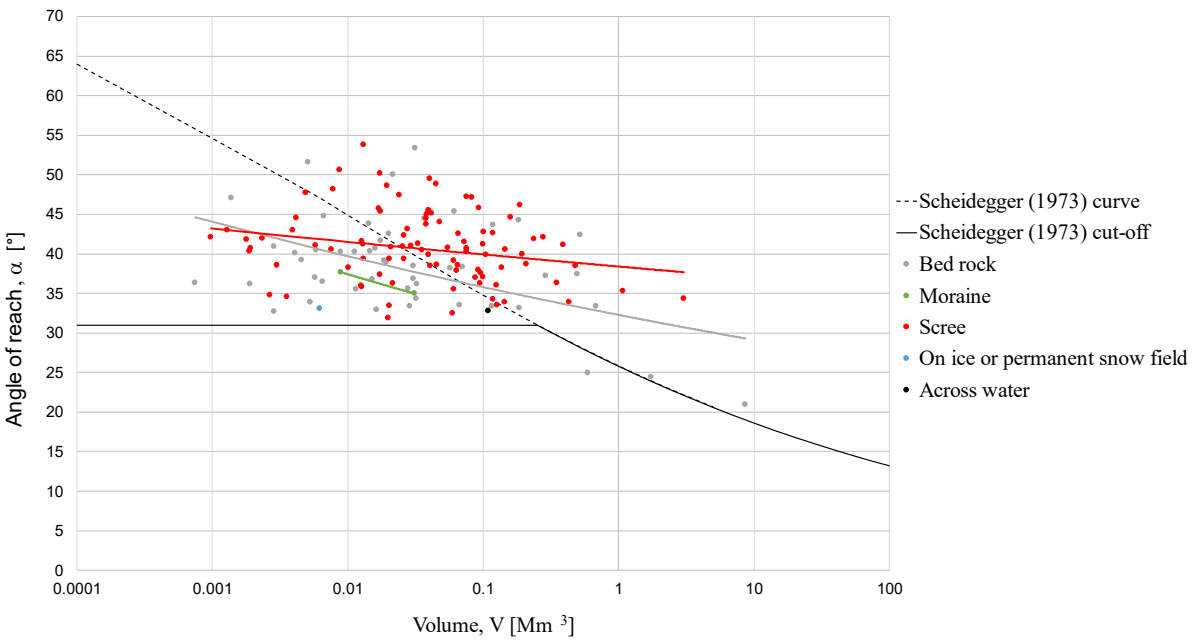

Figure 58 The angle of reach/volume ratio compared to the unobstructed events with different dominating substrates. The evets are also plotted with the Scheidegger curve (Scheidegger, 1973) and the cut-off of the Scheidegger curve at 31°, according to Corominas (1996). The best fit curves of the different data classes are also included. The volume is in a logarithmic scale

Table 11 Distribution of the different dominating substrates, with formula and R^2-values of the best fit curves.
*Not statistical representative (only occurring for one or two events or lands in water)
-- Excluded from the analyses

Type of substrate, dominating (unobstructed)	Number of events	Formula	R^2-value
Across water	1	*	*
Alluvial	0		
Bed rock	50	$32.289x^{-0.04}$	0.1706
Glaciofluvial	0		
Into water body	--	--	--
Moraine	2	28.441x-0.06	1*
On ice or permanent snow field	1	*	*
Scree	92	$38.405x^{-0.017}$	0.0521

4.2 α–β method with suitable coefficients for estimating the runout length of "steinskred" based on the mapped events

Based on the result from the earlier sections, the events below 250 000 m^3 seems to behave the same way. Events below this volume range have angle of reach above 31°. They have no excessive travel length and deviate therefore from rock avalanche. The new α–β method was developed for events with volumes between 10 000-250 000 m^3 (appendix B). This constitutes 144 events

The use of excel in the developing of the method for "steinskred" made it easy to change and test a large amount of different θ_β-angles and values for the m and n parameters. A separate Excel-file was used to present and test out the different scenarios of parameters, by calculating the standard deviation between measured (based on total fall height and the total travel length) and the "predicted" (based on the α–β method) angle of reach. 144 events are tested with different parameters combinations. 5 values for θ_β–angle, 7 values for the parameter m and 5 values for the parameter n were included. This constitutes 25 200 combinations (appendix C). The combination giving the lowest value of standard deviation is shown in equation 7:

$$\alpha = m \cdot \beta + n = 0.75 \cdot \beta + 5° \qquad (7)$$

Where β-point is tested to be where $\theta_\beta = 20°$. This equation resulted in a standard deviation for the events of 4.48°. The values were checked to see if the lowest value was found, by making graphs with the standard deviation values and different m-values, keeping the θ_β -angle and the

n-value constant. The graph showing the lowest value of standard deviation with the θ_β equal to 20° and the n-parameter equal to 0.75 is shown in figure 59.

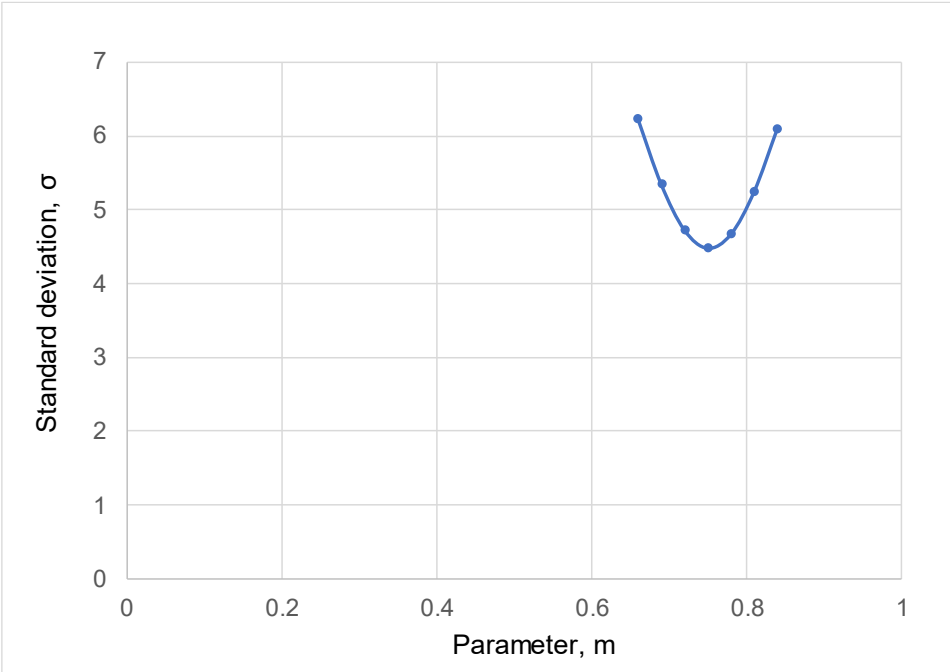

Figure 59 Testing of the constant θ_β-angle at 20° and n parameter of 5° together with different values for the m parameter. The graph show that the lowest standard deviation is given for the m value of 0.75

The results with different values of the parameters in the equation was also tested by comparing the "predicted" angle of reach to the measured angle of reach and look at the R^2- values for the linear best fit curve. These combinations of parameters and θ_β-angle gave no significant differences in the R^2-values and was therefore not used as a predictor for what values of the parameters that fits the best. However, the R^2-values for the parameter set with the lowest standard deviation are illustrated in figure 60 and listed in table 12. The R^2-values are close to 1 which indicate a relatively good statistical fit. This means that the estimated values for the angle of reach are close to the measured angle of reach. In addition, the equation also, when the best fit curve is passing the origin, show that the number multiplied with x is close to 1. This is favorable to be as close to one, as the x is the observed ("the real") value of the angle of reach. A multiplicator of 1 would mean that the method does not exaggerate or underestimates the reach angle.

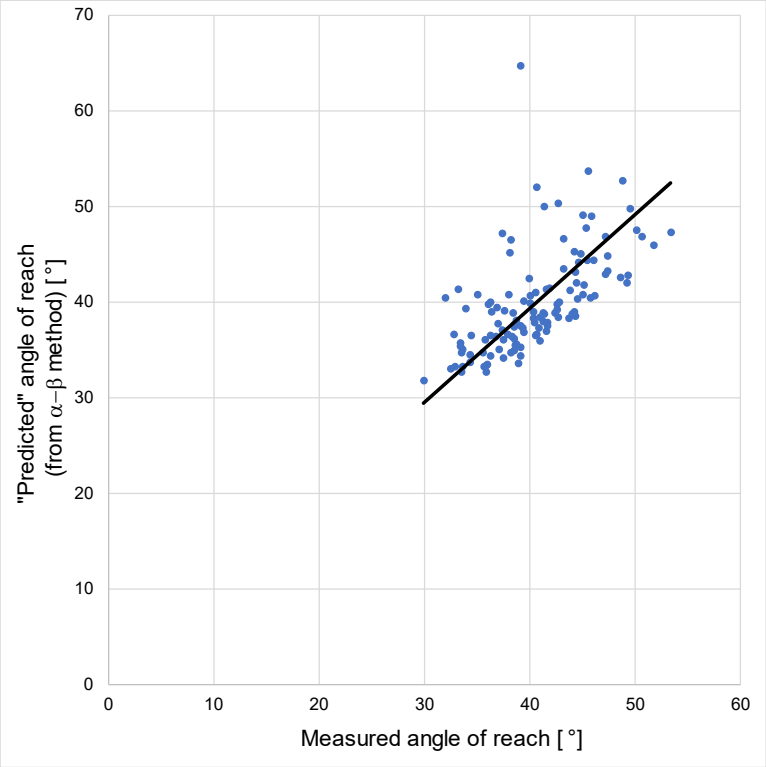

Figure 60 The "predicted" angle of reach (from the α−β method) vs the measured angle of reach. The best fit curve is set to go through 0

Table 12 Shows the formula and the R^2-value for the best fit curve for the comparison of the "predicted" angle of reach and the measured angle of reach

	Formula	**R^2-value**
"Predicted" vs measured angle of reach	y = 0.9843x	0.9879

4.3 Results from local mapping in Modalen

The deposit of the 14th of August 1953 event in Modalen was visited in the field. This event has eroded the scree and entrained it. This has led to deposited masses of a larger volume than the masses that first failed in the source area. It had a flow-like motion as seen in rock avalanches, despite the volume and angle of reach indicating "steinskred". In addition, it reached beyond what would be expected, compared to the rock falls on the side. The event did not only deposit in the valley, but also as levees along the flow path (figure 61). These levees have a height of 1.5-2 m. The erosion has made erosion features in the travelling path, and in the depositional area in the valley there was also observed some transversal ridges which could be mapped out. These have a height of 1-2 m above the internal depression and are spread over the entire deposit body.

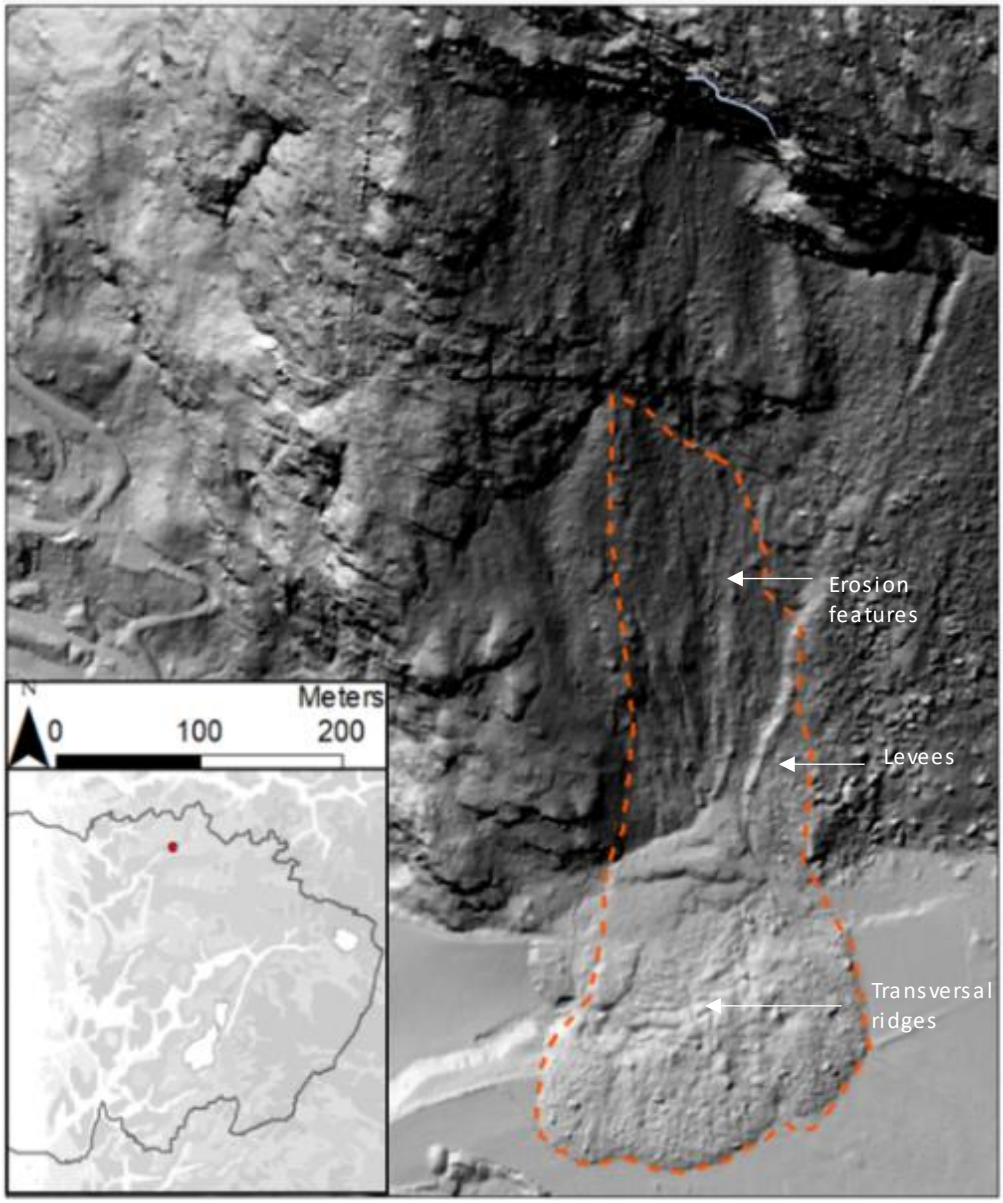

Figure 61 Hill shade map of the RSF event in Modalen. The orange line is representing the deposits and the light blue line is representing the back scar. In the upper part of the deposit area the erosion features and the levees are visible. In the lower part of the deposit area the translational ridges are visible

The measurements of roughness, blocks and tree density and the collecting of sediment samples (section 3.4) were meant to be used for modelling. However, more time than expected was used for the inventory mapping, which is due to large number of detected deposits. So instead, the data is included in the appendix of the thesis to make it easy to use for potential modelling of the RSF event at a later time (appendix D).

To get a better understanding of the flow behaviour of the masses in the failure in Modalen in 1953, the substrate samples were looked more closely into. This is done to investigate the possibility of a liquification of the sediments. The distribution of fragments after the sorting with wet and dry filtration is shown in table 13. The samples are not sorted at a smaller fraction than 0.063 mm, which corresponds to the border between silt and sand. This was because the amount of smaller fragments was considered to be insignificant.

Table 13 The result of the wet and dry filtration analyses of the four sediment samples taken in filed. The table show the percentage amount of the different fragment sizes in each sediment sample

Fragment diameter (mm)	Sediment sample 1 (%)	Sediment sample 2 (%)	Sediment sample 3 (%)	Sediment sample 4 (%)
>16	6	2	6	0
>8	6	12	11	4
>4	6	13	10	4
>2	7	31	7	6
>1	9	7	11	9
>0.5	10	6	25	13
>0.25	11	11	20	15
>0.125	13	5	4	17
>0.063	13	3	2	19
<0.063	20	10	4	13

The sediment samples are represented in a particle-size distribution graph in figure 62. This also shows the gradations which are potentially liquifiable (Obermeier, 1996). The particle-size distribution graphs for the sediment samples are lying inside of the area of potentially liquefiable sediments. Sediment sample 1 is classified as gravelly, sandy material, sediment sample 2 as gravelly, sandy material, sample 3 is sand, gravelly material, and sample 4 is classified as sand.

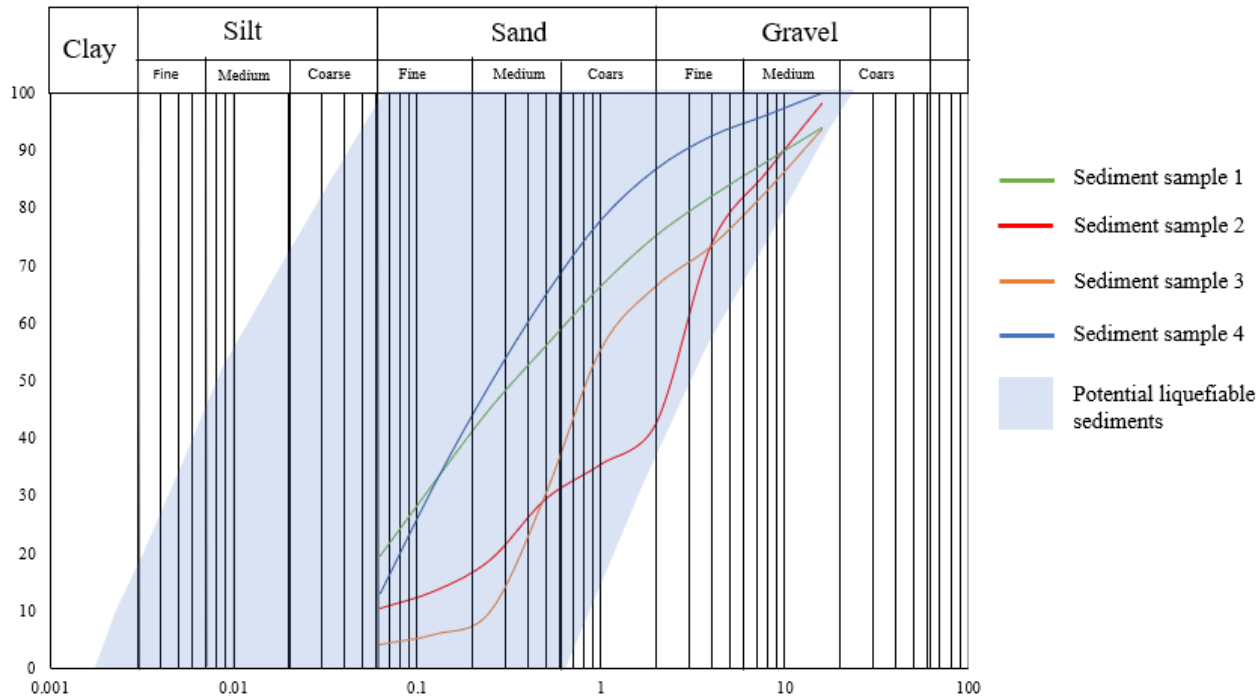

Figure 62 A particle-size distribution graph with the graphs for the four sediment samples. The light blue area indicates the area for potential liquefiable sediments (by Obermeier (1996)). All the sediments lie inside the area of potential liquefiable sediments

In addition to the substrate samples, a sand quarry close to the deposit area were looked at in the field (see location at figure 37, section 3.4). It was possible to study the original deposits and see the sedimentary structures. There was no indication of liquification. However, this investigation was done on the masses on the side of the deposited masses, not under.

Together with the sediment samples, observations in the field, already existing quaternary geological maps, hill shade maps and aerial photos, a new quaternary geological map of Modalen were made (figure 63).

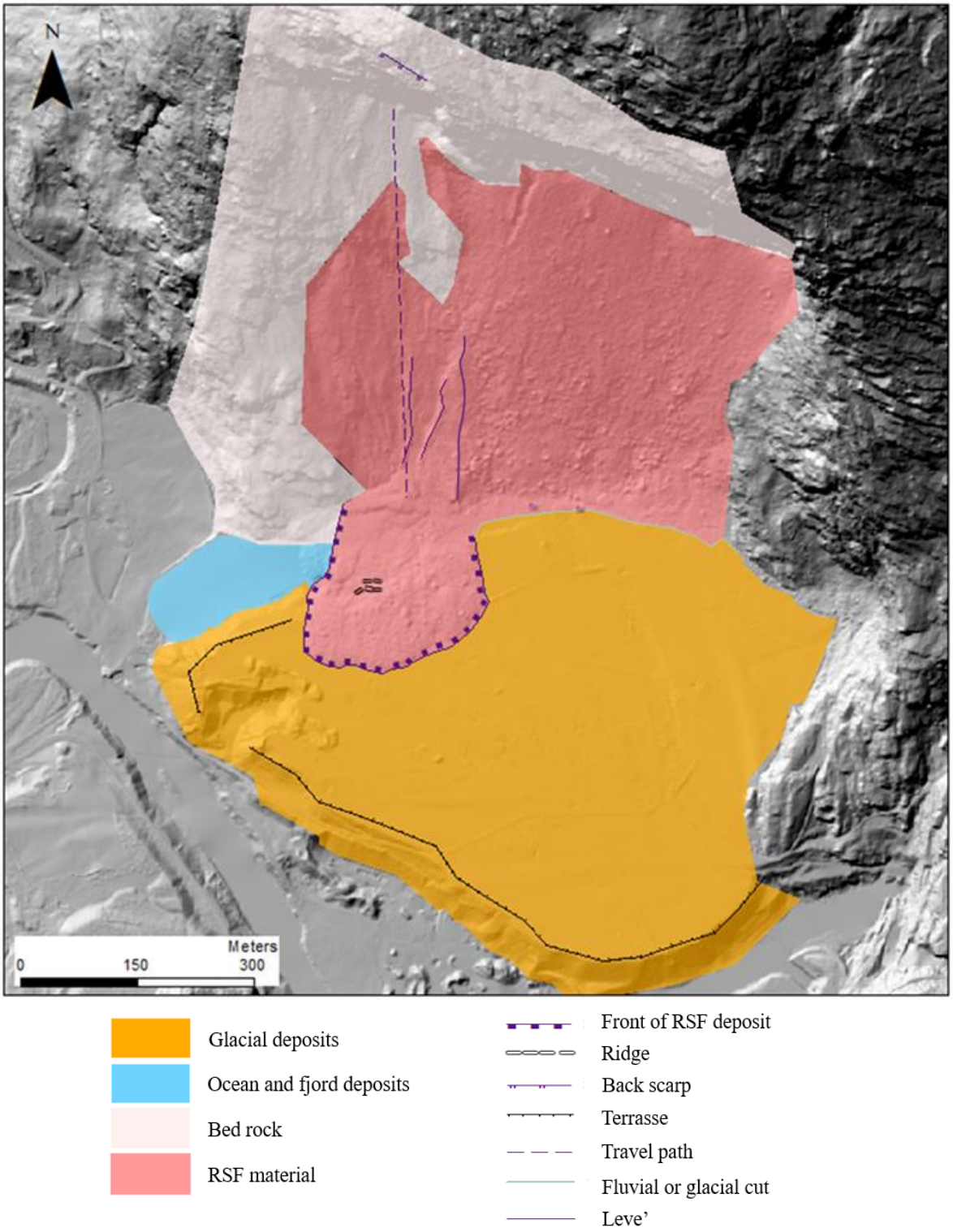

Figure 63 Quaternary geological map of the substrate in Modalen. The map is made based on the sediment samples taken in the field, already existing quaternary maps at NGU, field observations and aerial photos

Results of volume calculations

To make 3D models and volume estimates of the RSF event in Modalen, TLS scans and airborne TLS were used. Volume estimations have been done for the source area, the area of erosion and the deposit area (figure 64). The TLS scans taken from the field was used to make a 3D model of the source area and for the volume estimation of the source area (figure 65). The eroded masses and the deposition area were estimated with the use of airborne LiDAR from Hoydedta.no. The point clouds from the TLS scans and the airborne TLS were processed in the program called CloudCompare (section 3.4). The source area was measured to be 170 000 m^3 +/- 50 000 m^3. A calculation of the eroded mass is estimated to be about 260 000 m^3 (figure 66). Here it is taken in account that there is no deposited mass in the transportation area. Together, this will have a volume estimation of 430 000 m^3 of mobilized mass. However, the volume in the deposited mass in the bottom is measured to only be 140 000 m^3 (figure 67 and 68).

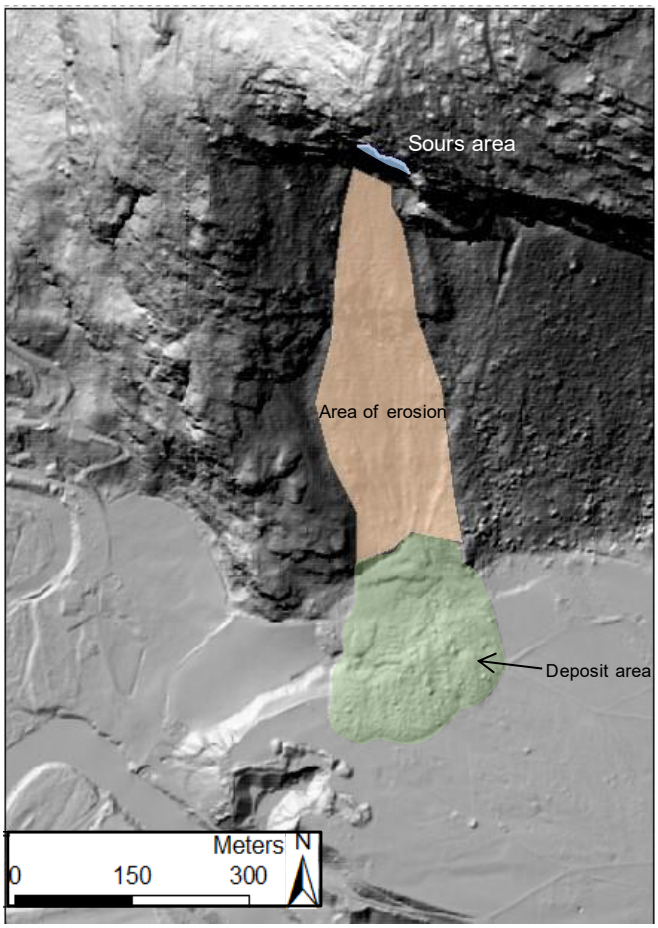

Figure 64 Overview of the source area, area of erosion and deposit area

Figure 65 3D view of the source area made by the scans taken from the LiDAR in the field

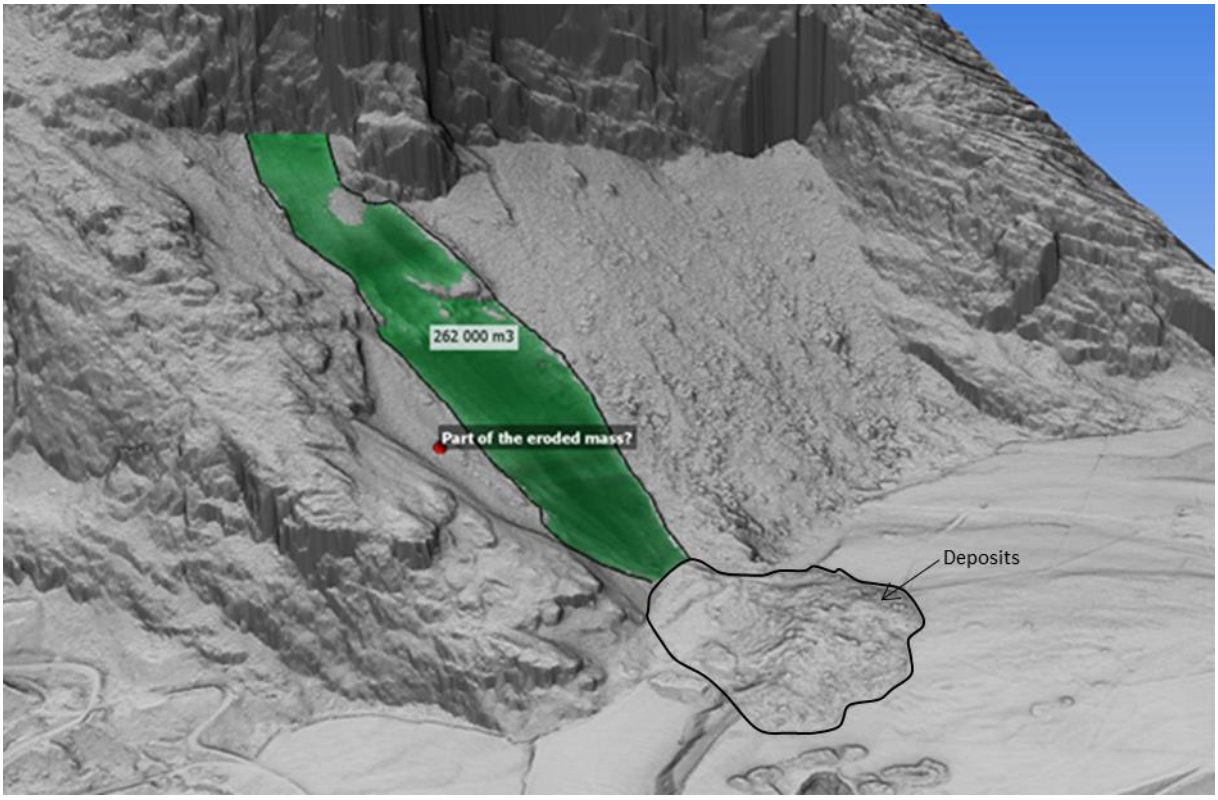

Figure 66 3D view of the slope in Modalen showing the eroded area of the scree (marked in green) and the deposits (outlined in black)

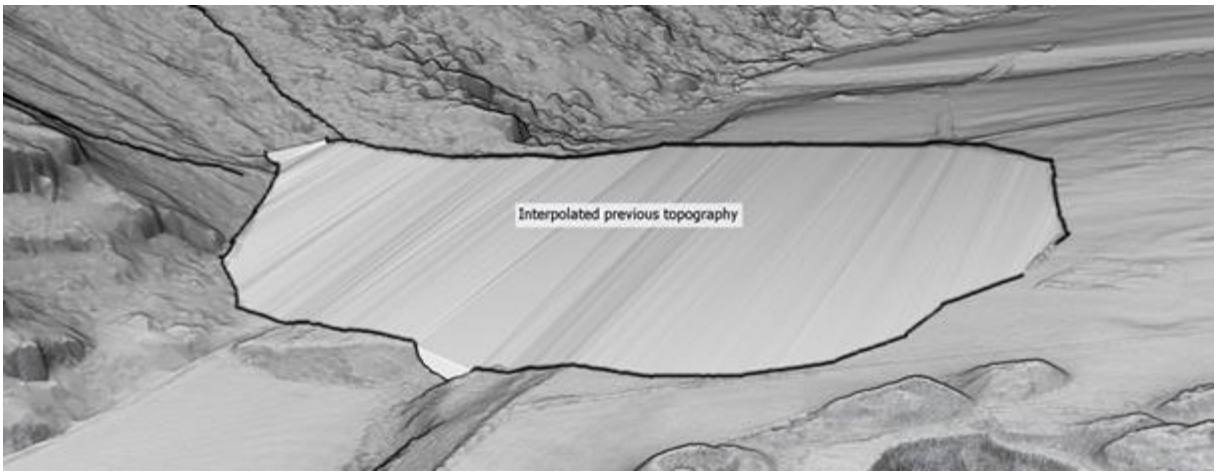

Figure 67 To estimate the volume of the deposit of the "steinskred" event, the previous topography had to be interpolated

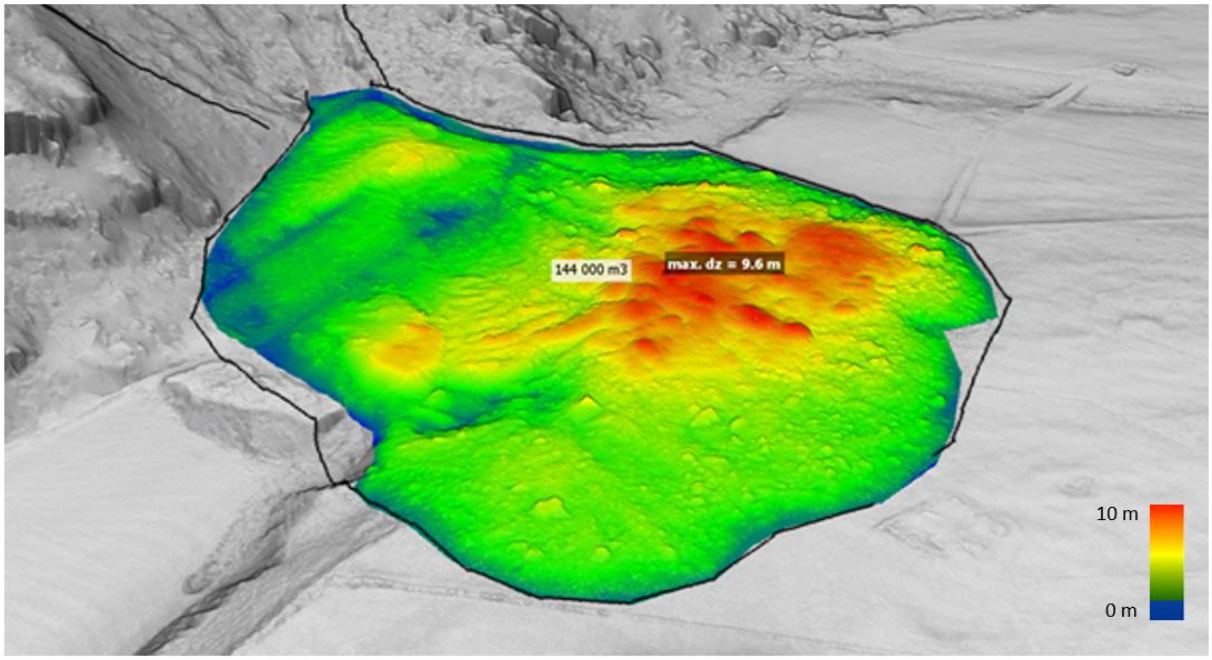

Figure 68 The deposits at the end of the slope is estimated to be ca. 144 000 m^3

The two volume estimations were plotted against the angle of reach, and compared with the Scheidegger curve (Scheidegger, 1973) and the cut-off of the Scheidegger curve at 31°, according to Corominas (1996) (figure 69). Thus, the smallest estimated volume is located on the Scheidegger curve, while the event will be located above this curve with a higher estimated volume.

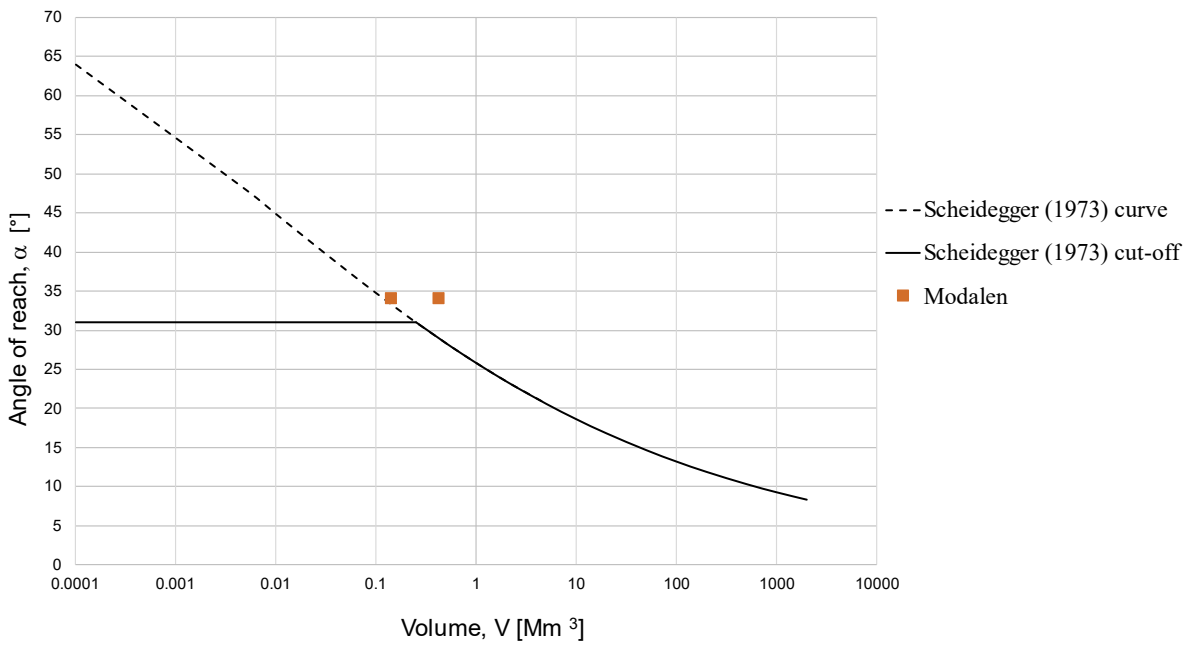

Figure 69 The two estimated volumes scenarios of the "steinskred" event in Modalen is plotted in an angle of reach/volume ratio together with the Scheidegger curve (Scheidegger, 1973) and the cut-off of the Scheidegger curve at 31°, according to Corominas (1996). The volume is presented in a logarithmic scale

The volume of the eroded masses in the slope estimated in CloudCompare did not consider that the masses of the event developed levees on the sides. To estimate a volume on a fast and easy way and consider the height of the levees, the volume of the eroded masses was done by estimating the area and multiplying it with the average height of the eroded masses (figure 70). The height of the eroded masses was estimated to be at maximum of about three meters and of an average, one meter. This was based on field photos and observations. The volume of the eroded part is estimated to be about 57 000 m^3. This estimated volume of the eroded mass compared to the volume of 260 000 m^3 estimated in CloudCompare, seem to correspond better to the estimated volume of the deposition area.

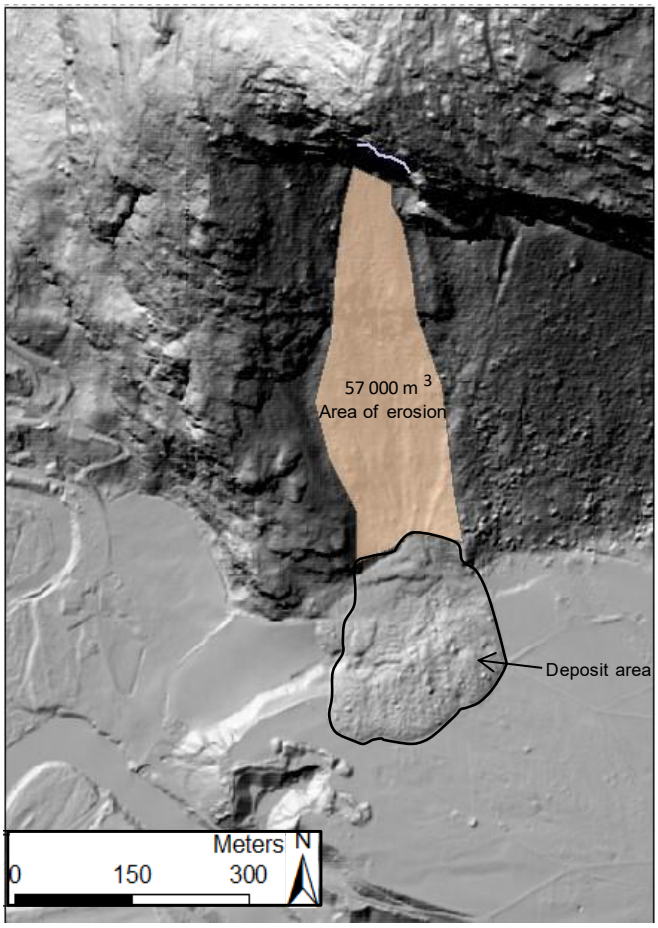

Figure 70 Estimation of the volume of the eroded masses in the slope taking the deposited levees in consideration

5. Discussion

5. 1 Empirical investigations of the controlling factors for the runout length of RSF events in Hordaland

216 events were mapped in Hordaland. However, the registered events will not represent the entire number of postglacial RSF events in the study area. This is because of the fjord environment, multiple overlaying deposits and likely erosion of deposit. Anyway, the large number of events were not expected to be found based on the events mapped in Møre og Romsdal, Troms and Sogn og Fjordane county (Velardi et al., 2020). This might be because the focus of the mapping in Møre og Romsdal, Troms and Sogn og Fjordane county might have been more on larger events and less on events as “steinskred”.

To have a measure on the quality of the data, all the events in Hordaland are subjectively divided into different certainty levels. When only comparing the certain and almost certain events the amount of data was reduced. Some categories ended up with so small number, which did not result in statistically representative data. However, the analyses of the certain and almost certain events show mostly the same trend as the result coming from the whole dataset. This was the case for both the analyses of the substrate and the topographical constraints. Even though most of the mapped events in the study area were classified as likely or uncertain they do not seem to influence the overall outcome of the results. However, because of the number of uncertainties, it was essential to be as consistent as possible when determining the different factors included in the database.

5.1.1 Volume estimation based on SLBL

Estimating the volumes of the deposits for the RSF events is a large part of the analyses performed in this work. The best way of determining volumes of deposits is to compare the DEM before and after the failure. Since there are no DEMs of the surfaces before the events, it is impossible to estimate the volume based on this method. The volume of the deposits for the mapped RSF events in the study area is done using the tool SLBL (section 3.2.1). The SLBL tool is a relatively new method, especially for estimating the volume of the deposit.

The pre-slope can be interpolated as flat or concave. It was observed that this could influence the result a lot. Selecting a concave pre-slope when the pre-slope is flat will overestimate the result. Difficulties of setting the deposit borders (section 3.1) and the cases where deposits have sunken or eroded down into the substrate will also lead to an under- or overestimation of the calculated volumes. However, since the result in this thesis are represented on a logarithmic scale, this potential overestimation does not make up a large importance. Gremmertsen (2021) did a test in QGIS and calculating the volume between the interpolated surface and the existing surface to check the reliability of using SLBL and concluded that the SLBL method is working for its purpose. For other use, the accuracy of volume estimation might be more important and should be considered.

5.1.2 Volume as a controlling factor for the runout length

The angle of reach/volume ratio for the events show that events with deposit volume above 250 000 m^3 have an angle of reach >31° (section 4.1.1), while events below have the possibility of excessive runout lengths (angle of reach <31°). The best fit curve for the rock avalanches (>250 000m^3) mapped in Hordaland shows a slightly increased angle of reach with the volume. This is in accordance with the Scheidegger curve (Scheidegger, 1973), which is a best fit curve for flow-like rock slope failures, indicating a continuous curve of the angle of reach to volume ratio. The best fit curve for the events in Hordaland is only more conservative. Corominas (1996) discussed that the Scheidegger curve is less valid for volumes smaller than 250 000 m^3. This is also shown in the angle of reach/volume ratio for the events in Hordaland. The best-fit curve for the events with deposit volumes <250 000 m^3 show a more constant angle of reach at about 41°. Therefore, the “steinskred” events in the study area are compared to the data by Corominas (1996), which make up the cut-off of the Scheidegger curve at 31° angle of reach. This cut-off is rather an envelope and not a best fit curve as the Scheidegger curve. This cut-off line at 31° makes a good envelope for the mapped events in Hordaland below 250 000 m^3. These results indicates that the limit between rock avalanche and “steinskred” can be discussed to lie more towards 250 000 m^3 than 100 000 m^3 as has been used up till now.

The line between when the angles of reach are more constant and when it increases with the volume is not a clear line. Several rock avalanches do not have excessive travel lengths but have, in fact, high angles of reach in the same way as “steinskred”. The reason for these high angles of reach can be a combination of many factors. This implies that the expectation of constant angle of reach might also show up valid for deposits larger than 250 000 m^3. These

high angles of reach for rock avalanches also indicates that the term of rock avalanches seems to be classified mostly based on volume.

Two events are outstanding and are located below the Scheidegger curve (Scheidegger, 1973) and the cut-off of the Scheidegger curve by Corominas (1996). It can be various reason for these two to be positioned below these lines. The topographical constraints might be one reason. The event with deposit volume below 250 000 m^3 has a channelized topography, and the other event is categorized as unobstructed. These are cases which are expected to go further than the events propagating onto the opposing valley wall. It is not a clear reason for the long runout length, and it is probably a combination of many factors.

The angle of reach/volume ratio and the comparison with the Scheidegger curve and the cut-off at 31° by Corominas (1996) have also been studied for other RSF events in other parts of Norway (Velardi et al., 2020, Blikra et al., 2001). In the same way as the data from Hordaland, these studies indicate that both "steinskred" and rock avalanches have lover excessive travel lengths and larger angles of reach than in other parts of the world. The explanation for this can be various:

- Different terrain. Narrow Norwegian valleys give shorter runout lengths.
- No report on the substrate in the world-wide data.
- Underrepresentation of events propagating on ice or liquifiable sediments in the data from Hordaland.

The threshold tendency indicated by Corominas (1996) is also seen in more recent studies of Velardi et al. (2020) and Gremmertsen (2021). Data by Velardi et al. (2020) and Gremmertsen (2021) and data collected from Hordaland show that the majority of the events with deposit volumes lower than 250 000 m^3 are located above angle of reach of 31°.

5.1.3 The effect of the maximum slope angle on the runout length

In general, H/L ratio increases with the maximum slope angle. However, when the maximum slope angle reaches a value of 45° and above, the H/L values seems to have less correlation with the maximum slope angle. This corresponds well with the result of the data collected from Møre og Rosdal, Sogn og Fjordane and Troms county (Velardi et al., 2020). This data had a threshold at 50° (figure 71), indicating that with at high max. slope angles, there are no-correlation with the H/L. Velardi et al. (2020) also showed that H/L often is correlated to the volume, where higher H/L values indicate higher volume.

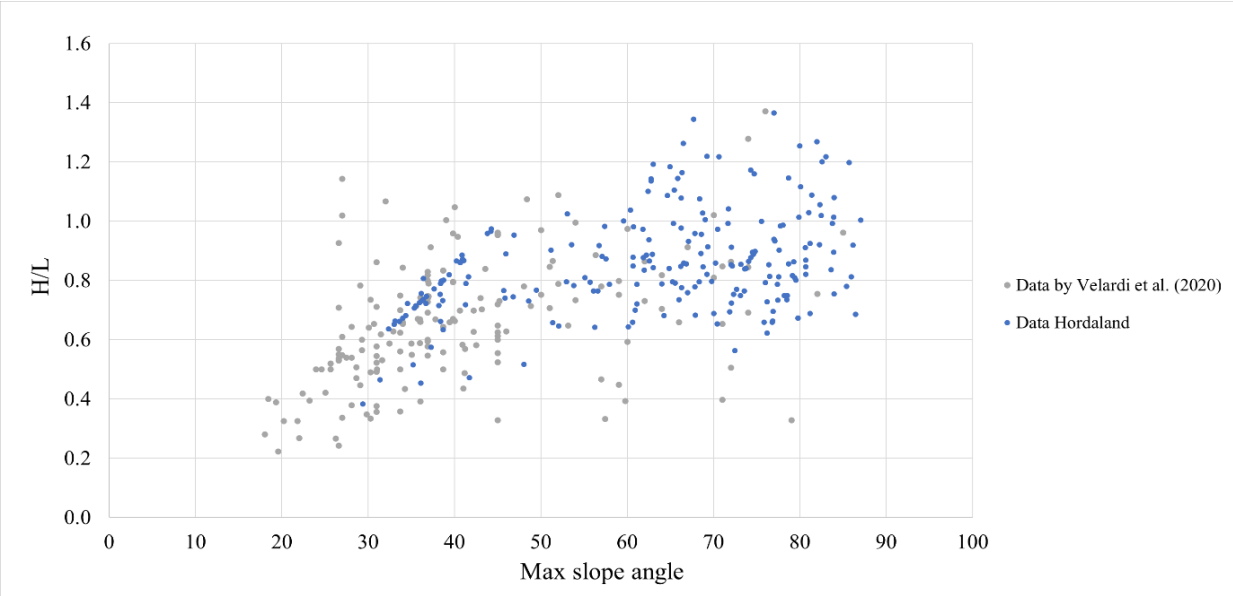

Figure 71 The max. slope angle data from Hordaland and Velardi et al. (2020) plotted against H/L values. Both the data show that maximum slope angle increases with higher H/L values up to slope angles of 45-50°. At higher angles, there is no correlation with the H/L values.

5.1.4 The slope profile geometry as a controlling factor for the runout length

The analyses of the slope profile geometry done in this thesis have not been investigated before. The events with a straight profile geometry of the runout path are shown to have the smallest angle of reach, followed by the ones with a small fall/bouncing area (fall/bouncing area are less than 1/3 of the slope) and a large fall/bouncing area (fall/bouncing area are more than 1/3 of the slope). This trend is independent of the volume. It suggests that a lot of energy is dissipated when there is a drop in the start of the slope. On the other hand, slopes with no break will preserved energy better, resulting in a longer runout length.

The results are in correspondence with earlier studies that have concluded that the angle of the slope influence the runout length (Legros, 2002, Crosta et al., 2017, Zhan et al., 2017). The more potential energy at the start, the further it goes. Crosta et al. (2017) discussed that the geometry of the break of slope causes a loss of momentum perpendicular to the basal layer. When the slope is smoothed, this will give a longer runout, which is also seen in the slope profile geometry analyse.

The normalized area of the slope profile against the angle of reach, as an analysis of the morphology of the slope, showed no correlation (figure 71). The method is taken from the study by Colas et al. (2018). Their result showed a strong relationship between the slope morphology and observed energy line angle (angle of reach) values. This study included 7039 events with a

large variety of angles of reach. This is in contrast to the 218 in this work, with less variation of the angle of reach. However, if placing the data from Hordaland into the graph together with the dataset by Colas et al. (2018), the data might fit in the correlation they found since the data here have a narrow normalized area ratio range, except for a few outliers. The data from Colas et al. (2018) where not available so this could therefore not be tested.

5.1.5 Topographic constraints as a controlling factor for the runout length

The study of RSF events in Hordaland also indicated that the topography along the "runout" path impacts the runout length. For the rock avalanches and steinskred deposit above ~0.09 Mm^3, the results indicate that the angle of reach is lowest for the events with a channelized path, followed by unobstructed failures and the events travelling up the opposite wall. This is an expected result and corresponds to earlier work by Nicoletti and Sorriso-Valvo (1991), Corominas (1996) and Velardi et al. (2020). The events mapped in Hordaland indicate that when the volumes get below ~0.09 Mm^3, the channelized events are no longer the ones with the smallest angle of reach. This result indicates that the rocks lose energy when hitting the walls in the channelized path. Rock falls lose energy with every contact or obstacle, which are implied by Wyllie (2014). Considering the lower limit for rock avalanches as more towards 250 000 m^3 the analyse of the topographic constraints indicates that large "steinskred" can have long runout lengths when it is channelized, while smaller "steinskred" might have the longest runout lengths in unobstructed runout paths. The best fit curves in the results are all located above the Scheidegger cut-off by Corominas (1996), which needs to be considered for hazard assessment in Norway.

Note that an event classified as an unobstructed event in this dataset might be affected by other obstructions like bending of the runout path. These types of obstructions are not studied in this work. Corominas (1996) has considered more types of obstructions and concluded that in general, the scattering in the plots of his results is due to obstacles and topographic constraints in the path.

5.1.6 The effect of the substrate and path material on the runout length

The substrate analysis indicates that the "steinskred" event below ~0.08 Mm^3 will have shorter runout lengths when running on soft material. This is in accordance with Bozzolo and Pamini (1986) and Vick et al. (2019), indicating that rock falls travelling or landing on the softer ground leads to damping and dissipation of the kinetic energy as the soil deforms. In contrast, larger "steinskred" and rock avalanches will rather have longer runout length when travelling on softer material. It is shown that large rock avalanches which have interacted with liquefiable sediments have led to excessive travel lengths, e.g. the 1903 Frank Slide of southern Alberta (Hungr and Evans, 2004) and the rock slide of Elm in Switzerland in 1881 (Buss et al., 1881). This is discussed to be due to the reduction of the friction of coefficient (Aaron and McDougall, 2019) or the rapid undrained loading of the saturated sediments (Sassa and hui Wang, 2005).

The events which are categorized as crossing water have the lowest angles of reach. This was not expected. The data collected from Møre og Romsdal, Troms and Sogn og Fjordane county indicates high angles of reach for crossing water events (Velardi et al., 2020). The reason for the low angles in Hordaland might be because the two events registered are of high volumes, consequently, longer runout lengths can be expected. Additionally, there are only two events in the data from Hordaland, which is registered as crossing water. This is not a good statistical representative.

There is a considerable variation in the number of the different substrate types in analyses of both the substrate in the toe area and the dominating substrates. This makes the reliability of the impact of some of the substrate categories uncertain. Only one event is, for example, registered with ice or permanent snowfields and debris flow and is therefore statistically uncertain. More events in Hordaland might have landed on ice or permanent snowfields, but this is hard to state because of the high uncertainty of the timing of the ice or snow melting. The deposit that was categorized as propagating over ice or permanent snowfields indicates a long runout length, but one case is too small to quantify this potential relationship. De Blasio (2014) argues that friction of coefficient is lower with ice than in rocky terrain, as scree, which leads to higher mobility. That cases that propagate over glaciers are the most mobile is also confirmed by empirical statistics by Aaron and McDougall (2019). Also, studies of Norwegian sites by Schleier et al. (2015) and Velardi et al. (2020) showed high mobility of rock avalanches over ice or permanent snowfields. Most of the events mapped in Hordaland are registered with a substrate in the slope being bedrock or scree. The other substrate types are found in the valley. "Steinskred" are processes that rather affects slope deposits and not valley deposits.

The R^2-values of the best fit curves for the different substrate categories showed a large scattering in the data, indicating that other factors are additionally controlling. The attempt of getting a less scattered result of the analyses of the substrate by excluding channelized and opposing wall events did not show any less scattering. However, it gave the same trend as the analyses from the whole dataset. The result from the whole dataset is therefore considered as reliable.

The substrate categories alluvial, glaciofluvial, scree, debris flow, moraine and bed rock are not included in the currently existing NGU database or in the analyses by Velardi et al. (2020). This addition of substrate categories seems to be essential. It made it possible to study the difference in impact on "steinskred" compared to rock avalanches. Velardi et al. (2020), categorized these substrates added in this mapping of the events in Hordaland as "on land". The mapped events in Hordaland show considerable differences in the runout length for the different new added substrates. For example, scree substrate tends to give a larger angle of reach than moraine substrate. This is probably because of the larger roughness of the terrain when propagating on scree. This importance of dividing into more substrate categories was also apparent during the mapping in the field, especially when analyzing the event in Modalen when the failure set the scree in the slope in motion.

5.2 The α–β model for "steinskred"

Because the observed trend of volumes below 250 000 m^3 shows the same behaviour, the α–β method was tested for the volume range 10 000–250 000 m^3. The resulting equation estimated by using the developed method in Excel is set to:

$$\alpha = m \cdot \beta + n = 0.75 \cdot \beta + 5° \tag{8}$$

Where the β-point is tested to be where $\theta_\beta = 20°$. This is the same as for debris flow. The α–β equation for "steinskred" resulted in a standard deviation of 4.48°. This standard deviation is high compared to the standard deviation found in the already existing equations for rock fall, snow avalanches, and debris flows which are in between the values of 1.5° to 2.3°. (Bakkehoi et al., 1983, Lied and Bakkehøi, 1980, Lied and Kristensen, 2003, Norem and Sandersen, 2012) (section 3.3 and equation 5).

The developed method used to test a new α–β model for "steinskred" makes it is easy to change the variables in the equation and the smoothing of the slope in an effective way. The method is

also consequent when calculating the variables and locating the β-point. However, the method had to be automized because of time limitations, and details in each event were not double checked. This can be one of the reasons for the large standard deviation.

The method needs to be further tested. This might be with, for example, more values for m or the method could favorably be tested for negative n values as in the α−β equations for snow avalanches and debris flows. Additionally, field investigations of the events included in the analyses can make a higher certainty of the estimation of the β-point. The comparison of the "predicted" angles of reach, based on the α−β method, with the measured angles of reach (section 4.2) showed that there were some outliers. There was in particular one case where the "predicted" angle of reach was a lot larger than the measured angle of reach. It might be an advantage to exclude these outliers and the special cases where the results are dominated by features.

5.3 Modalen

As shown, the event in Modalen is of several reasons a special case of a RSF event. The volume estimations (section 4.3) showed that the eroded masses together with the masses loosened from the source area are of too large volume compared to the deposited volume in the valley. The explanation for this is difficult to conclude, but it might be:

- The source area may perhaps be estimated from the wrong location, or the failure surface was overestimated
- An overestimated volume calculation of the eroded masses on the slope. This has probably been done when estimating the volume in CloudCompare, because the levees in the slope was not considered. Also, the slope profile might have been transversely concave prior to failure
- Some of the deposits are deposited in the slope and was not included in the calculation of the volume of the deposits. The levees in the slope were not included in the estimations but were observed in the field as deposited mass. This will lead to an underestimation of the total volume deposited
- The masses might have sunken down into the substrate in the deposit area and does not show at the surface

The flow-like motion was investigated. The substrate has been analysed for the possibility of liquification, which is studied to make a large runout length (Buss et al., 1881, Hungr and

Evans, 2004, Schleier et al., 2017). The sediment samples show that the sediments that the deposit was landing on was composed of glaciofluvial sediments and the particle-size distribution graphs of the sediment samples showed that they are potentially liquifiable sediment based on the fragment distribution. However, it was, based on observations in a quarry and a small trench that was dug in the field, concluded that the sediments were not saturated and have not been liquified. The information collected right after the event also shows that there was no heavy rainfall in the period before the failure, which might be decisive for a potential liquification. However, this theory of no liquification cannot be entirely excluded since this conclusion is based on the substrate outside the deposition area and not inside. If the answer is not lying in the substrate, there has to be other reasons. This might, for example, be due to the entrainment of the scree.

The data collected can, additionally to the results in this thesis, be used to investigate the site further and implement a modeling of the runout to challenge existing simulation models and potentially develop better ones for "steinskred" events. There are no modeling programs specified to the volume range of "steinskred". However, modeling programs for both rock avalanches and rock fall could potentially be tested to see the usefulness for "steinskred".

5.4 "Steinskred" as a definition

The term "steinskred" is a Norwegian term and is not used internationally. "Steinskred" is currently defined based on volume and is, according to Devoli et al. (2011), classified as a RSF event with a volume between 10 000 and 100 000 m^3.

Such arbitrary limits are not supported in this work. The definition might be considered to be further based on the propagation of material of the RSF and the way it acts. This work indicates that events up to the volume of 250 000 m^3 behave similar and have an angle of reach >31°. This indicates that events with deposit volumes between 100 000 m^3 and 250 000 m^3, also act like a "steinskred". The volume range of a "steinskred" may lie more correctly in between 10 000–250 000 m^3. "Steinskred" lies between rock fall and rock avalanches. Rock avalanches have excessive travel lengths and have more flow-like runout behaviour while rock falls have not. Modalen had this flow-like motion, as indicated by the morphology of the deposits. Simultaneous, the volume and angle of reach indicated that the event is a "steinskred". This flow behaviour is not typical for "steinskred", and none of the other mapped events in Hordaland with that volume range had this type of motion. This leads to the question if events as "steinskred" also might have the ability of flow-like motion such as rock avalanches.

The analyses of the effect of substrate and slope topography for the runout length also substantiates the fact that steinskred is an in-between phenomenon. For events laying in the upper part of the volume scale for “steinskred” the substrate and topography will affect the runout length in the same way as in rock avalanches. In the lower volume range, the substrate and the topography will affect the runout length more similarly as for rock falls. None of the analyses showed a good statistically fit based on the R^2- values. This indicates that there is not one factor affecting the runout length for “steinskred”, but several. This also highlights the importance of the study of the different factors affecting the runout length for “steinskred”.

In the national database over landslide and avalanches in Norway it is registered that the term “steinskred” is not clear. The term is used for different types of events, independent of the volume. For example, small events with volumes of rock falls are several times called “steinskred”. Also, in the Norwegian website, Skredregistrering.no where RSF events in Norway are registered, the term does not exist but is defined as small rock avalanches. Even though the term is not clearly defined yet and is not analysed enough, it is essential to know about the uncertainties. Maybe there should not be any specific volume threshold between the different terms. A process-based terminology might be better than a volume-based terminology. The volume-based distinction between “steinskred” and rock avalanche should be investigated further.

6. Conclusions

The main findings of the study can be summarized as followed:

- The events mapped in Hordaland show a threshold in the behaviour at 250 000 m^3. Events below this ("steinskred") have angle of reach >31°, while the rock avalanches are beyond 250 000 m^3 and have the ability of excessive travel lengths (angle of reach <31°). "Steinskred" is always >31°, while rock avalanches are volume dependent.
- The flow motion rock avalanche events in Hordaland have a larger angle of reach, leading to shorter runout lengths for equivalent fall height, than the world wide data collected by Scheidegger (1973). This is corresponding to other analysed events in Norway (Blikra et al., 2001, Velardi et al., 2020). The "steinskred" events where compared to the world wide data and the envelope by Corominas (1996). This envelope is a good fit for the "steinskred" events mapped in Hordaland.
- The most used factor for estimating the runout length is the volume. In this study, the best fit curve of angle of reach is nearly constant within the range of "steinskred", independently of the volume. For rock avalanches the angle of reach shows a slight correlation with volume.
- For events beyond ~0.09 Mm^3 the deposits with channelized travel path (n=9) are travelling the furthest. Under ~0.09 Mm^3 it is the unobstructed (n=109) events that travells the furthest, like commonly seen for rockfalls (they go less far in gullies), suggesting a transition in the controlling factors toward the same as for rock falls in smaller volumes.
- The RSF events in the study area have the largest angle of reach when propagating on scree. Large events, above 0.08 Mm^3, have the longest runout on softer material such as moraine and alluvial, while the events below this will have larger angle of reach on soft material and lower when propagating on bed rock.
- The maximum slope angles are increasing with the H/L up to ~45°. At higher slope angles there are no correlation between the maximum slope angle and the H/L.
- The RSF events slope profile geometry is, in this study, divided into straight, small and large fall/bouncing area. Events with small fall/bouncing area are defined as events where the fall/bouncing area makes up less than 1/3 of the total fell height. Events with large fall/bouncing area are defined as events where the fall/bouncing area makes up more than 1/3 of the total fall height. The RSF events with straight slope profile

geometry have the lowest angles of reach, followed by the events with a small falling/bouncing area and the events with large fall/bouncing area. The analyses with categorization of the slope profile geometry shows a clear correlation with the angle of reach, suggesting a strong control of the terrain profiles.

- The automated developed approach tested for a new $\alpha-\beta$ model for "steinskred" led to this equation: $\alpha = m \cdot \beta + n = 0.75 \cdot \beta + 5°$, where β–point is where $\theta_\beta = 20°$. The standard deviation is 4.48°, which is high compared to the already existing equations for rock fall, debris flows and snow avalanches (Bakkehoi et al., 1983, Lied and Bakkehøi, 1980, Lied and Kristensen, 2003, Norem and Sandersen, 2012). The method needs to be further tested.
- The term "steinskred" should be discussed further. Currently the separation between "steinskred" and rock avalanche is at 100 000 m^3, but based on the data from Hordaland, the suggest transition should lie at 250 000 m^3. The blurry transition of behaviour from "steinskred" to rock avalanche is not well understood and therefor the line should be more flexible, and the term rather defined on processes.
- The event in Modalen is a flow behaviour event with small volume. The factors contributing to the eroding of the scree should be investigated further.

6.1 Recommendations for further work

- Investigate if there is another way of presenting the result from the slope profile geometry, since geometry of the terrain profile is shown to be an important controlling factor.
- Test the categorization of different slope profile geometry with data collected by Velardi et al. (2020).
- Detailed fieldwork, as done in Modalen, for the failure events classified as uncertain or outliers, to understand why they stand out.
- Look at bathymetric data for the events going out in the fjord or lakes and investigate further what effect this might have on the runout length.
- Now the counties Vestland (Hordaland and Sogn og Fjordane), Møre og Romsdal, Troms and Oppland are mapped. Other counties in Norway should be mapped to make a whole done dataset for the entire Norway.

- Test different modelling programs developed for both rock falls and flow-based phenomena to see if it is possible to use these to analyse the runout length events with volume defined as “steinskred”.
- Map further events in detail to take benefit of the high resolution DEMs of today which will result in much more precise volume calculations.

7. References

AARON, J. & MCDOUGALL, S. 2019. Rock avalanche mobility: The role of path material. *Engineering Geology,* 257**,** 105126.

AUGUSTINUS, P. C. 1992. The influence of rock mass strength on glacial valley cross-profile morphometry: A case study from the Southern Alps, New Zealand. *Earth Surface Processes and Landforms,* 17**,** 39-51.

AZZONI, A., LA BARBERA, G. & ZANINETTI, A. Analysis and prediction of rockfalls using a mathematical model. 1995 1995. Elsevier, 709-724.

BAKKEHOI, S., DOMAAS, U. & LIED, K. 1983. Calculation of snow avalanche runout distance. *Annals of Glaciology,* 4**,** 24-29.

BALLANTYNE, C. K. 2002. Paraglacial geomorphology. *Quaternary Science Reviews,* 21**,** 1935-2017.

BLIKRA, L. H., LONGVA, O., BRAATHEN, A., ANDA, E., DEHLS, J. F. & STALSBERG, K. 2006. Rock slope failures in Norwegian fjord areas: examples, spatial distribution and temporal pattern. *Landslides from massive rock slope failure.* Springer.

BLIKRA, L. H., SKURTVEIT, E. & BRAATHERN, A. 2001. Hazard evaluation of rock avalanches; the Baraldsnes-Oterøya area.

BOULTBEE, N., STEAD, D., SCHWAB, J. & GEERTSEMA, M. 2006. The Zymoetz River rock avalanche, June 2002, British Columbia, Canada. *Engineering Geology,* 83**,** 76-93.

BOURRIER, F., DORREN, L. & HUNGR, O. 2013. The use of ballistic trajectory and granular flow models in predicting rockfall propagation. *Earth Surface Processes and Landforms,* 38**,** 435-440.

BOZZOLO, D. & PAMINI, R. 1986. Simulation of rock falls down a valley side. *Acta Mechanica,* 63**,** 113-130.

BRAATHEN, A., BLIKRA, L. H., BERG, S. S. & KARLSEN, F. 2004. Rock-slope failures in Norway; type, geometry, deformation mechanisms and stability. *Norwegian Journal of Geology/Norsk Geologisk Forening,* 84.

BUSS, E., HEIM, A., BECKER, F., HOFER, J. J. & GANZ, J. 1881. *Der Bergsturz von Elm den 11. September 1881: Denkschrift*, Verlag nicht ermittelbar.

COLAS, B., BERGER, F. & TOE, D. Run-out of rockfall: towards objective assistance in determining the angles of the energy line method. 2018 2018.

COROMINAS, J. 1996. The angle of reach as a mobility index for small and large landslides. *Canadian Geotechnical Journal,* 33**,** 260-271.

CROSTA, G. B., DE BLASIO, F. V., DE CARO, M., VOLPI, G., IMPOSIMATO, S. & RODDEMAN, D. 2017. Modes of propagation and deposition of granular flows onto an erodible substrate: experimental, analytical, and numerical study. *Landslides,* 14**,** 47-68.

CRUDEN, D. M. & VARNES, D. J. 1996. Landslide types and processes. Dalam: Turner, AK Landslides Investigation and Mitigation. Special Report. National Academy Press.

DE BLASIO, F. V. 2014. Friction and dynamics of rock avalanches travelling on glaciers. *Geomorphology,* 213**,** 88-98.

DELINE, P., ALBERTO, W., BROCCOLATO, M., HUNGR, O., NOETZLI, J., RAVANEL, L. & TAMBURINI, A. 2011. The December 2008 Crammont rock avalanche, Mont Blanc massif area, Italy. *Natural Hazards and Earth System Sciences,* 11**,** 3307-3318.

DEVOLI, G., EIKENÆS, O., TAURISANO, A., HERMNNS, R., FISCHER, L., OPPIKOFER, T. & BUNKHOLDT, H. 2011. Plan for skredfarekartlegging - Delrapport steinsprang, steinskred og fjellskred. *NVE report,* 15**,** 2011.

DOMAAS, U. 1994. Geometrical methods of calculating rockfall range. *Norwegian Geotechnical Institute, Report,* 585910.

DORREN, L. K. A. 2003. A review of rockfall mechanics and modelling approaches. *Progress in Physical Geography,* 27**,** 69-87.

DORREN, L. K. A. 2015. Rockyfor3D (v.5.2) revealed - Transparent description of the complete 3Drockfall modell. (www.ecorisq.org): 32 p.

ERISMANN, T. H. 1986. Flowing, rolling, bouncing, sliding: synopsis of basic mechanisms. *Acta Mechanica,* 64**,** 101-110.

EVANS, S. G. & HUNGR, O. 1993. The assessment of rockfall hazard at the base of talus slopes. *Canadian geotechnical journal,* 30**,** 620-636.

FOSSEN, H., DALLMAN, W., ANDRESEN, A. & RAMBERG, I. B. 2008. The mountain chain rebounds and founders. The Caledonides are worn down: 405–359 million years. *The Making of a Land. Norwegian Geological Association, Trondheim,* 232**,** 259.

FREDIN, O., BERGSTRØM, B., EILERTSEN, R., HANSEN, L., LONGVA, O., NESJE, A. & SVEIAN, H. 2013. Glacial landforms and Quaternary landscape development in Norway. *Quaternary Geology of Norway, edited by: Olsen, L., Fredin, O., and Olesen, O., Geological Survey of Norway Special Publication, Geological Survey of Norway, Trondheim,* 525.

GREMMERTSEN, C. 2021. *Empirisk mobilitetsanalyse av steinskred i Oppland og vurdering av InSAR Norge som predikativt verktøy.* Det matematisk-naturvitenskapelige fakultet, Universitetet i Oslo. Available: https://www.duo.uio.no/.

HEIM, A. 1932. Landslides and human lives (Bergstürz and Menchen leben), Translated by: Skermer, N. *Bi-Tech Publishers, Vancouver*.

HERMANNS, R. L. 2018. Landslide. *In:* BOBROWSKY, P. T. & MARKER, B. (eds.) *Encyclopedia of Engineering Geology.* Cham: Springer International Publishing.

HERMANNS, R. L., HANSEN, L., SLETTEN, K., BÖHME, M., BUNKHOLT, H., DEHLS, J. F., EILERTSEN, R., FISCHER, L., L'HEUREUX, J. S. & HØGAAS, F. 2012. Systematic geological mapping for landslide understanding in the Norwegian context. *Landslide and engineered slopes: protecting society through improved understanding. Taylor & Francis Group, London***,** 265-271.

HERMANNS, R. L., SCHLEIER, M., BÖHME, M., BLIKRA, L. H., GOSSE, J., IVY-OCHS, S. & HILGER, P. Rock-avalanche activity in W and S Norway peaks after the retreat of the Scandinavian Ice Sheet. 2017 2017. Springer, 331-338.

HSU, K. J. 1975. Catastrophic debris streams (sturzstroms) generated by rockfalls. *Geological Society of America Bulletin,* 86**,** 129-140.

HUNGR, O. 1995. A model for the runout analysis of rapid flow slides, debris flows, and avalanches. *Canadian geotechnical journal,* 32**,** 610-623.

HUNGR, O. & EVANS, S. G. Engineering evaluation of fragmental rockfall hazards. 1988 1988. 685-690.

HUNGR, O. & EVANS, S. G. 2004. Entrainment of debris in rock avalanches: an analysis of a long run-out mechanism. *Geological Society of America Bulletin,* 116**,** 1240-1252.

HUNGR, O., LEROUEIL, S. & PICARELLI, L. 2014. The Varnes classification of landslide types, an update. *Landslides,* 11**,** 167-194.

JABOYEDOFF, M., BAILLIFARD, F., COUTURE, R., LOCAT, J. & LOCAT, P. 2004. Toward preliminary hazard assessment using DEM topographic analysis and simple mechanical modeling by means of sloping local base level. *Landslides evaluation and stabilization. Balkema***,** 199-205.

JABOYEDOFF, M. & DERRON, M.-H. 2005. A new method to estimate the infilling of alluvial sediment of glacial valleys using a sloping local base level. *Geografia Fisica e Dinamica Quaternaria,* 28**,** 37-46.

JABOYEDOFF, M., OPPIKOFER, T., ABELLÁN, A., DERRON, M.-H., LOYE, A., METZGER, R. & PEDRAZZINI, A. 2012. Use of LIDAR in landslide investigations: a review. *Natural hazards,* 61**,** 5-28.

KOLDERUP, N. H. 1955. Raset i Modalen 14. august 1953. *Norsk Geol. Tidssk,* 34**,** 211-217.

LAGERBÄCK, R. 1990. Late Quaternary faulting and-paleoseismicity in northern Fennoscandia, with particular reference to the Lansjärv area, northern Sweden. *Geologiska Föreningen i Stockholm Förhandlingar,* 112**,** 333-354.

LATO, M. J., DIEDERICHS, M. S. & HUTCHINSON, D. J. 2010. Bias correction for view-limited Lidar scanning of rock outcrops for structural characterization. *Rock mechanics and rock engineering,* 43**,** 615-628.

LEGROS, F. 2002. The mobility of long-runout landslides. *Engineering geology,* 63**,** 301-331.

LIED, K. 1977. Rockfall problems in Norway. *ISMES Publication,* 90**,** 51-53.

LIED, K. & BAKKEHØI, K. 1980. Empirical calculations of snow–avalanche run–out distance based on topographic parameters. *Journal of Glaciology,* 26**,** 165-177.

LIED, K. & KRISTENSEN, K. 2003. *Snøskred: håndbok om snøskred*, Vett & Viten.

MANGERUD, A. J. 1976. Fra istid til nåtid.

MANGERUD, J., AARSETH, I., HUGHES, A. L. C., LOHNE, Ø. S., SKÅR, K., SØNSTEGAARD, E. & SVENDSEN, J. I. 2016. A major re-growth of the Scandinavian Ice Sheet in western Norway during Allerød-Younger Dryas. *Quaternary Science Reviews,* 132**,** 175-205.

MCKERROW, W. S., MAC NIOCAILL, C. & DEWEY, J. F. 2000. The Caledonian orogeny redefined. *Journal of the Geological society,* 157**,** 1149-1154.

MITCHELL, A., MCDOUGALL, S., NOLDE, N., BRIDEAU, M. A., WHITTALL, J. & AARON, J. B. 2020a. Rock avalanche runout prediction using stochastic analysis of a regional dataset. *Landslides***,** 1-16.

MITCHELL, A., MCDOUGALL, S., AARON, J. & BRIDEAU, M.-A. 2020b. Rock avalanche-generated sediment mass flows: Definitions and hazard. *Frontiers in Earth Science***,** 412.

NGU. 2015. *Terrestrial laser scanning.* [Online]. Available: https://www.ngu.no/en/topic/terrestrial-laser-scanning [Accessed 25.07.21].

NICOLETTI, P. G. & SORRISO-VALVO, M. 1991. Geomorphic controls of the shape and mobility of rock avalanches. *Geological Society of America Bulletin,* 103**,** 1365-1373.

NOREM, H. & SANDERSEN, F. 2012. Flom-og sørpeskred: Høringsutgave av veileder.

NVE 2014. Flaum- og skredfare i arealplanar. *NVE report 2/2011 - Revidert 22.mai 2014.* Oslo: Norges Vassdrags- og energidirektorat. Available: http://publikasjoner.nve.no/retningslinjer/2011/retningslinjer2011_02.pdf [Accessed 20.07.21].

NVE 2020. Veileder for utredning av sikkerhet mot skred i bratt terreng. Available: https://veileder-skredfareutredning-bratt-terreng.nve.no/ [Accessed 02.05.21].

OBERMEIER, S. F. 1996. Use of liquefaction-induced features for paleoseismic analysis—an overview of how seismic liquefaction features can be distinguished from other features and how their regional distribution and properties of source sediment can be used to infer the location and strength of Holocene paleo-earthquakes. *Engineering Geology,* 44**,** 1-76.

RITCHIE, A. M. 1963. Evaluation of rockfall and its control. *Highway research record*.

ROCKSCIENCE 2021. Rocfall. https://www.rocscience.com/software/rocfall.

SASSA, K. & HUI WANG, G. 2005. Mechanism of landslide-triggered debris flows: Liquefaction phenomena due to the undrained loading of torrent deposits. *Debris-flow hazards and related phenomena.* Springer.

SCHEIDEGGER, A. E. 1973. On the prediction of the reach and velocity of catastrophic landslides. *Rock mechanics,* 5**,** 231-236.

SCHLEIER, M., HERMANNS, R. L. & ROHN, J. Rock avalanches in a changing landscape following the melt down of the scandinavian ice sheet, Norway. 2017 2017. Springer, 369-377.

SCHLEIER, M., HERMANNS, R. L., ROHN, J. & GOSSE, J. C. 2015. Diagnostic characteristics and paleodynamics of supraglacial rock avalanches, Innerdalen, Western Norway. *Geomorphology,* 245**,** 23-39.

SIGMOND, E. M. O. 1998. Odda. Bergrunnskart Odda M 1:250 000; trykt i farger. *NGU*.

SOSIO, R., CROSTA, G. B., CHEN, J. H. & HUNGR, O. 2012. Modelling rock avalanche propagation onto glaciers. *Quaternary Science Reviews,* 47**,** 23-40.

STATENS VEGVESEN 2005. Håndbok 014 Laboratorieundersøkelser.

STEAD, D. & EBERHARDT, E. 2013. Understanding the mechanics of large landslides. *Ital. J. Eng. Geol. Environ. Book Ser,* 6**,** 85-112.

VARNES, D. J. 1978. Slope movement types and processes. *Special report,* 176**,** 11-33.

VELARDI, G., HERMANNS, R. L., PENNA, I. & BÖHME, M. Prediction of the Reach of Rock Slope Failures Based on Empirical Data From Norway. 2020. International Society for Rock Mechanics and Rock Engineering.

VICK, L. M., ZIMMER, V., WHITE, C., MASSEY, C. & DAVIES, T. 2019. Significance of substrate soil moisture content for rockfall hazard assessment. *Natural Hazards and Earth System Sciences,* 19**,** 1105-1117.

WYLLIE, D. C. 2014. Calibration of rock fall modeling parameters. *International Journal of Rock Mechanics and Mining Sciences,* 67**,** 170-180.

ZHAN, W., FAN, X., HUANG, R., PEI, X., XU, Q. & LI, W. 2017. Empirical prediction for travel distance of channelized rock avalanches in the Wenchuan earthquake area. *Natural Hazards and Earth System Sciences,* 17**,** 833-844.

8. Overview of appendices

The appendices are gathered in an own ZIP-file delivered together with the thesis.

Appendix A: Data of the mapped events and the belonging data as:

- Deposit volume
- H/L
- Angle of reach, α
- Substrate (in the toe area and the dominating)
- Topographic constraints
- The slope profile geometry
- Maximum slope angle
- Certainty level

Appendix B: The new method for estimating the $\alpha-\beta$ model

Appendix C: Testing of the parameters m and n and θ_β in the new $\alpha-\beta$ equation in order to find the lowest standard deviation

Appendix D: Data collected in the field from the "steinskred" event in Modalen, 1953

NTNU

Norwegian University of
Science and Technology